The Design of Apparatus for Measuring Ocean Wave Parameters

A thesis presented in partial fulfilment of the requirements
for the degree of

Master of Technology

at Massey University, Palmerston North, New Zealand.

Frank John van der Hulst

2003

Abstract

This document describes the design of a low-cost apparatus for the measurement of ocean wave parameters. The design is implemented using magnetometers to measure attitude of a free-floating buoy, and accelerometers to measure motion of the buoy, and a microprocessor to analyse the data. Calibration of the sensors is described, as well as the use of digital filtering in the analysis of the signals to determine attitude and motion. Testing of the system, both on land and on water, is described, including protection of the devices from the corrosive effects of salt water.

Table of Contents

Table of Figures

Acknowledgments

My thanks go to the following, who were assisted in bringing this research project to fruition:

- Dr Roger Browne of Massey University, my supervisor and mentor, for his patience and guidance.

- Dr Bruce van Brunt, of Massey University's Dept of Mathematics who helped me to visualise the three dimensional mathematics.

- Ken Mercer and Colin Plaw of Massey University's Institute of Information Sciences and Technology, who shared with me their skills and knowledge of electronics and hardware design.

- My colleagues and students at Wanganui Regional Community Polytechnic (now Wanganui UCOL), who provided me with support and encouragement.

1 Introduction

Measurement of ocean waves is important for

- **Engineering purposes**
  - Ship design. Pitching and rolling can slow down the progress of the ship, as well as causing cargo to move and causing other damage. Knowledge of the size and frequency of waves likely to be encountered allows the ship designer to minimise the negative effects of waves.
  - Design of structures to be erected in the sea (eg oil drilling platforms, wharves).Waves are the most important environmental factor producing forces on offshore structures. Not only can there be high stress loads from individual waves, but fatigue from significant wave activity over a long period must be designed for.
  - Wave-driven electricity generation. An average of 25MW of electricity could be generated per km of coastline. However, this is variable, so knowledge of wave climate is needed to properly estimate the return from investing in a wave-driven power station.
  - Military. During World War II, much effort was put into oceanography to predict wave characteristics for beach landings. Pressure-operated mines, which need to be set off by ships but not wave action is another example.

- **Environmental reasons**
  - Study of erosion in coastal areas. This is becoming increasingly important with the predicted rise in sea level due to greenhouse effects. Not only do waves erode cliffs and beaches, but material is also carried by 'longshore drift' to be deposited elsewhere.
  - Changed ocean climate. Measurements suggest a significant worsening of the eastern North Atlantic wave climate between 1960 and 1977. [Draper 1986]
  - Study of ocean/atmosphere interaction and weather prediction. The oceans have a great effect on the atmosphere and vice versa. It is increasingly becoming recognised that ocean waves are an important mechanism for energy exchange between the ocean and air, and an important part of ocean currents. [Melville 2002]

The height of ocean waves is the property of the most interest because it gives a measure of the amount of energy being carried by the wave, and therefore its destructive power. Also of interest is the direction of the wave.

A central problem to ocean wave study is that observations need to be made over an extended period of time (months to years) to gain an understanding of the wave climate. In addition, the location of interest is often in a remote part of the ocean, rarely visited by people.

Often, data needs to be gathered from locations in deep water. In these circumstances, it is necessary for the sensors to be mounted on a buoy that floats on the ocean surface. Typically, the motion of the buoy is measured as it follows the ocean surface. In many cases, mooring a buoy in the correct location is prohibitively expensive, so

buoys are deployed and allowed to drift. This in turn is expensive, since the time that buoy is providing the required data is limited. Only 37% of drifting buoys are still fully operational after 18 months [Meindl 1992].

The following properties are therefore desirable in a device to measure ocean waves in deep water:

1. Autonomy. It is desirable to place the device at the desired location and record ocean wave data over long time periods without human intervention.
2. Measurement of wave height.
3. Measurement of wave direction.
4. Self-powered. To allow this, all components must have minimal power requirements so that batteries or solar cells can power the system.
5. Stable sensors or a self-calibrating system.
6. Data transmission. Data should be transmitted by the device to a remote base station, possibly in batches, or at least stored for later retrieval.
7. Data analysis. Analysing data in situ will reduce the amount of data transmission/storage required. Data may be analysed in real time (eg. for weather prediction) or batch mode (for longer-term studies).
8. Robustness. Due to remoteness of data gathering locations, it may be very expensive to repair faults. This suggests a minimum of mechanical devices.
9. Corrosion resistance. Sea water is extremely corrosive to metallic devices.

The School of Electronic and Software Engineering at the Central Institute of Technology, Trentham, New Zealand has been developing a solar-powered boat as a research project [van der Hulst 2001]. It is an autonomous vessel designed to operate far from land for long periods of time. This capability makes it suitable for use as a self-positioning data buoy for monitoring weather or ocean conditions, if suitable sensors are constructed.

This report will begin by outlining the current theory of ocean wave motion, and the current techniques used to measure ocean waves (Chapter 2: Context). The following chapters will describe alternative techniques that can be applied (Chapter 3: This Project), the hardware and software implemented during this research project (Chapters 4 and 5), and the outcome of testing of the system (Chapter 6: Results). Finally, possible directions for further research based on the outcome of this project are outlined in Chapter 7, and conclusions discussed in Chapter 8.

2 Context

2.1 Ocean Waves

Waves on the ocean are produced by surface friction with wind. Once a small unevenness appears, it feeds back positively to the wind, causing the wind to speed up beyond the crest causing a low-pressure area. This in turn causes the wave to increase in size, and further increases the effect on the wind.

Wave sizes vary from capillary ripples (centimetres in length, millimetres in amplitude, surface tension is a significant aspect) to storm surges (kilometres in length, metres in amplitude, days in period).

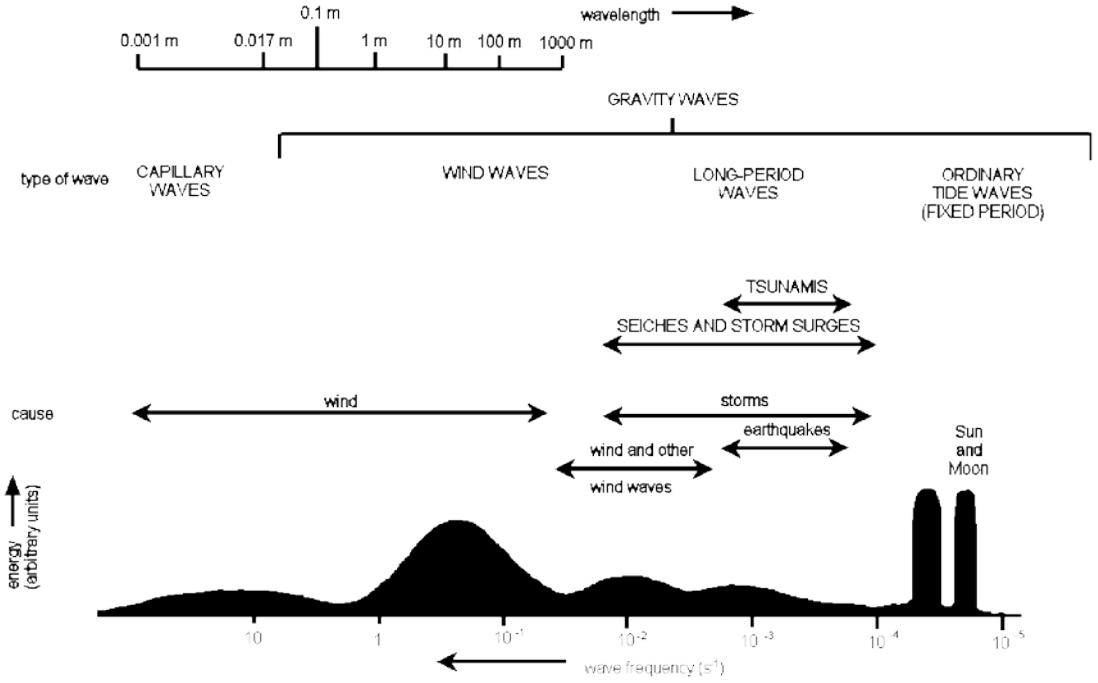

Figure 2-1: Ocean Wave Spectrum

Waves with a shorter period (less than 10 seconds) are known as seas. These tend to be non-symmetrical, are caused by local influences, and tend to dissipate quickly. Longer-period waves are known as swells. These are produced by wind action on the large scale (pressure changes from storms), are relatively symmetrical, and travel great distances from the area where they originate. Collectively, these large motion waves are known as gravity waves.

The first study of a wave system and its component frequencies by [Barber 1948] identified swells with a period of 20 seconds which had travelled over 1500 miles across the North Atlantic, taking 2 days to do so.

For small waves, the hydrodynamic equations are linear and can be modelled as sinusoidal motion [Tucker 1991, Chapter 11]. In a sinusoidal wave train in deep water there is no significant interaction with the seabed, and the water particles travel in circular orbits.

However, the motion is somewhat complex, with wave trains of different frequencies and amplitudes travelling in different directions. Waves of different frequency travel at different speeds; in general, those with lower frequency travel faster and further and transport more energy than higher frequency waves.

*Trochoidal moti*on models the movement water particles in ocean waves better than a sinusoidal model; it allows a small net displacement of water particles in the direction of the wave train. A *trochoid* is the locus of points traced by a fixed point *P* on the radius of a circle that rolls on a straight line without slipping. If the straight line is the x-axis, the circle has radius *B*, and *P* is at a distance *A* from the centre of the circle, then parametric equations for the trochoid are given by $x = B*Z - A\ sin(Z)$ and $y = A\ cos(Z)$ where *Z* is the angle of rotation of the circle. In general, trochoidal waves have sharper peaks and flatter troughs than sinusoidal waves.

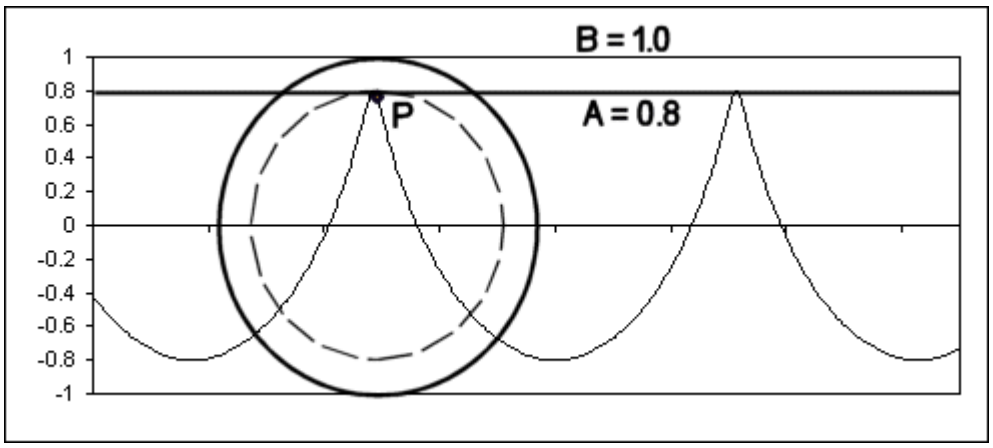

Figure 2-2: Trochoidal Motion: Locus of $x = Z - 0.8\ sin(Z)$ and $y = 0.8\ cos(Z)$

As waves become steeper (the ratio of height to wavelength increases), they tend to become less sinusoidal and more trochoidal. The extreme case is a breaking wave, where the steepness exceeds the ability of the water particles to maintain the surface.

Wave heights follow a Rayleigh probability distribution; about a third of waves are 1.60 times the mean height, and 1% are 2.66 times the mean height.

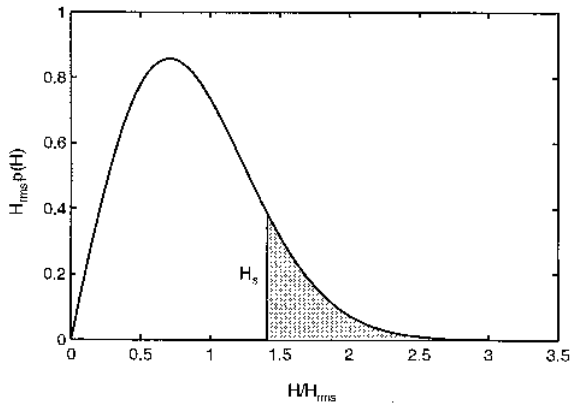

Figure 2-3: The probability function for wave height as defined by the Rayleigh distribution

The range of wave heights varies with latitude and season; highest waves occur in July at about 50°S with one third being over 6m in height. [Young 1999, chapter 3] Extreme waves may reach heights of 27m (South Atlantic, Indian Ocean, TR = 30 years) [Massel 1996, chapter 8]

2.2 Theory of Ocean Waves

Ocean wave theory has been developed since the mid-1800s [Airy 1845; Jeffreys 1924; Jeffreys 1925]. Due to the complexity of the mathematics involved, many simplifying assumptions have been made:

- Water is of constant depth.
- Water is incompressible.
- Viscosity, turbulence, and surface tension have negligible effect.
- Waves have constant wavelength and period.
- Waves have constant form.
- Wave height is small compared to water depth and wavelength.
- No forcing of waves by wind.

Given these assumptions, formulae have been developed to describe the initial formation of waves, and to describe the behaviour of these waves – *Linear Wave Theory*. This predicts sinusoidal motion and consequently assumes that water particles move in closed orbits (there is no net transport of water) and that crest and trough heights are equal (the wave is distributed evenly about the still water level).

For periodic motion, a Fourier series can calculate water surface position as the sum of a number of sine waves:

$$z(t) = \sum_{i=1}^{N} a_i \sin(k_i - 2\pi f_i t + \phi_i)$$

where $z(t)$ represents the surface elevation at time t, and a_i, f_i, and ϕ_i are the amplitude, frequency, and phase of the ith wave in the summation. a_i^2 is related to the energy content of the wave. Although the number of frequencies measured is discrete, as $N \rightarrow \infty$ the amplitude spectrum can be transformed into a continuous spectrum and it is common to describe wave data in this manner.

[Borgman 1977] describes a further extension to the Fourier model to cover wave components propagating in different directions:

$$z(x, y, t) = \sum_{i=1}^{N} a_i \cos[k_i (x \cos\theta_i + y \sin\theta_i) - 2\pi f_i t + \phi_i]$$

where θ_i is the angle between the x axis and direction of propagation of the wave and k_i is the wave number = $2\pi/L_i$

The limitations of Linear Wave Theory have been investigated and attempts to reduce one or more have been made, resulting in *Finite Amplitude Wave Theories*. These theories consider the influence of the wave itself on its own properties – phase speed, wavelength, water surface shape, and other properties are considered to be functions of the actual wave height. These theories can predict peaked crests, and flat troughs and a small net fluid transport, in accordance with trochoidal particle motion.

Gerstner Wave Theory (also called trochoidal wave theory since the elevation profile takes the form of a trochoidal curve) was developed for periodic waves of finite height. The solutions are exact and satisfy continuity as well as the pressure conditions at the water surface, and experimental studies have shown that the theory closely approximates the profiles of real waves on a horizontal bottom. Drawbacks include that mass transport is not predicted, the velocity field is rotational, and the particle movements are opposite to that expected in real waves (and found in other theories) [LeMehaute 1976].

The two most commonly adopted theories are *Stokes' Wave Theory* [Stokes 1847; Stokes 1880; Miche 1944] which is applicable to deep water, and *Cnoidal Wave Theory* [Korteweg and De Vries 1895; Keulegan and Patterson 1940; Wiegel 1960] which is applicable to shallow water. These theories require that waves be of a single period and length.

Water is considered to be 'deep' if the water depth is more than ¼ of the wavelength. In water deeper than this, waves are not significantly affected by interaction with the bottom.

The predictions of both Gerstner and Stokes wave theories agree equally well with measured wave profiles. This is explained by the fact that if the Gerstner wave equations are expanded into a series the first three terms are identical to those in the Stokes solution. This similarity in predictive ability and greater ease of use means that Gerstner wave theory is preferred in many engineering applications.

2.3 Limiting Wave Parameters

In a simple wave, the limiting wave has a sharp angle at the crest of 120° [Bascom 1980]; each side slopes down at 30° to the horizontal. At the crest, the particles are moving forward at exactly the phase speed of the wave. If the wave is any steeper, the particle speed exceeds the wave speed and water particles spill down the front of the wave. For this wave, the downward acceleration of particles at the crest is –0.5G.

However, it has been shown [Longuet-Higgins 1985] using Stokes Wave Theory that the minimum crest acceleration tends towards –0.39G and maximum trough acceleration is +0.30G.

The highest wave has a steepness (height/wavelength ratio) of 1/7 (0.14) [Michell 1893]. The phase velocity (speed) of this wave is 1.2 times that of a low-amplitude wave of the same wavelength.

[Hidy 1971] states that $c = \sqrt{gh}$ for waves with a steepness less than 0.05

Where c = the wave's speed, g = gravitational constant, h = wave height

The minimum speed for gravity waves in water is 0.23 m/sec [Hidy 1971, p131].

The theoretical minimum and maximum frequencies for wind-induced gravity waves are 0.03Hz and 13.6Hz [Massel 1996]

In standing waves, water particles only move vertically; there is no horizontal component. When the downward acceleration at the crest exceeds –1G, water leaves the top of the wave and it breaks. At the limiting height, the water surface angle is 45°. Standing waves are not found in a real wind-formed sea. However, fast-moving storms can produce high wave energies moving in opposite directions. This produces waves similar to standing waves, but with short crest lengths, known as ‘pyramidal waves’.

2.4 Measurement

Historically, human visual observation and estimation has been the standard technique for recording wave information. However, this is subjective and consequently inaccurate and unreliable. People tend to remember extraordinary rather than ordinary waves. Another disadvantage is the need for a human presence; this has resulted in a rather patchy record of wave data.

Many different automated wave measurement techniques have been described [Bascom 1980, Chapter 8; Young 1999, Chapter 9; Massel 1996, Chapter 9; Tucker 1991, Chapter 3-4]. They may be divided into two categories: in situ and remote sensing.

2.4.1 In Situ Instruments

In situ instruments are instruments that are physically located on or in the sea. They may be further categorised as Fixed or Surface Following.

2.4.1.1 Fixed Instruments

These are physically connected to the seabed in some way and measure the motion of the waves as they pass by. Instruments may either pierce the surface and use the difference in properties between air and seawater to determine the location of the water surface, or they may measure the distance to the surface remotely.

2.4.1.1.1 Surface piercing

Early wave recorders were based on the tide gauge invented by Lord Kelvin in 1882. This consisted of a float constrained in a pipe mounted vertically in the sea, and open to it. The float is connected mechanically to a pencil, which draws the record on paper on a chart recorder moving at a constant speed (Figure 2-4).

By varying the size of the opening, the system is ‘tuneable’ to record waves in a desired frequency range. By measuring the difference between a ‘low frequency’ instrument and a ‘high frequency’ instrument, it is possible to remove low frequency (tides, etc) information.

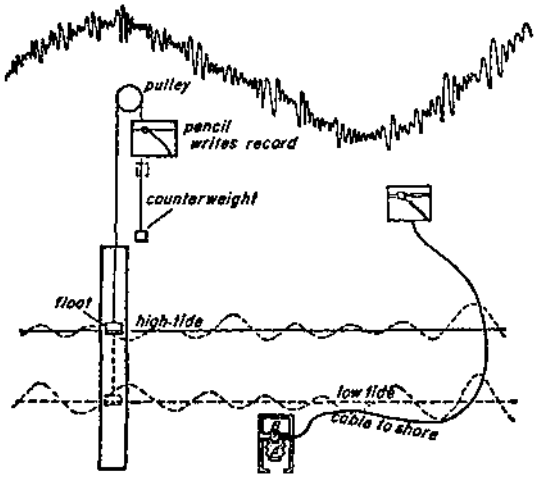

Figure 2-4: Simple Wave recording mechanisms [Bascom 1980, p166]

Electrical variations of this consist of

- Resistive Gauge: A pair of wires of known resistivity is mounted vertically in the water. As the water level rises and falls, it 'shorts' the resistive circuit. The voltage drop will therefore vary depending on the water level. The resistance varies depending on the salinity of the water.
- Wave staff: A series of contacts mounted on a pole. As the water level rises, the contacts are closed by water. The contacts are connected to a series of resistors.
- Capacitance: Water forms the dielectric in a capacitor consisting of two wires or plates mounted vertically in the water. As the water level rises, the capacitance changes. The capacitance is measured, and is proportional to water level.
- Zwarts Pole: A pole is mounted vertically in the water. An electromagnetic wave transmitted down the pole reflects off the water surface, and the time for the signal to return is a direct measure of water surface elevation.

All of these have the disadvantage that they are subject to fouling by marine organisms because they must be at the ocean surface where much biological activity occurs.

2.4.1.1.2 Sub-surface

- The weight of a column of seawater varies with depth of the column. A pressure transducer at the bottom of the sea, measuring this weight, can therefore measure the height of waves as they pass over. However, wave bottom pressure decreases rapidly with depth… at depths greater than $\lambda/2$ they are less than one tenth of the surface pressure. Therefore bottom-mounted sensors are useful in relatively shallow water only. In addition, they have poor HF performance, being useful only for frequencies below 1.2Hz. Movement of sand may cover the sensor, rendering it unreliable or even inoperative.
- An echo-sounder (sonar) may be mounted on the sea floor and look upward to measure the distance to the sea surface. However, when the water aerates during a storm, it will produce inaccurate measurements.

- A horizontal current meter mounted below the surface may measure the orbital motion of water particles. However, measurement of wave direction is difficult.
- In deeper water, a buoy may be anchored to the bottom so that it 'floats' a few metres below the surface. The transducer is mounted on this buoy. However, the effects of currents and tides may move the buoy laterally.
- A submarine or subsurface buoy equipped with a motion-sensing system and an upward-looking echo sounder may be workable.

2.4.1.2 Surface Following

2.4.1.2.1 Buoys

The standard technique is to measure the motion of a buoy on the water surface. The buoy may be a small sphere or platform. Spheres that float just below the surface follow the motion of water particles in a Lagrangian manner. A discus buoy will follow the water surface in an Eulerian manner.

In shallow water, a buoy or boat may use an echo sounder to measure water depth.

Typically, however, an accelerometer is mounted in the buoy in such a way that it remains vertical. By measuring the vertical acceleration, then integrating twice, the surface position can be calculated. Buoys do not follow the wave surface exactly – their response varies with wave frequency. It is necessary to compensate for the response of large buoys [Steele 1993; Tucker 1989; Gnanadesikan 1993].

Buoys may be tethered to the ocean floor to prevent them drifting away. In this case, the buoy's response will also depend on the mooring constraints, current, tides, and wind speed. Alternatively, buoys may be allowed to drift. In this case, the buoy may tend to ride around wave crests rather than over them.

Various brands and models of data buoys are in use. However, the market is dominated by the Waverider, manufactured by Datawell bv, The Netherlands.

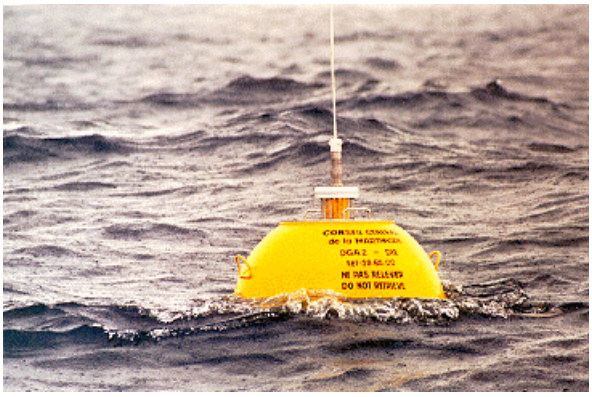

Figure 2-5: Datawell Waverider (Photo Meteo-France)

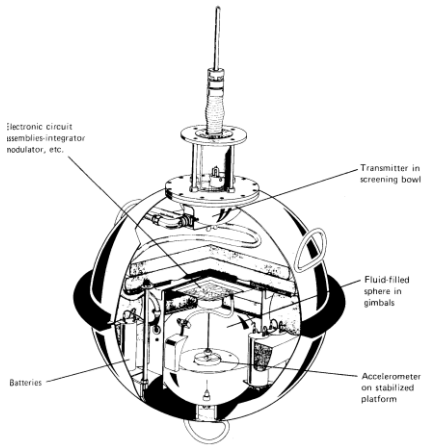

Figure 2-6: Waverider Internals [Tucker 1991]

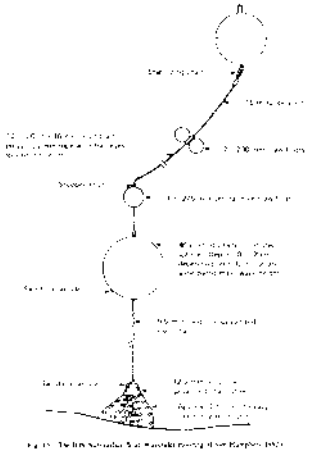

Figure 2-7: Waverider Mooring [Tucker 1991]

This is a buoy of 0.7 or 0.9m diameter. It is tethered to a flexible rubber cord 15m in length. To ensure that the accelerometer remains vertical, the Waverider uses a fluid filled sphere mounted on gimbals. The accelerometer itself is mounted on a horizontal disk, suspended on wires inside the sphere. This arrangement gives a compound pendulum with a natural period of approximately 120 seconds, so that at the 0.04-0.2Hz frequencies (5-25 second periods) typical of ocean waves the accelerometer remains approximately vertical. The accelerometer mounting mechanism is somewhat fragile, being easily damaged by mishandling or steep breaking waves.

Despite having 900N of buoyancy, the Waverider underestimates the highest waves by being dragged through the crests or floating around them [Allender 1989]. [Longuet-Higgins 1986] concluded that it results in slight underestimation of water surface elevation. The buoy's response varies with wavelength – for periods below 1.8 secs (wavelength below 5m) it does not follow the wave's surface. [Tucker 1991] concluded that the motion of the buoy reduces the magnitude of higher frequencies. The response is flat for wave periods of 5-10 secs, and there is some attenuation between 10-25 secs. The buoy samples the accelerometer at 0.3906 second intervals, meaning that the maximum frequency that can be sampled accurately is 1.2801Hz. Maximum wave height is 20m, and the maximum current for deployment is 1m/s. [Datawell Web]

A hybrid approach combining surface-following and 'fixed' sensors may be applied. For example, a pressure sensor may be mounted below the water on a buoy or ship which is relative unresponsive to waves. This may be a large ship, or a buoy that supports a massive damping disk hanging below it [Bascom 1980, p172]. An example described in [Bascom 1980, p150] is FLIP (Floating Laboratory Instrument Platform), which has a heave period of 28 seconds. In a storm with seas up to eighty feet, the platform moved about six inches vertically. To compensate for movement of the platform, its own motions may be measured and combined with the sensor measurements to provide more accurate readings.

2.4.1.2.2 Shipborne Recording

These are somewhat inaccurate by modern standards, but have been widely used. They are a combination of a vertical accelerometer and a pressure sensor, mounted so

that even in the steepest waves they will remain below water level. The accelerometers measure the ship's motion, and the water pressure is added to these measurements to calculate wave height. The vessel must be stationary while wave recording, or Doppler shifts cause problems with calculating wave frequency. The response of the vessel needs to be factored into the wave calculations.

Using a small ship itself as a wave measurement device is considered in [Tucker 1991, section 3.5.2]. He suggests using a triaxial accelerometer to measure the ship's motion, from which vertical acceleration can be derived mathematically and used to calculate vertical displacement. He suggests that this might be successful up to about 0.2Hz.

2.4.2 Remote Sensing

Satellites and aircraft have been used extensively to remotely sense wave information. Both have disadvantages over in situ methods in that they give low-resolution answers; i.e. they give an average reading over a large area (perhaps hundreds of square metres). In addition, a typical satellite orbits once per 100 minutes. Thus events of less than 100 minutes duration may not be recorded at all. A satellite may only overfly the same location once every 17 days.

A radar altimeter is used to remotely sense wave height from a satellite. A radar pulse is beamed vertically downwards, and the shape of the return pulse gives wave height. This technique is relatively inaccurate (± 0.5m or 10%), and low resolution (approximately 10km diameter). This gives wave height only; no period or direction information can be derived.

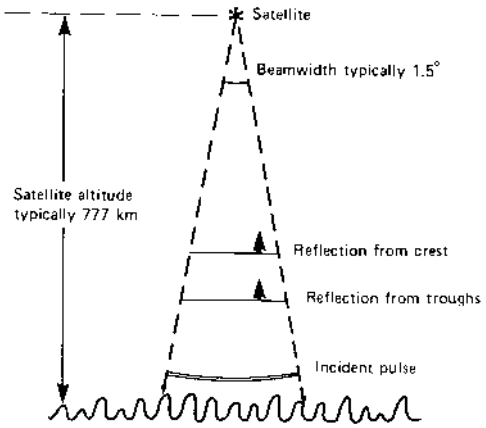

Figure 2-8: Satellite radar altimetry

In a similar approach to the satellite radar altimeter, an aircraft equipped with a laser altimeter can collect wave information. Whilst there may be some low-frequency drift due to the aircraft's movements, this can be removed during data analysis.

2.4.3 Directional Measurement

Measurement of the directional spectrum of a wave field relies on measuring several properties of the waves in that field. Properties that have been used include

- Elevation
- Water velocity
- Surface slope
- Dynamic pressure

Another approach to estimate direction is to employ multiple spatially distributed sensors. Numerous researchers [Barber 1963, Davis 1977, Howell 1993, Krylov 1966, Panicker 1970, Borgman 1977, Krogstad 1988, Nwogu 1989, Young 1994] have used spatial arrays made up of multiple surface piercing or bottom-mounted transducers to make directional measurements of waves. In general, a polygonal arrangement of at least 3 sensors is needed to measure waves in an omnidirectional spectrum. The number and arrangement of sensor elements defines the performance of the array. [Carvalho 2000]

Combined pressure/water velocity gauges may also be used. These instruments are typically bottom-mounted (eg the Woods Hole directional current meter), and measure the water pressure to determine wave height and measure the velocities of water particles in two orthogonal directions [Simpson 1969, Kobune 1986].

In deep water, buoys are used to measure wave directional data. The buoy measures heave (vertical displacement) to determine wave height, and measures pitch and roll to determine the direction of the wave's motion. Whilst there are several manufacturers, by far the most popular heave-pitch-roll buoy is the Datawell Directional Waverider. This buoy uses the same technique as the Waverider to measure vertical motion of the buoy. To determine wave direction, the Directional Waverider is equipped with a magnetic compass and two accelerometers, mounted horizontally and at right angles to each other. From these sensors, it is possible to determine the instantaneous pitch and roll of the buoy, and therefore the slopes of the wave surface in the X and Y directions. [Longuet-Higgins 1962, Ewing 1987, Tucker 1989, Brisette 1994]

Another in-situ approach, which has not had great success, was to use a cloverleaf buoy (Figure 2-9). A cloverleaf buoy consists of three buoys, connected together mechanically such that they can move independently of each other. The relative movement of the parts is then measured and can be used to determine the wave's slope. Effectively a cloverleaf buoy produces the same data as a heave-pitch-roll buoy. [Mitsuyasu 1975]

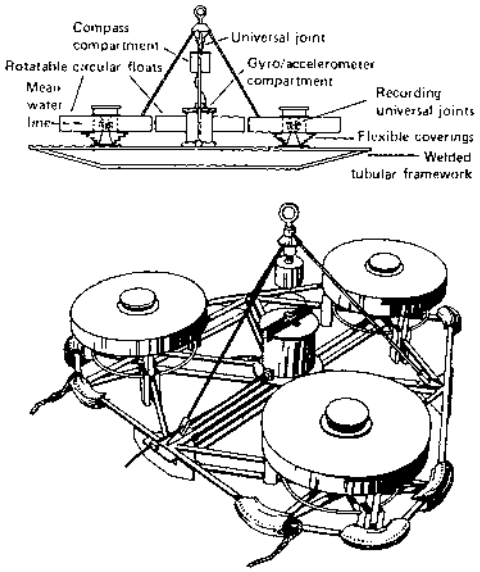

Figure 2-9: Cloverleaf buoy

Various remote-sensing techniques have been used to determine the directional wave spectrum:

- Stereophotogrammetry [Simpson 1969]
- Marine Radar [Young 1985]
- HF Radar [Tyler 1974, Trizna 1977, Trizna 1980]
- Side-looking airborne radar [McLeish 1980, Bascom, p175]
  This has been reported to allow measurement of wavelength (10-50m resolution) and wave direction (2°)
- Synthetic Aperture Radar (SAR) [Beal 1986, Rufenach 1991, Alpers 1981]
  SAR is computationally difficult, but resolution is about 20m, and a 100km wide swath is scanned. In addition, it is possible to derive information about the 2D spectrum from SAR data.

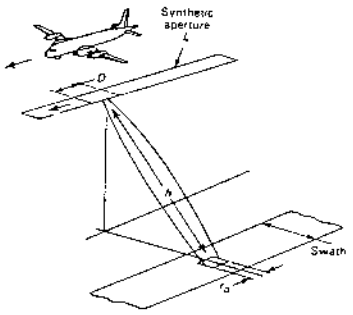

Figure 2-10: Aircraft Synthetic Aperture Radar

2.5 Analysis

Having gathered a time series of wave height and slope information, there are several ways to analyse the data [Massel 1996, p408]:

- Fourier Expansion Method: This assumes a linear wave model (i.e. sinusoidal motion). Fourier series measurement can also be used to represent trochoidal waves, which are another example of periodic motion.
- Maximum Likelihood Method: This is marginally better than the FEM
- Maximum Entropy Method: Autoregressive/FEM based on a probability density distribution. A combined MLM/MEM approach gives better results than MLM
- Bayesian Directional Method: This method is difficult to implement, but very accurate. It is preferred when at least 4 wave properties have been recorded. [Long 1979]

3 This Project

To measure the height and direction of a wave in deep water using a surface-following buoy, it is necessary to determine the vertical displacement and the attitude of the buoy in three dimensions. To do this, the buoy must use either an internal inertial reference platform, or some external reference that is fixed and measurable. There are few suitable external references because, in the waves of the open ocean, there are few features that are motionless. For small boats and buoys, the normal to the local water surface is the direction of the 'apparent vertical'. Therefore gravity cannot be accurately sensed to provide a 'vertical' reference. An apparent 'horizon' (when visible) may not be horizontal.

Therefore, the central problem is how to determine the attitude of the buoy

3.1 Attitude Determination

3.1.1 Sun Sensors

Sun sensors are relatively simple; they are used in virtually all spacecraft to provide an attitude reference. However they are not useful as a sole reference on a terrestrial device. The sun is not visible at night, and may often be obscured during daytime. At low elevations, it may be difficult to separate the sun's image from its reflection off the sea surface.

3.1.2 Gyroscopes

Gyroscopes can be used to produce an inertial reference platform. Typically, they measure the rate of rotation about an axis. This rotation rate can then be integrated to derive the angle of rotation about each axis. If the gyroscope axes are aligned with the three cardinal axes, then this gives the attitude of the platform.

There are four main types of gyroscope:

3.1.2.1 Spinning Mass Gyroscope

Classically, a gyroscope has a mass spinning at a constant rotational velocity mounted on gimbals (a freely movable axis). When the gyroscope is tilted, gyroscopic effect causes precession (a force orthogonal to the direction of tilt) on the gimbals (Figure 3-2). This force is measured to determine the angle moved. Because mechanical constraints cause numerous error factors, the axis is fixed with springs and the spring tension is proportional to the precession speed. The spring tension is integrated to get the angle. An angular velocity (rate of turn) sensor, therefore, is known as a rate-gyroscope.

Spinning mass gyros are fragile, require regular maintenance, and have large energy requirements.

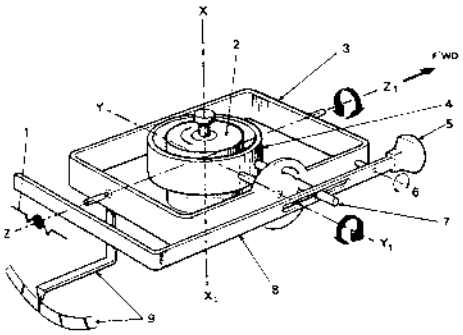

Figure 3-1: Artificial Horizon

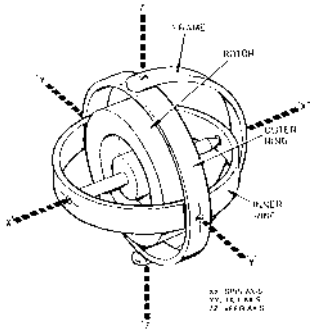

Figure 3-2: Mechanical Gyroscope

3.1.2.2 Optical Gyroscope

A laser beam is passed many times around a fixed path within an enclosure. If the enclosure rotates, the duration from the moment of laser emission to eventual reception will vary. In a Ring Laser Gyroscope, mirrors inside the enclosure form the laser beam path. In a Fibre Optic Gyroscope, a coil of optical-fibre creates the path.

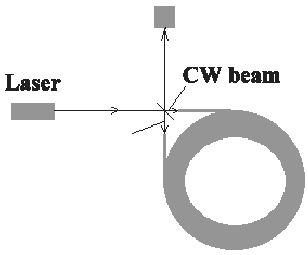

Figure 3-3: Fibre-optic Gyroscope

3.1.2.3 Vibratory Gyroscope

A vibratory gyroscope is comprised of a proof mass mounted on a suspension that allows the proof mass to move in two orthogonal directions. Typically, vibratory gyroscopes are manufactured using micromachining techniques; they are engineered using the same techniques as used to manufacture computer chips.

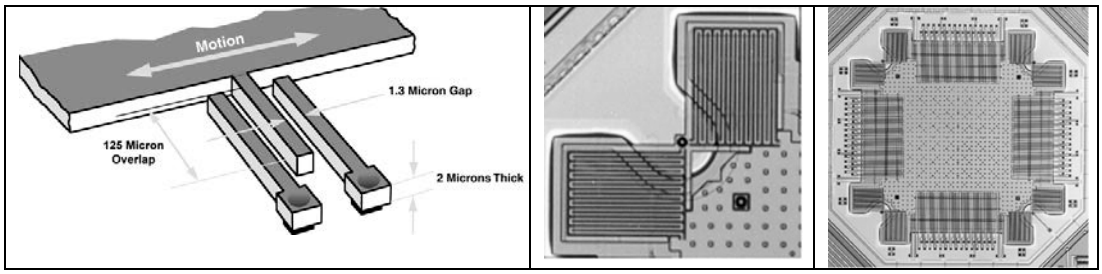

Figure 3-4: Micromachined vibratory gyroscope chip.

Vibratory gyroscopes rely on the generation and detection of Coriolis acceleration. For Coriolis acceleration to be generated, the proof-mass must be in motion. To this end, the proof-mass is electrostatically forced to oscillate in one direction parallel to the chip surface. If the gyroscope chip is rotated about the axis perpendicular to the chip surface, then Coriolis acceleration causes the proof-mass to deflect at right angles. The amplitude of this oscillatory deflection is proportional to rotation rate; capacitive sensing is used to produce a voltage proportional to angular rotation rate.

These devices, whilst being cheap and robust, are prone to drift over a period of time.

3.1.2.4 Gas Rate Gyroscope

A gas rate gyroscope fires a gas jet onto heated wires. When the housing is rotated, the gas that is in motion continues in a straight line, and therefore curves relative to the housing. This in turn causes a change in the temperature of the wires, and therefore their resistance. Numerous factors including fluid mechanics uncertainties and convectional heat transfer prevent the practical usage of gas rate gyroscopes.

3.1.3 GPS Attitude Measurement

The Global Positioning System (GPS) uses a constellation of satellites whose positions in space are known very precisely. Each satellite transmits a coded timing signal; by measuring the time for the signal to travel from the satellite to the receiver, it is possible to calculate the distance between the satellite and receiver. This places the receiver on the surface of a sphere centred on the satellite. Simultaneously measuring distances from four satellites uniquely resolves the location of the receiver.

GPS satellites transmit two timing signals; an encrypted military-only signal (P code), and an unencrypted signal called the Coarse Acquisition (C/A) code. The C/A code is transmitted encoded as CDMA – a pseudo-random bit stream, unique to each satellite. This signal is transmitted every millisecond. Receivers compare the received signal with the known codes, sliding the codes forward/backward in time until one matches with the received signal. The amount of slew needed to create a match is the delay due to the signal's travel time, and used to calculate the receiver's position.

The C/A code bits are about one microsecond long. At the speed of light, this corresponds to a distance of 300 metres. Therefore it is very important to synchronise the receiver very accurately with the received signal. Receivers basing their location on the C/A code can calculate their locations to one or two metres at best.

However, there are numerous errors in the time taken for the signal to travel through the atmosphere. These errors reduce the accuracy of the receiver to about 25 metres or so, depending on conditions. To remove these errors, Differential GPS (DGPS) is used. A base station at a fixed and accurately known location calculates the errors in the times received from each satellite and broadcasts these corrections to the mobile station. If the baseline (the distance between base station and rover) is reasonably short (a few kilometres), the rover can calculate its location to about 1 metre accuracy.

Clearly, using these techniques will not allow the attitude of a buoy to be measured accurately.

Survey-grade GPS instruments can measure locations to centimetre and even millimetre accuracy. They do this by using DGPS to get an approximate location, then using the phase of the carrier frequency (1.575GHz, with a wavelength of about 20cm) to calculate a precise position. However, within the one metre accuracy derived from the C/A code there are possibly 5 or 6 carrier waves. Identifying exactly how many carrier waves there are between the satellite and the receiver is a problem known as "carrier phase ambiguity". Resolving a position using this technique may take 3-5 minutes. [Hofmann-Wellenhof 1994]

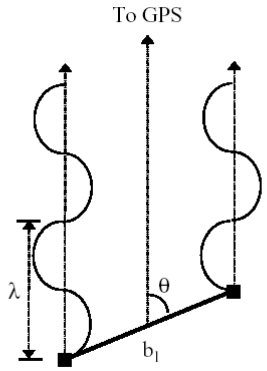

Figure 3-5: GPS Attitude Determination

By using ultra-short baselines (under 0.5 metres), there are a limited number of ambiguities, giving a high level of integrity. However, for ultra-short baseline attitude systems, phase errors translate into larger angular errors than they do in long baseline systems. For precision installation situations antenna phase errors can be as much as 1 cm. In less ideal installations, the antenna phase errors can easily be as much as 2cm. Inertial reference is not required for calibration. [Hayward 1998]

3.1.4 Magnetometers

The Earth's magnetic field has been used as a directional reference for many years. Although it doesn't point due North, the declination (angle between Magnetic North and True North) is well known for all points on the Earth's surface.

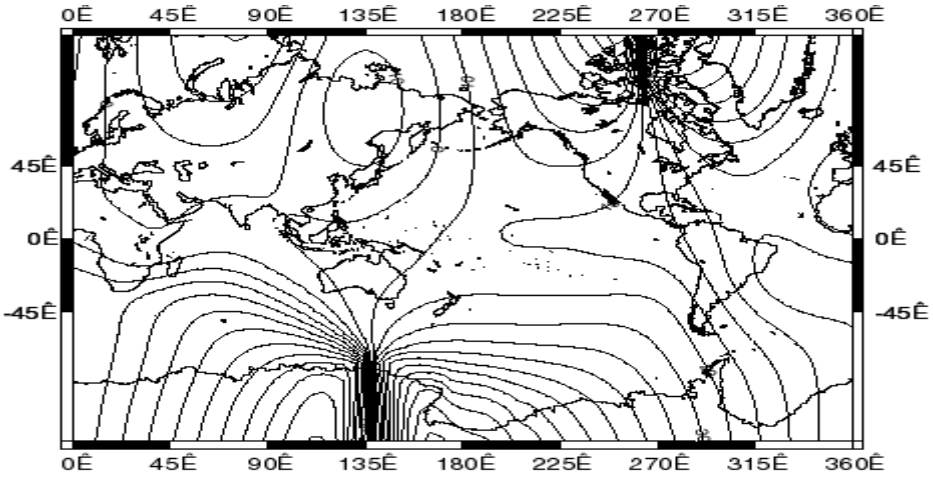

Figure 3-6: Magnetic field declination (1992) [Tauxe Web]

In general, the Earth's magnetic field is not horizontal. Again, this inclination (the angle between the horizontal and the direction of the magnetic field) is well known for various points on the Earth's surface.

Although the Earth's magnetic field direction changes over time, this change is so slow (of the order of less than 1% per year) that it can be considered to be constant for the purposes of this project.

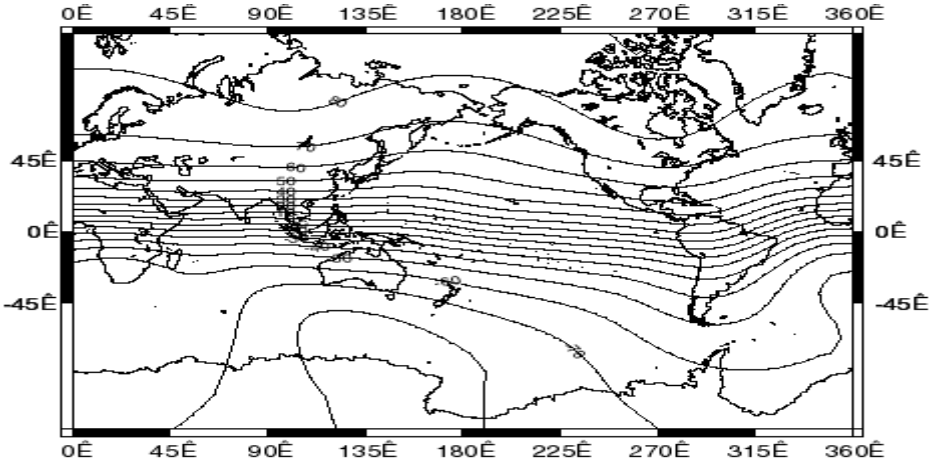

Figure 3-7: Magnetic field inclination (1992) [Tauxe Web]

The International Association of Geomagnetism and Aeronomy (IAGA) International Geomagnetic Reference Field (IGRF) is an empirical model that can be used to calculate the Earth's magnetic field at a particular location, for dates between 1945 and 2005 [Barton 1997]. Therefore, the Earth's magnetic field can be used as a reference vector against which the absolute attitude of the buoy can be measured.

Sensor attitude can be determined by solving what is known as *Wahba's problem*:

> Given two sets of n vectors $\{B_1, B_2, \ldots B_n\}$ (magnetic field as measured by sensors) and $\{M_1, M_2, \ldots M_n\}$ (magnetic field as estimated based on position estimate), find the rotation matrix C which brings the first set into best least-squares coincidence with the second.

Numerous solutions to Wahba's problem have been devised.

However, a simpler solution is possible when the attitude is constrained. Although the single vector of the magnetic field does not provide enough information to fully determine attitude in a fully free 3D environment, [Wang 1993] shows that pitch, roll, and azimuth (heading) can be determined for a discus buoy. This relies on the following assumptions:

- the average pitch and roll angles are zero
- pitch and roll angles are relatively small
- yaw angle varies slowly

If yaw angle varies slowly compared to pitch and roll angles, changes in the measured magnetic field vector may be divided into two parts:

- B_L is the low-frequency (below 0.03Hz) part, due to the buoy's azimuth (yaw) motion
- B_H is the high-frequency part, due to the buoy's tilting (pitch and roll) motion

[Wang 1993] includes corrections for fixed and induced magnetic fields due to the hull of the buoy carrying the sensors. For simplicity, these corrections will be ignored. Then,

$$\sin(A) = -B_{Ly} / B_{Ey}$$
$$\cos(A) = B_{Lx} / B_{Ey}$$

and

$$A = \tan^{-1}(\sin(A)/\cos(A))$$

Since the denominator of both terms is the same (B_{Ey}), it can be cancelled out and the azimuth angle calculated by

$$A = \tan^{-1}(-B_{Ly} / B_{Lx})$$

$$\sin(P) = B_{Hx} / B_{Ez}$$
$$\sin(R) = -B_{Hy} / B_{Ez}$$

Where

A = azimuth angle
P = pitch angle
R = roll angle
B_{Lx} = low frequency part of measured magnetic field (buoy's x axis)
B_{Ly} = low frequency part of measured magnetic field (buoy's y axis)
B_{Hx} = high frequency part of measured magnetic field (buoy's x axis)
B_{Hy} = high frequency part of measured magnetic field (buoy's y axis)
B_{Ey} = Earth's magnetic field intensity (Earth's Y axis (North))
B_{Ez} = Earth's magnetic field intensity (Earth's Z axis (Up))

3.2 Digital Filtering

A filter can be thought of as a "black box" that transforms a set of inputs to a set of outputs. The transformation may involve smoothing, differentiating, integrating, or performing any other convolution of the set of inputs.

An *analog* filter accepts an analog signal and produces an analog output. Both signals are analog functions: continuous in time, and able to take an infinite number of values.

A *digital* filter is a filter that operates on digital signals (ordered sequences of numbers), such as sound, represented inside a computer. The data is discrete, both in time and in value. It is a computation that takes one sequence of numbers (the input signal) and produces a new sequence of numbers (the filtered output signal). A digital filter can do anything that an analog filter can do; that is, any analog filter can be simulated to an arbitrary degree of precision digitally.

Thus, a digital filter is a formula for going from one digital signal to another, typically involving addition, multiplication, and delay operators. A digital filter may exist as a subroutine (software), may be implemented in hardware, or as a combination of both in a Digital Signal Processing (DSP) chip.

There are two types of filters: a *non-recursive filter* (also known as a *Finite Impulse Response* filter) generates its output by weighting only the inputs by coefficients. A *recursive filter* (*Infinite Impulse Response* filter) uses the previous output values in calculating a new output value. A simple example of a recursive digital filter is given by

$$y_n = x_n + y_{n-1}$$

In other words, this filter determines the current output (y_n) by adding the current input (x_n) to the previous output (y_{n-1}).

Linearity means that the output due to a sum of input signals equals the sum of outputs due to each signal alone. *Time-invariance* means that the filter does not change over time. When a filter is both linear and time-invariant, then it is guaranteed to produce a sinusoid in response to a sinusoid, and at the same frequency.

3.2.1 Filter Combinations

Filters may be combined into larger systems. Any filter system can be thought of as combinations of parallel and/or serial digital filters.

For parallel filters, the output is the sum of the outputs of the two parallel filters. For serial filters, the output is the convolution (multiplication) of the outputs of the two serial filters.

3.2.2 Frequency response

This is the most important characteristic of a filter. It is a pair of functions that describe

a) Selective amplification or attenuation of input signals depending on frequency. The ratio of the peak output amplitude to the peak input amplitude is the filter *gain* at this frequency. The frequency response depends on the weighted sums of the coefficients. It is standard practice to describe the attenuation/amplification in decibels.
b) Delay of the output relative to the input. This is known as *phase shift*, and described in terms of angles in radians. The phase shift will always be in the range $-\pi$ to $+\pi$.

Filters can be designed to amplify signals above or below a particular frequency (pass-band) and attenuate signals at other frequencies (stop-band). Filters that attenuate low frequencies are known as high-pass filters, and filters that attenuate high frequencies are known as low-pass filters. By combining a high-pass with a low-pass filter, it is possible to create a band-pass filter. The inverse of a band-pass filter is called a notch filter.

The frequency at which the change from stop-band to pass-band occurs is known as the *corner frequency*. In reality, there is not an instantaneous change from pass-band to stop-band; instead there is a *transition region* where the attenuation changes.

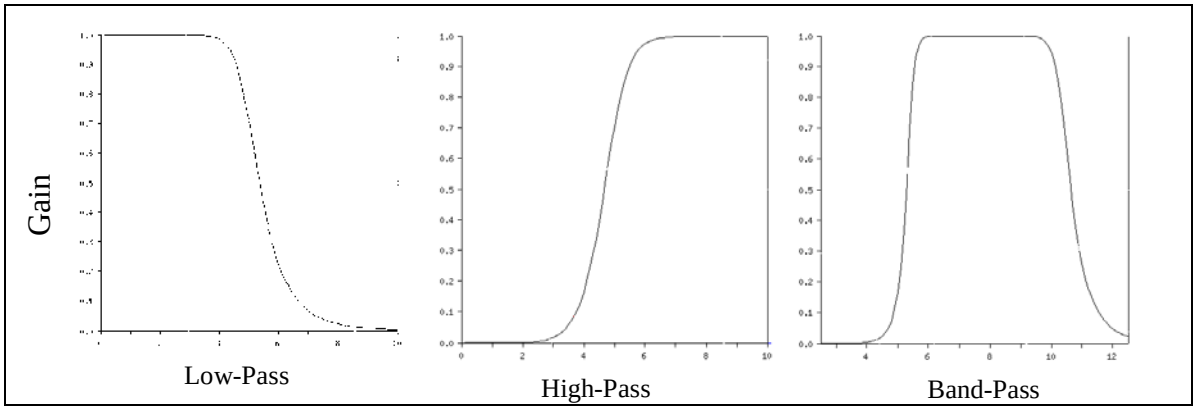

Figure 3-8: Butterworth Filter Frequency Response Curves

3.2.3 Integrating Filters

Integration is the calculation of the area under a curve represented by a series of numbers. For example, given a series of velocity data, distance covered can be calculated. Several integrators are known; all operate well at low frequencies, but they have varying qualities at higher frequencies:

Running sum	$y_k = x_k + y_{k-1}$	High gain at high frequency
Trapezoid rule	$y_k = x_k/2 + x_{k-1}/2 + y_{k-1}$	Low gain at high frequency
Simpson's rule	$y_k = x_k/3 + 4x_{k-1}/3 + x_{k-2}/3 + y_{k-2}$	Best for mid-range frequencies Very bad for high frequencies
3/8 rule	$y_k = 3(x_{k-3} + 3x_{k-2} + 3x_{k-1} + x_k)/8$	Similar to Simpson's rule Better for data with higher-order curvature.

3.2.4 Differentiating Filters

A differentiator is the inverse of an integrator; it calculates the slope of a curve represented by a series of numbers. For example, given a series of distance data, the velocity at each point can be calculated. Both of these differentiators are close to ideal at low frequencies.

a) Difference:
$y_k = x_k - x_{k-1}$

b) Central difference:
$y_k = (x_k - x_{k-2})/2$
Useful for attenuating high-frequency differentials

3.2.5 Common Filters

Three common digital filters are:

3.2.5.1 **Butterworth filter**

This is popular because there are no ripples in the passband or stopband – it is maximally flat. This means that all frequencies in the passband are equally amplified, and all frequencies in the stopband are equally attenuated. The tradeoff for this feature is a relatively wide transition region.

The Butterworth filter has two design parameters: the order of the filter, and the corner frequency. Higher-order filters generate flatter stopbands and passbands and shorter transition regions. See Figure 3-8 for examples).

3.2.5.2 Chebyshev Filter

The Chebyshev filter has a narrower transition region than the same-order Butterworth filter, but has ripples in either the stopband or passband. The Chebyshev filter minimises the height of the maximum ripple. Higher-order filters have more ripples and a shorter transition region.

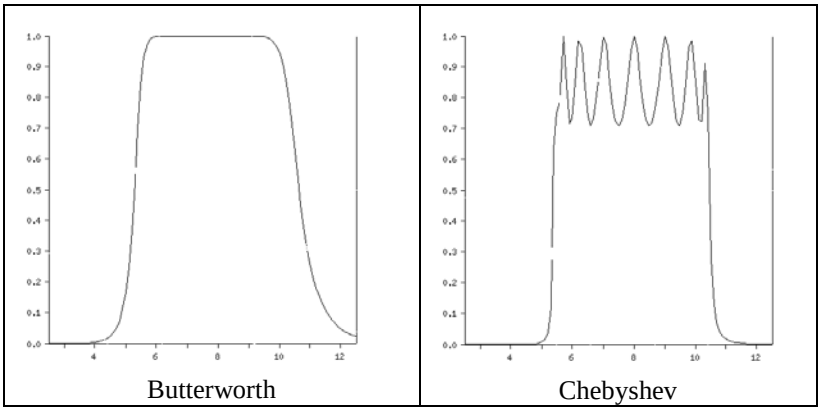

Figure 3-9: Butterworth and Chebyshev Filter Frequency Response Curves

3.2.5.3 Elliptic Filters

An elliptic filter has the narrowest transition region because it allows ripples in both the passband and stopband. The designer specifies the width of transition region.

3.2.6 Filter Design

To perfectly match a desired analog filter's characteristics, an infinite number of coefficients are necessary. For practical purposes, some finite number of coefficients is chosen; this is the *order* of the filter. Higher order means more coefficients, and therefore more processing time, in return for a more precise filter.

Filter design involves complex mathematics (real and imaginary numbers). These can be represented as (x, y) pairs, or as (magnitude, direction) pairs. The *poles* of a filter represent frequencies that are amplified, whilst *zeroes* represent frequencies that are attenuated. These correspond to digital filter coefficients. If a pole's magnitude is greater than one, a filter will be unstable.

One design technique is the "*Impulse Invariant Technique*". In this scheme, a digital filter is designed so that its response to a unit impulse is the same as that of an analog filter. This will result in digital filter whose frequency response being an approximation of the analog filter's frequency response.

There are several Web sites which offer interactive Java applets to calculate coefficients for a filter with specified characteristics (order, filter type, pass- and stop-bands). One such web site is http://www-users.cs.york.ac.uk/~fisher/mkfilter/

For more detail on digital filter theory, see [Rabiner 1975].

3.3 Sampling Rate

Nyquist's Sampling Theorem states that, when sampling a signal at discrete intervals (eg converting from an analog signal to digital), the sampling frequency must be greater than twice the highest frequency of the input signal in order to be able to reconstruct the original perfectly from the sampled version.

Since the frequency range of interest lies between are 0.03Hz and 13.6Hz (see section 2.3: Limiting Wave Parameters), sampling rates need to be greater than 27.2Hz – a sampling interval of 36 milliseconds or smaller.

Higher sampling rates will allow more accurate filtering of data.

If the end user of the data is only interested in waves of lower frequency, then lower sampling rates can be used. For example, if the end user of the data is only interested in swells (waves with a frequency less than 0.1Hz), then a sampling rate as low as 0.2Hz (5sec sampling interval) could be used.

Note that the industry standard Waverider's sampling rate is 2.56Hz.

4 Hardware Implementation

It was decided to implement a solution based on magnetometers and accelerometers. These would be interfaced to a microcontroller that would merge the data streams from the sensors to calculate attitude and motion.

Two buoys, one 0.5m and one 1.0m in diameter, were constructed from polystyrene backed with aluminium, to provide buoyancy, rigidity, and strength. Fins were mounted on the aluminium bottom, to maximise drag so the buoy would move very little relative to the water.

Because of the corrosive nature of seawater, the entire instrumentation package, including battery, microcontroller, and sensors, was mounted in a sealed box on the top of the buoy. This simplified construction and improved protection for the vulnerable instruments, since no wires needed to pass through the waterproof container. The instruments were positioned so that the accelerometers were as close as possible to the centre of mass of the buoy.

Figure 4-1: 0.5m buoy top & underside

A set of 3 accelerometers was mounted mutually at right angles to measure the components of the acceleration vector in each of the buoy's axes. Since the buoy follows the motion of the wave surface, the accelerometer readings give the acceleration of the water particles.

Similarly, a set of 3 magnetometers was mounted mutually at right angles to measure the components of the magnetic field vector in each of the buoy's axes. Since the direction of the field vector is constant, any change in readings relates to a corresponding change in attitude of magnetometers, and therefore of the buoy and accelerometers.

4.1 Magnetometers

4.1.1 Description

The magnetometers selected were FGM-1 and FGM-2 models manufactured by Speake & Co. [Speake Web]

The FGM-series of devices are high sensitivity magnetic field sensors operating in the range of the Earth's magnetic field (±50 microtesla = ±0.5 oersted). The FGM-2 is a single package containing two FGM-1 sensors at right angles to one another.

These sensors are simple, essentially three-terminal devices, operating from a single +5 volt supply, the connections being ground, +5V and output. The output is a robust 5 volt rectangular pulse whose period is directly proportional to the field strength, making it very easy to interface to a microprocessor.

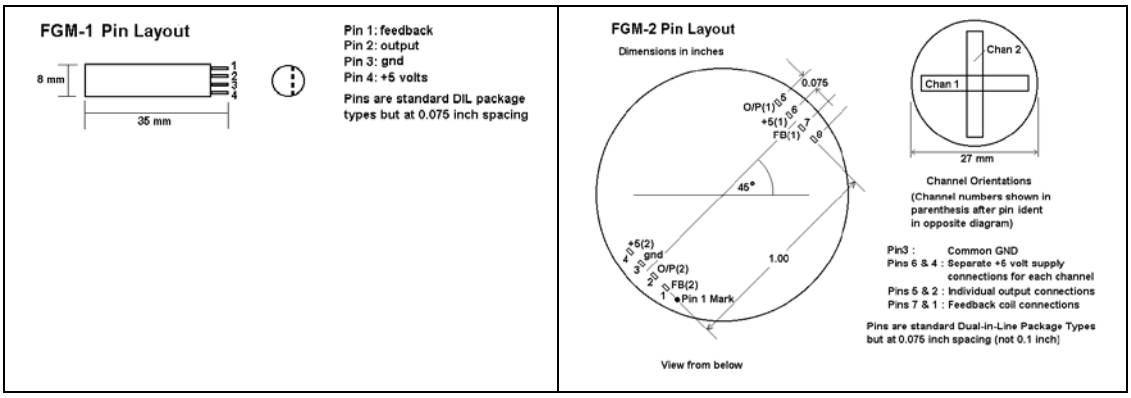

Figure 4-2: FGM-1 and FGM-2 layout

Unlike Hall Effect field sensors which are sensitive to temperature, the FGM-series sensors have a very low temperature coefficient.

4.1.2 Microcontroller Interface

The FGM-1 and –2 series magnetometers output frequency-modulated (FM) signals in the range 50 – 100 kHz (periods ranging from 10μs to 20μs). Since the lowest effective Nyquist sampling rate is ~50 kHz, appropriate filtering can provide an AC field bandwidth from DC to ~25kHz.

If this signal was fed directly into a microcontroller, it would generate one interrupt for each cycle. This would be an overpowering load for all but the most powerful microcontrollers. Given that the rate of attitude change on an ocean wave is relatively slow, this responsiveness is not required. Therefore each of the signals from the magnetometers is divided by 2048. As well as reducing interrupt frequency to a manageable level, this also effectively averages the signal from the magnetometer over a longer period of time, reducing quantisation noise and the effect of transients.

4.1.3 Calibration algorithm

The FGM-series sensor has an output in the form of a large rectangular pulse whose period is approximately proportional to the external magnetic field along its principal axis.

The FGM sensors are generally stable enough for orientation purposes without continuous recalibration if supplied from a stable voltage source. Calibration is required:

- To overcome the effects of drift from any potential source (for example, in the power supply voltage).
- To correct for variations in the Earth's magnetic field. Strength varies from place to place on the Earth's surface.
- Because no two sensors are alike.

Continuous autocalibration is possible when three orthogonal sensors are used to determine the alignment of the earth's field with respect to their axes. The calibration can be carried out at whatever intervals are considered appropriate to maintain a suitable compromise of stability and speed of data acquisition.

4.1.3.1 Linearisation

The calibration technique presented below depends on a linear relationship between field strength and sensor output period. However, the sensor's output period is not linear relative to the observed field. The manufacturers recommend adding a constant frequency of 18 kHz to the incoming frequency, so that over the range of the Earth's field (-0.5 to +0.5 oersted) the slope is close to linear. Figure 4-3 shows a plot of T' = T/(1+cT), c=18 kHz vs Field for a typical sensor.

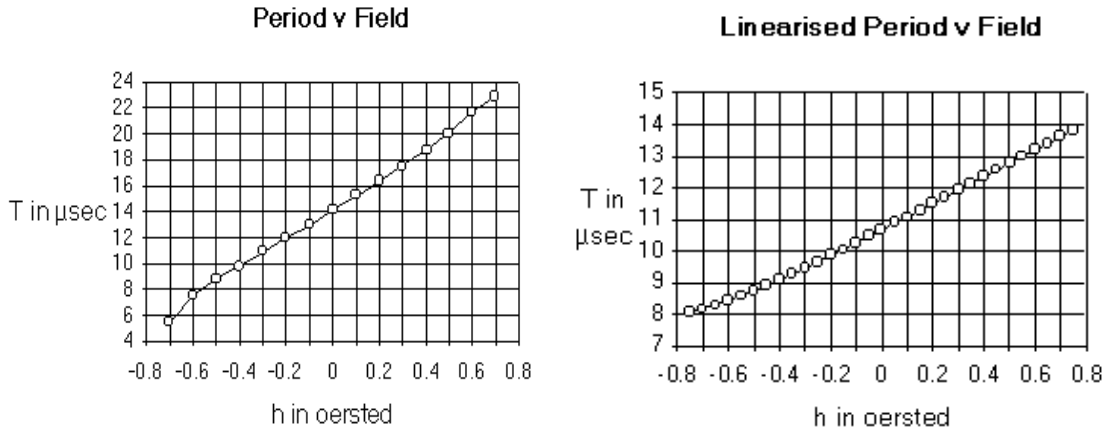

Figure 4-3: Raw and Linearised Periods v Magnetic Field

A further improvement in linearity can be obtained by making use of the built-in overwound coil intended for feedback systems. For perfect linearisation, the response of the sensor to known magnetic fields could be measured, and used to correct the reading obtained from the sensor.

4.1.3.2 Calibration

Since the output cannot have a negative period, there must be a zero-field period in the form of a zero-offset large enough to accommodate negative values of magnetic field.

Therefore there are two unknown parameters associated with each sensor

- the slope of the relationship between period and magnetic field (*sensitivity*)
- the period corresponding to zero magnetic field (*zero-offset*)

Both these parameters need to be taken into account, when using sensor combinations to determine orientation information using the Earth's field.

The other requirement for this type of calibration is that several separate readings are taken. This is easily accomplished if the sensor platform is in continuous or intermittent motion. If this is the case it is possible to continuously determine and update the values of the three sensitivities and the three zero-offsets, using the readings taken in normal operation.

The fundamental principle behind the method is the fact that the Earth's field can be regarded as fixed in both magnitude and orientation and the sum of the squares of the orthogonal field components will therefore remain constant regardless of the orientation of the platform. If the field components are $\mathbf{h_x}$, $\mathbf{h_y}$ and $\mathbf{h_z}$ then the field strength **h** can be calculated by:

$$h_x^2 + h_y^2 + h_z^2 = h^2 \qquad (1)$$

Any variation of the measured values from this relationship indicates one or more incorrect zero-offset and/or sensitivity values. Indeed, the variation of the measured readings from this relationship can be used to calculate the required corrections.

It should be noted that any errors observed in the calibration are due to uncorrected nonlinearity in the sensor's outputs and the limited precision used in the calculation of the calibration. The algorithm itself is precise when fed with precise input values.

4.1.3.3 Three dimensional calibration method

For an earth field vector, **h,** having orthogonal components $\mathbf{h_x}$, $\mathbf{h_y}$ and $\mathbf{h_z}$ in the planes of the sensor axes, assume the sensors give output periods of $\mathbf{t_x}$, $\mathbf{t_y}$, and $\mathbf{t_z}$.

If the sensors have differing sensitivities, $\mathbf{s_x}$, $\mathbf{s_y}$ and $\mathbf{s_z}$ and differing zero-offset periods, $\mathbf{t_{x0}}$, $\mathbf{t_{y0}}$, and $\mathbf{t_{z0}}$, such that:

$$t_x = s_x.h_x + t_{x0} \qquad (2)$$
$$t_y = s_y.h_y + t_{y0} \qquad (3)$$
$$t_z = s_z.h_z + t_{z0} \qquad (4)$$

The above equations can be rewritten as:

$$(t_x - t_{x0}) / s_x = h_x \qquad (5)$$
$$(t_y - t_{y0}) / s_y = h_y \qquad (6)$$
$$(t_z - t_{z0}) / s_z = h_z \qquad (7)$$

Substituting these into equation (1) we obtain:

$$(t_x - t_{x0})^2/ s_x^2 + (t_y - t_{y0})^2/ s_y^2 + (t_z - t_{z0})^2/ s_z^2 = h^2 \quad (8)$$

If the field magnitude is defined to be in the range 0 – 1 of some arbitrary units, this effectively converts the field components into their direction cosines, independent of the field magnitude. All components must also be in the range 0 – 1. Note that the $\mathbf{h^2}$ term (a constant) disappears from the equation as a result of this operation; the absolute magnitude of the field is not needed to determine orientation.

$$(t_x - t_{x0})^2/ s_x^2 + (t_y - t_{y0})^2/ s_y^2 + (t_z - t_{z0})^2/ s_z^2 = 1 \quad (9)$$

Multiplying equation (9) through by $\mathbf{s_x^2}$ will yield:

$$(t_x - t_{x0})^2 + (t_y - t_{y0})^2 s_x^2/ s_y^2 + (t_z - t_{z0})^2 s_x^2/ s_z^2 = s_x^2 \quad (10)$$

Now, substituting $\mathbf{Q = s_x^2 / s_y^2}$ and $\mathbf{R = s_x^2 / s_z^2}$ yields:

$$(t_x - t_{x0})^2 + Q(t_y - t_{y0})^2 + R(t_z - t_{z0})^2 = s_x^2 \quad (11)$$

This is the equation, in $\mathbf{t_x}$, $\mathbf{t_y}$ and $\mathbf{t_z}$ of an ellipsoid with centre located at ($\mathbf{t_{x0}, t_{y0}, t_{z0}}$), having principal axes $\mathbf{s_x}$, $\mathbf{s_y}$ and $\mathbf{s_z}$.

All measured triples of sensor readings, $\mathbf{t_x}$, $\mathbf{t_y}$ and $\mathbf{t_z}$, **must** lie on this ellipsoid and hence, given sufficient resolution, any six different points are sufficient to define the ellipsoid completely.

It is therefore possible to deduce the centre, ($\mathbf{t_{x0}, t_{y0}, t_{z0}}$) and the principal axes, $\mathbf{s_x}$, $\mathbf{s_y}$ and $\mathbf{s_z}$ from any six different triples of sensor readings.

If the six points are denoted by ($\mathbf{t_{xi}, t_{yi}, t_{zi}}$), i = 1,2,3,4,5,6 then six equations of type (11) above are available, having the typical form:

$$(t_{xi} - t_{x0})^2 + Q(t_{yi} - t_{y0})^2 + R(t_{zi} - t_{z0})^2 = s_x^2 \quad (12)$$

Subtracting these from one another successively will yield five equations of the typical form:

$$((t_{xi} - t_{x0})^2 - (t_{xi+1} - t_{x0})^2) + Q((t_{yi} - t_{y0})^2 - (t_{yi+1} - t_{y0})^2) + R((t_{zi} - t_{z0})^2 - (t_{zi+1} - t_{z0})^2) = 0 \quad (13)$$

Expanding, we get:

$$(t_{xi}^2 - 2t_{xi}t_{x0} + t_{x0}^2) - (t_{xi+1}^2 - 2t_{xi+1}t_{x0} + t_{x0}^2) + Q((t_{yi}^2 - 2t_{yi}t_{y0} + t_{y0}^2) - (t_{yi+1}^2 - 2t_{yi+1}t_{y0} + t_{y0}^2)) + R((t_{zi}^2 - 2t_{zi}t_{z0} + t_{z0}^2) - (t_{zi+1}^2 - 2t_{zi+1}t_{x0} + t_{z0}^2)) = 0 \quad (14)$$

Collecting like terms:

$$(t_{xi}^2 - t_{xi+1}^2 - 2t_{xi}t_{x0} + 2t_{xi+1}t_{x0} + t_{x0}^2 - t_{x0}^2) + Q(t_{yi}^2 - t_{yi+1}^2 - 2t_{yi}t_{y0} + 2t_{yi+1}t_{y0} + t_{y0}^2 - t_{y0}^2) + R(t_{zi}^2 - t_{zi+1}^2 - 2t_{zi}t_{z0} + 2t_{zi+1}t_{z0} + t_{z0}^2 - t_{z0}^2) = 0 \quad (15)$$

$$(t_{xi}^2 - t_{xi+1}^2) - 2t_{x0}(t_{xi} - t_{xi+1}) + Q((t_{yi}^2 - t_{yi+1}^2) - 2t_{y0}(t_{yi} - t_{yi+1})) + R((t_{zi}^2 - t_{zi+1}^2) - 2t_{z0}(t_{zi} - t_{zi+1})) = 0 \quad (16)$$

Substituting

$$a_i = 2(t_{xi} - t_{xi+1})$$
$$b_i = 2(t_{yi} - t_{yi+1})$$
$$c_i = 2(t_{zi} - t_{zi+1})$$
$$d_i = -(t_{yi}^2 - t_{yi+1}^2)$$
$$e_i = -(t_{zi}^2 - t_{zi+1}^2)$$
$$f_i = (t_{xi}^2 - t_{xi+1}^2)$$

into equation (16) will yield five equations of the form:

$$f_i - a_i t_{x0} + Q(-d_i - b_i t_{y0}) + R(-e_i - c_i t_{z0}) = 0 \qquad i = 1,2,3,4,5 \quad (17)$$

Rearranging:

$$f_i - a_i t_{x0} - d_i Q - b_i (Q t_{y0}) - e_i R - c_i (R t_{z0}) = 0$$

$$a_i t_{x0} + b_i (Q t_{y0}) + c_i (R t_{z0}) + d_i Q + e_i R = f_i \qquad i = 1,2,3,4,5 \quad (18)$$

These five equations are linear in $\mathbf{t_{x0}}$, ($\mathbf{Qt_{y0}}$), ($\mathbf{Rt_{z0}}$), **Q**, and **R** and are therefore soluble for these values, using the Gaussian elimination method of solving simultaneous linear equations.

If the set of data points being used for the calibration are not sufficiently different from each other, then two or more of these equations will also be very similar. If they are too similar (where "too similar" depends on the resolution and accuracy of the data reading), this set of equations will be ill-conditioned, and Gaussian elimination will fail to provide a solution, or will provide an incorrect solution. In any case, there will be errors inherent in the calibration. To minimise these, the outputs from the calibration routine are passed through low-pass filters. Selection of data points for calibrating is covered in more detail in section 4.1.3.3.1 below.

This will immediately provide the values of $\mathbf{t_{x0}}$, **Q**, and **R**. By dividing ($\mathbf{Qt_{y0}}$) and ($\mathbf{Rt_{z0}}$) by **Q** and **R** respectively, the values of $\mathbf{t_{y0}}$ and $\mathbf{t_{z0}}$ can also be easily determined.

Finally, applying the last of the type (12) equations, viz.

$$(t_{x6} - t_{x0})^2 + Q(t_{y6} - t_{y0})^2 + R(t_{z6} - t_{z0})^2 = s_x^2 \quad (19)$$

can be solved for $\mathbf{s_x}$ and hence $\mathbf{s_y}$ and $\mathbf{s_z}$ calculated by dividing $\mathbf{s_x^2}$ by **Q** and **R**.

This gives the required sensitivities and zero offsets of the individual sensors, which can now be used to correct the incoming readings to give valid direction cosines for the orientation calculations, as follows:

By inserting the calculated the sensitivity and offset values into equations (5)-(7) along with the values of a triple of readings, ($\mathbf{t_x, t_y, t_z}$) :

$$h_x = (t_x - t_{x0}) / s_x$$
$$h_y = (t_y - t_{y0}) / s_y$$
$$h_z = (t_z - t_{z0}) / s_z$$

the corrected values of the magnetic field components can be calculated.

4.1.3.3.1 Calibration Point Selection

Although, mathematically, any six points will provide a solution, the precision of calculation with measurements of finite accuracy will be adversely affected if the points are very close together. This is not usually a problem with orientation systems that are in constant motion and the algorithm is designed to wait until it has collected sufficiently different inputs before proceeding to calculate.

However, if there is little motion about one axis (eg, when all waves are coming from the same direction) then the attitude of the buoy will follow an arc. In this case, the data points in will not be well-distributed in the hemisphere of possible attitudes.

Furthermore, if the 6 data points to be used for calibration are close together in time, it is likely that they will also be similar in attitude. Therefore the points selected should be reasonably well distributed in time.

The calibration point selection algorithm compares the raw readings received with fixed readings for 6 predetermined attitudes; perfectly upright, and 5 points corresponding to a 90° tilt to points spread equally around the horizon (ie, at 72° intervals). Points nearest to these ‘target’ attitudes are chosen... if a new data point is closer to a target point than any previously selected point, then it replaces one of the selected points, and an attempt is made to calculate calibration settings. When a successful calibration occurs, the 6 points used are discarded and the process begins again.

To avoid an expensive floating point calculation that is likely to fail, the 6 points must be a reasonable distance apart before the calculation will start.

To avoid a single erroneous reading from remaining in the calibration points set, each point is ‘aged out’... if it has been a long time and no successful calibration has occurred, the oldest point in the set is discarded and the process resumes with the next data point.

Similarly, to attempt calibrations when the sea state is relatively calm, or waves are very mono-directional, as time goes by the ‘reasonable distance apart’ required for a calibration attempt is reduced. Conversely, a failed calibration attempt will increase

this parameter so that excessive CPU time is not wasted making calibration attempts which are unlikely to succeed.

If more than six points are collected, the system is over-determined and calibration of the magnetometers becomes a minimisation problem, searching for values for the centre and axes of the ellipsoid that minimise the errors in the calculation.

4.2 Accelerometers

4.2.1 General Description

The ADXL202E is a low-cost, low-power, complete 2-axis accelerometer with digital outputs on a single monolithic IC. It will measure positive and negative accelerations with a full-scale range of ±2 G. Signals below 2mG can be resolved. The ADXL202E can measure both dynamic acceleration (eg vibration) and static acceleration (eg gravity). It outputs both analog voltages and digital signals whose duty cycles (ratio of pulse width to period) are proportional to acceleration. The duty cycle outputs can be directly measured by a microcontroller counter.

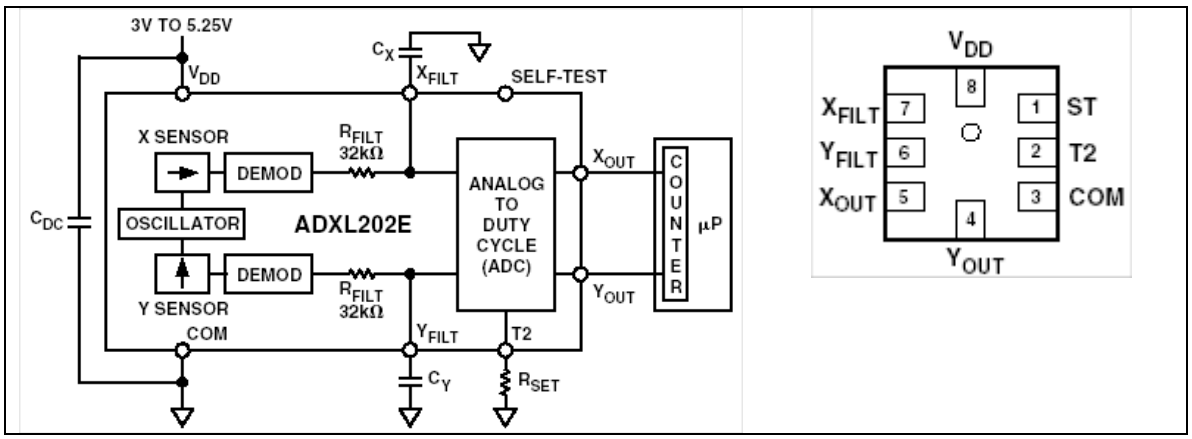

Figure 4-4: ADXL202E accelerometer block diagram and pinout

The bandwidth of the accelerometer is set with capacitors C_X and C_Y at the X_{FILT} and Y_{FILT} pins.

The output of the accelerometer is a digital signal whose duty cycle varies with acceleration. The period of the signal (T2) is approximately constant, being set via a resistor (R_{SET}) to a time between 0.5 ms and 10 ms). The width of the 'on' part of the cycle (T1) varies with acceleration. Thus the duty cycle (the Ratio of "on" time (T1) to the total cycle time (T2) ie T1/T2) varies with acceleration. [Analog Web].

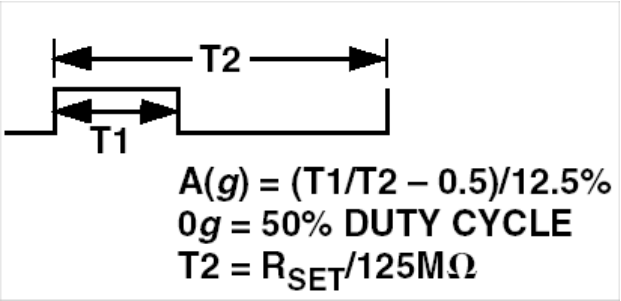

Figure 4-5: Typical Accelerometer Output Duty Cycle

4.2.2 Theory of Operation

The ADXL202E contains a polysilicon surface micromachined sensor (MEMS) structure built on top of a silicon wafer. Polysilicon springs suspend the structure over the surface of the wafer and provide a resistance against acceleration forces. Deflection of the structure is measured using a differential capacitor that consists of independent fixed plates and central plates attached to the moving mass. The fixed plates are driven by 180° out-of-phase square waves. An acceleration will deflect the beam and unbalance the differential capacitor, resulting in an output square wave whose amplitude is proportional to acceleration. Phase sensitive demodulation techniques are then used to rectify the signal and determine the direction of the acceleration.

The output of the demodulator drives a duty cycle modulator (DCM) stage through a 32 kΩ resistor. At this point a pin is available on each channel to allow the user to set the signal bandwidth of the device by adding a capacitor. This filtering improves measurement resolution and helps prevent aliasing.

After being low-pass filtered, the analog signal is converted to a duty cycle modulated signal by the DCM stage. A 0G acceleration produces a nominally 50% duty cycle. The acceleration signal can be determined by measuring the length of T1 and T2.

4.2.3 Microcontroller Interface

The ADXL202E is specifically designed to work with low-cost microcontrollers. This section will outline a general design procedure and discuss the various trade-offs that need to be considered.

4.2.3.1 Filters: The Noise/Bandwidth Trade-Off

The accelerometer bandwidth selected determines the measurement resolution (smallest detectable acceleration). Filtering is used to lower the noise floor and improve the resolution of the accelerometer. Resolution is dependent on both the analog filter bandwidth at X_{FILT} and Y_{FILT} and on the speed of the microcontroller counter.

The analog output of the ADXL202E has a typical bandwidth of 5 kHz, while the duty cycle modulators' bandwidth is 500 Hz. A filter at this point limits. To minimise DCM errors the analog bandwidth should be less than 1/10 the DCM frequency. A table in the ADXL202E datasheet lists values of the X_{FILT} and Y_{FILT} capacitors and the corresponding bandwidth; values of 0.1μF were used, giving a bandwidth of 50Hz.

4.2.3.2 Counter Frequency and Resolution

The second determinant of accelerometer resolution relates to the measurement resolution of the counter when decoding the duty cycle output.

The ADXL202E's duty cycle converter has a resolution of approximately 14 bits; better resolution than the accelerometer itself. The actual resolution of the acceleration signal is, however, limited by the time resolution of the counting devices used to decode the duty cycle. The faster the counter clock, the higher the resolution of the duty cycle and the shorter the T2 period can be for a given resolution. The accelerometer's noise floor sets the lower limit on the resolution.

In this application, the T2 period has been set to the maximum value of 10ms. The counter clock used is set to 500 kHz giving 5000 counts per T2 cycle, and consequently an average 625 counts/G and a resolution of 1.6mG.

4.2.3.3 Power Saving

It is possible to reduce the ADXL202E's average current from 0.6mA to less than 20μA by using the following techniques:

1. Power Cycle the accelerometer.

   Depending on the value of the filter capacitors, the ADXL202E is capable of turning on and giving a good reading in 1.6ms.

2. Power Cycling When Using the Digital Output

   An alternative is to run the microcontroller at a higher clock rate and shut it down between readings. Tthe ADXL202E should be set at its fastest sample rate (T2 = 0.5 ms), with a 500 Hz filter, acquiring a reading as quickly as possible and then shut down the ADXL202E and the microcontroller until the next sample is needed.

In either of the above approaches, the ADXL202E can be turned on and off directly using a digital port pin on the microcontroller to power the accelerometer without additional components.

4.2.4 Calibrating the ADXL202E

The initial value of the offset and scale factor for the ADXL202E will require calibration. These calibrations take place in the software of the microcontroller used to decode the duty cycle signal. Calibration factors can be stored in non-volatile memory.

The force of gravity is the most stable, accurate and convenient acceleration reference available. To calibrate, the accelerometer's measurement axis is pointed directly at the earth. The 1G reading is saved and the sensor is turned 180° to measure –1G. The sensitivity can be determined by the two measurements.

Using the two readings:
Let A = Accelerometer output with axis oriented to +1G
Let B = Accelerometer output with axis oriented to –1G
Then:

Sensitivity = (A – *B)*/2G
Zero-G Offset = (A + B)/2 G

For example, if the +1G reading (A) is 55% duty cycle and the –1G reading (B) is 32% duty cycle, then:
Sensitivity = (55% – 32%)/2G = 11.5%/G
Zero-G Offset = (55% + 32%)/2G = 43.5%

This calibration technique is not particularly useful on a buoy; because the buoy is in an accelerating environment, a reading due the force of gravity alone cannot be made. However, over a long time, the average attitude of the buoy will be vertical, with no

horizontal acceleration. Therefore, by applying low-pass filters to the accelerometer readings, these readings can at least be determined.

4.3 Microcontroller

Desirable features:

- three timer/counters suitable for reading FM inputs (magnetometers)
- three timer/counters suitable for reading DCM inputs (accelerometers)
- low power usage
- fast processor
- non-volatile memory for data storage
- development environment including
  - efficient high-level language
  - debugging and diagnostic software
  - hardware interfacing
- serial I/O interface
- Flash memory for program storage

Given the accelerometers and magnetometers both provide variations of pulse-width modulated output signals, there is no requirement for the microcontroller to be able to process analog signals.

4.3.1 Mitsubishi M16C/62 Features

The M16C/62 single-chip microcontroller is a CMOS processor packaged in a 100-pin plastic moulded QFP. It has a sophisticated instruction set, with many instructions executing in a single cycle. It features a built-in multiplier, making it ideal for high-speed processing applications. With 1MB of address space, there is plenty of room for large programs or data storage.

The Mitsubishi M16C/62 microcontroller has all of the desirable features listed above available on a single IC:

- six timer/counters suitable for reading frequency or duty cycle modulated inputs
- 175mW typical power usage, with low-power modes also available
- 16MHz processor (62.5ns cycle time)
- 256KB of flash memory which can be used for program or data storage
- up to 4 serial I/O interfaces
- development environment including
  - efficient C compiler and assembler
  - remote debugger and monitor
- a development platform is available which brings all the CPU pins to a 96-pin connector

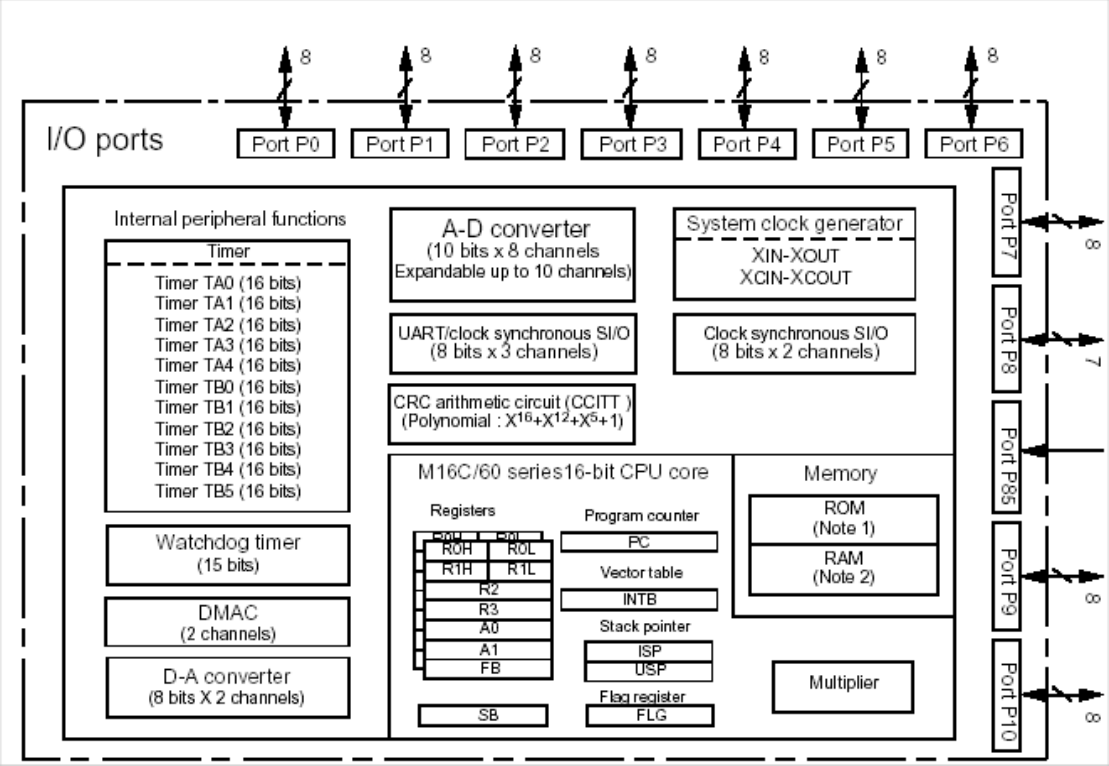

Figure 4-6: M16C/62 block diagram

4.3.2 Timers

The M16C has eleven 16-bit timers. The timers are classified into two types:

- Output timers, known as timers A0 – A4. These include an output pin which is automatically controlled by the timer when it overflows.
- Input timers, known as timers B0 – B5

The count source of each timer may be programmed individually, and selected from

- f1 (the CPU's clock (16MHz))
- f8 (the CPU clock divided by 8 (2MHz))
- f32 (CPU clock divided by 32 (500kHz))
- fC32 (CPU secondary clock divided by 32).

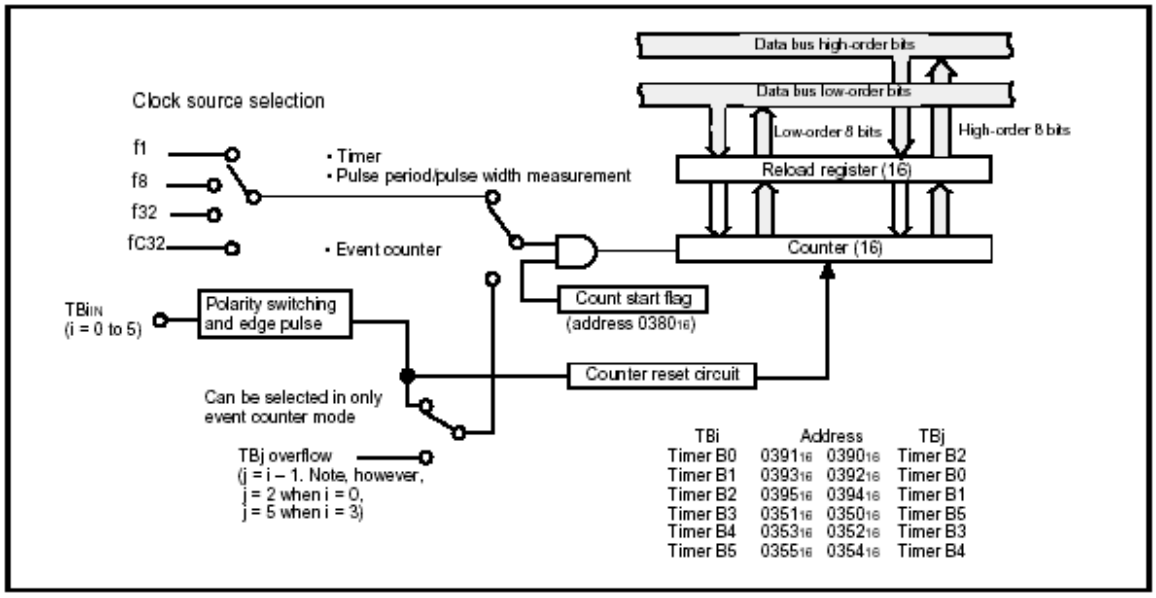

Figure 4-7: Timer B block diagram

Each TimerB can be individually programmed to measure the pulse period or pulse width of an external signal. It does this by counting pulses from an internal source, and transferring the count to the “Reload” buffer register on external rising or falling edges. At this point, the count register is also reset to zero, and an interrupt generated.

With a 5V supply, the high and low parts of a cycle must both be at least 200ns long.

For period measurement, either rising or falling edges may be used to trigger the transfer (Figure 4-8).

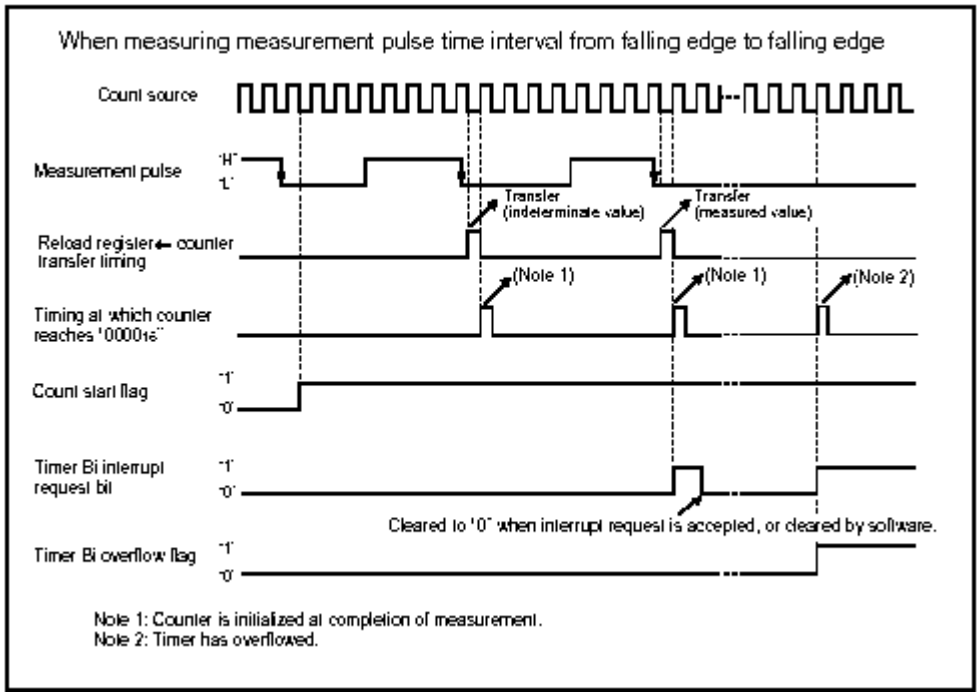

Figure 4-8: Period measurement with Timer B

For pulse width measurement, both rising and falling edges trigger transfers (Figure 4-9). An interrupt service routine must distinguish between a rising or falling edge by checking the state of the external input. To measure pulses of long duration, a counter overflow may cause an interrupt and the overflows counted in software.

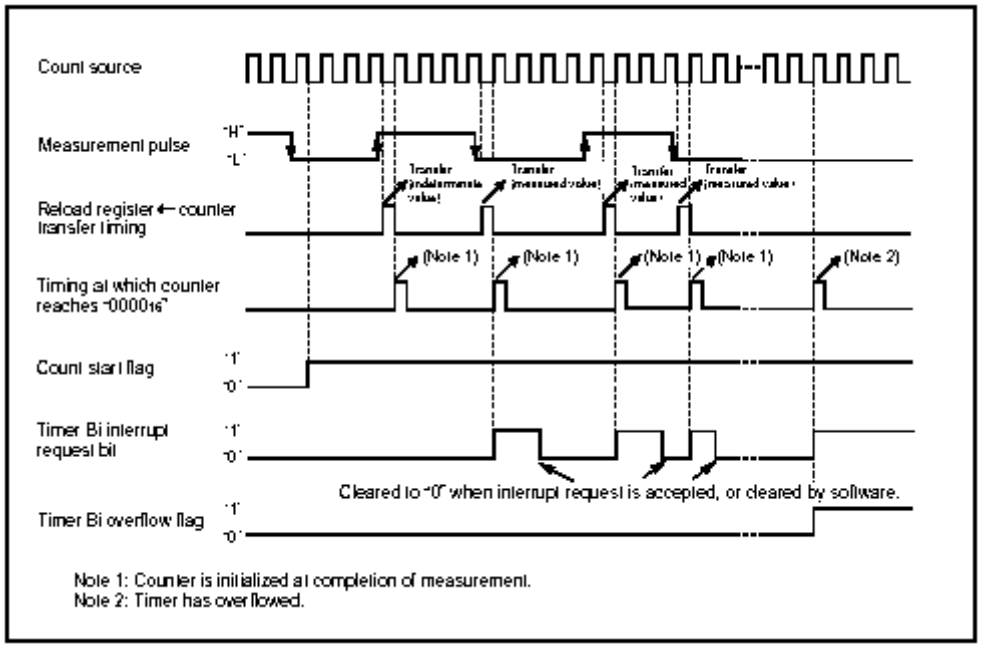

Figure 4-9: Pulse width measurement with Timer B

4.3.3 Interrupt Latency

"*Interrupt Latency*" is the time from an interrupt request until it is responded to. This time comprises

- Time to complete the current instruction
- Time required to execute the interrupt initiation sequence
- Time required to process the interrupt

For a 16MHz clock, the worst case is 3.125 microseconds: (30 clock cycles (1.875 microseconds) for the DIVX instruction plus 20 clock cycles (1.25 microseconds)), plus the time to save registers and input data from a port.

This may be exacerbated by multiple interrupts occurring simultaneously. The M16C has an interrupt resolution circuit to select the interrupt with the highest priority level for execution. In this case, a low priority interrupt may be delayed for a considerable period, depending on the total execution time of higher priority interrupt service routines. An interrupt request that is not accepted because of low priority will be held. If the held interrupt is of sufficient priority then it will be accepted when the Return from Interrupt (REIT) instruction is executed. Enabling interrupts within an interrupt routine allows higher priority interrupt requests to be accepted.

4.3.4 Power control

The M16C has three available power control modes:
(a) Normal operation mode: Current requirements (5V supply, 16MHz): 35mA typically, 50mA max
(b) Wait mode: The CPU is stopped. The oscillators do not stop.

(c) Stop mode: All oscillators stop. The CPU and all built-in peripheral functions stop. Current requirements: 1uA

4.3.5 Flash memory

The M16C contains “Divided NOR” flash memory that can be rewritten with 5V. The flash memory can be manipulated via parallel or serial I/O under the control of an external programmer, or it can be controlled by the CPU.

The flash memory is divided into several blocks as shown below; each block can be erased independently. There is an additional separate boot-ROM area which is used to store a serial I/O mode control program. This boot ROM area can only be rewritten in parallel I/O mode.

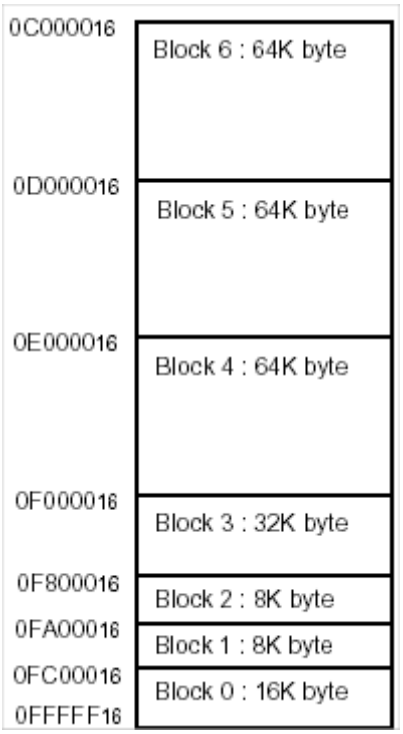

Figure 4-10: M16C Flash memory map

4.3.6 Development System

Mitsubishi manufactures a development system for the M16C/62 known as the "Starter Kit 2" (SK2).

Figure 4-11: Mitsubishi M16C SK2 development board

This includes the following components:

- Starter Kit board with M16C/62 with 256KB Flash meory & 20KB RAM, two 7-segment LEDs, 16MHz main clock & 32KHz subclock, reset IC, switches, 5V regulator, RS232 driver chip, 96-pin DIN connector for application board interface
- C Compiler
- Tool Manager (Integrated Development Environment)
- Debugger via PC serial port
- Flash ROM programming software
- Sample C programs
- Serial cable

The SK2 has drawbacks for embedded system development:

- the 96-way DIN connector is expensive and somewhat inappropriate for prototyping systems
- the onboard RS-232 driver is used for interfacing to the debugger (which runs on a PC) and consequently is not available for program use during debugging

Therefore a "breakout board" was developed which allows easy access to the M16C's ports, and which also includes an EIA RS-232 port for serial communications (see section 4.4.3)

4.4 Mounting and interfacing

4.4.1 Magnetometers

The magnetometers were mounted inside a plastic medicine bottle. A wooden dowel sized to fit the bottle was drilled longitudinally, and this holds the FGM-1 (single) magnetometer precisely at right angles to the FGM-2 (dual-package) magnetometers. Also included in the bottle are capacitors for power-supply decoupling, and resistors, etc required by the magnetometers. Connection to the magnetometer package is via a 1.5m long, 5-way cable that carries +5V, ground, and the 3 signal outputs from the magnetometers.

Figure 4-12: Magnetometer and accelerometer packages

4.4.2 Accelerometers

The two ADXL202E packages are mounted on individual printed circuit boards. These boards are mounted at right angles on a plastic block. Of the 4 available accelerometers in the two packages, two are aligned in the same direction (vertically) – one of these is unused. The self-test pin on the accelerometer chips is unused. Also included on the accelerometer boards are capacitors for power-supply decoupling, and resistors, etc required by the accelerometer. Connection to the accelerometer package is via a 1.5m long, 5-way cable that carries +5V, ground, and the 3 signal outputs from the accelerometers.

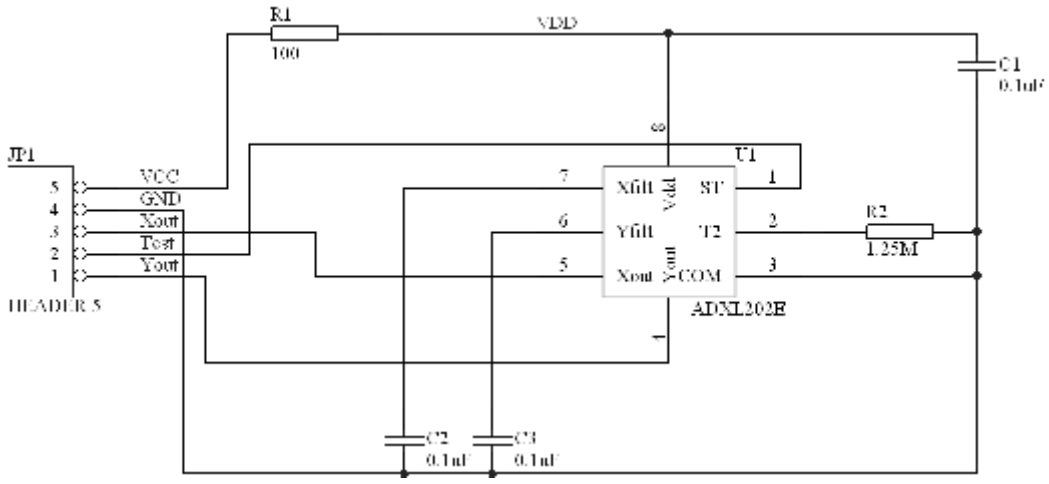

Figure 4-13: Accelerometer board schematic

4.4.3 M16C Interface

A general-purpose breakout board for the SK2 was designed and constructed. For each of the 8-bit I/O ports plus V_{CC} and GND, a 10-pin connector is provided. Also included on the breakout board was an EIA-232 driver chip connected to the M16C's UART0, and indicator LEDs for transmit and receive. Schematics, etc of this board are available in Appendix 3: Hardware.

A specialised interface board (Figure 4-14) was built to interface the accelerometers and magnetometers to the general purpose breakout board. The power supply for the magnetometers and accelerometers is provided via this interface board.

Also on this board are three 4020 14-bit binary ripple counter ICs to divide the 50-100 KHz magnetometer output signals by 2048 to 24-48Hz (20-40ms period), which are fed to the TimerB0, TimerB1, and TimerB2 inputs on the microcontroller.

The outputs from the accelerometers are fed directly to the TimerB3, TimerB4, and TimerB5 inputs on the M16C.

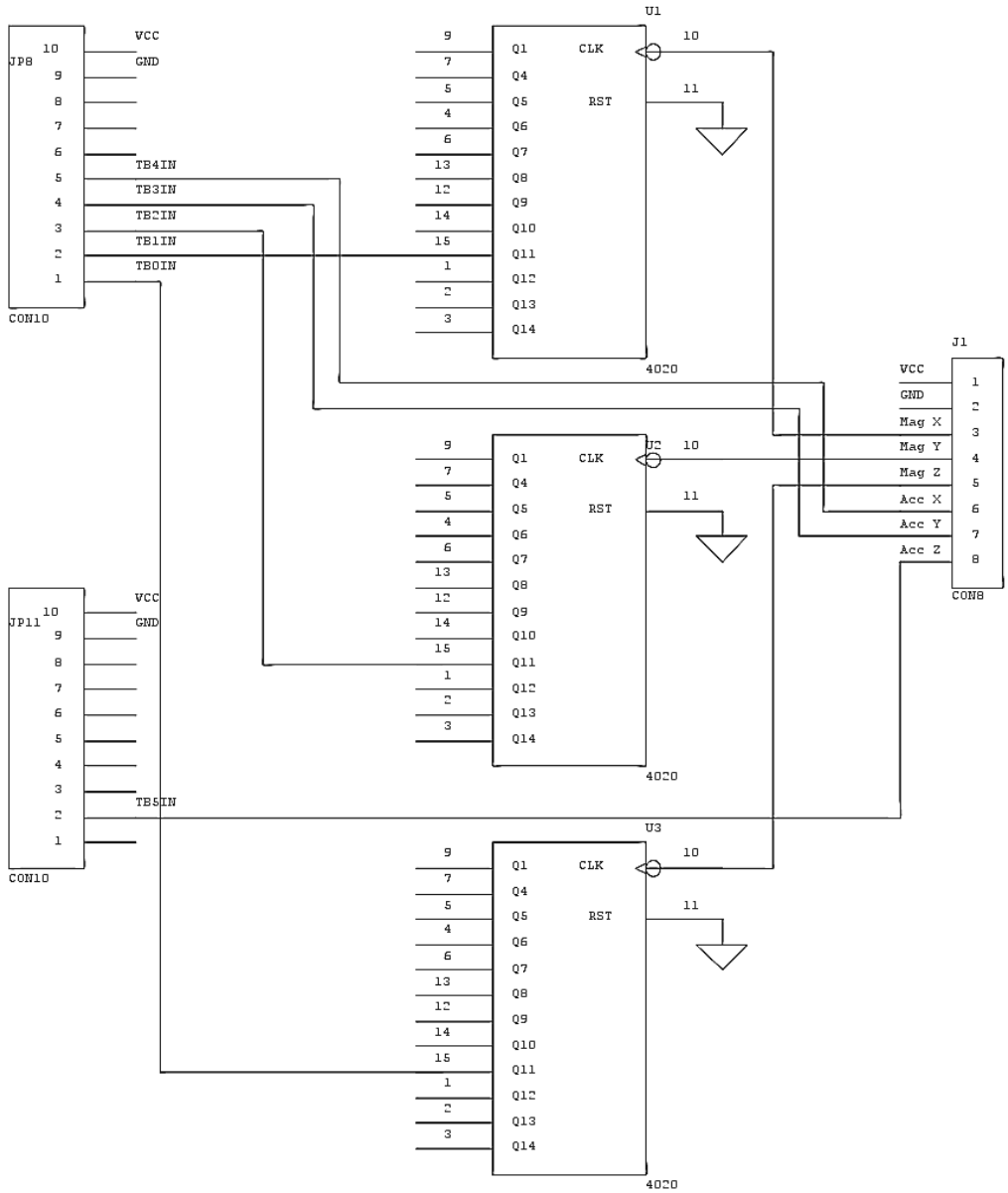

Figure 4-14: Magnetometer interface board schematic

5 Software Implementation

The general strategy used in developing the wave analysis software was to develop across two platforms; the embedded M16C system described in section 4.3.1 above, and a standard desktop PC environment. As software was developed on the PC environment, it was migrated to the embedded environment. The application was developed in several phases:

1. M16C as a data input device.
2. M16C as a simple data logger
3. Once algorithms had been tested in phase 2, they were coded in C and run on the PC against the data logged in phase 2 to compare C results with the spreadsheet results. Once tested in the PC environment, it was transferred to the embedded environment. This was relatively straightforward, with both systems having ANSI C compilers available.

5.1 Data Input Device

In this development mode, the M16C was used as a simple data input device. The M16C was connected directly to the PC using a serial cable. Data was read from the input devices, and the raw readings output to the PC. This mode was used in the laboratory for testing and calibrating the sensors. Software could also be developed in the relatively user-friendly PC development environment to analyse and display the data being read by the M16C.

Data comes from two sources, a set of 3 magnetometers, and a set of 3 accelerometers. The magnetometers vary the period of a square wave depending on the magnetic field they detect, and the accelerometers vary the mark/space ratio of a square wave. To measure these, the M16C's TimerB counters are used, under interrupt control.

This source code is available in Appendix 1: Data & Programs.

5.2 Data Logger

The M16C has 256KB of flash memory and 20KB of RAM on-chip. The flash memory is typically used to store the program to be executed. However, it is possible to also use some of this memory for data storage.

In this mode, the M16C recorded the sensor readings into Flash memory. On command, this raw data could later be downloaded to the PC. Data was output in a comma-delimited decimal format, so that it could be easily imported into programs such as Microsoft Excel. This permitted easy data visualisation, and algorithms could be rapidly tested and evaluated.

The data logger was tested in two ways:

- The embedded system was used to record data whilst being driven in a car. The motion sensed by the embedded system could then be compared to known and repeatable motion.
- The data logger was then deployed on a buoy to provide raw data for later PC analysis.

Once the logger program has been loaded into flash memory, the microcontroller board plus attached sensors and a 9V battery is completely autonomous.

As the data is logged, bits 12-19 of the address are displayed in hex on the onboard 7-segment LEDs to give an indication of how much memory has been used. The multiplexing of the two displays is controlled by TimerA1, which is configured to interrupt at 10ms intervals. This timer also provides the time base for the data logging.

The INT0 and INT1 pushbuttons on the SK2 board are used after startup/reset to choose the function to be performed: pressing INT0 results in Flash erasure and data logging, whilst pressing INT1 results in data output via UART0 (19200bps).

This program can coexist in the SK2 board with Mitsubishi's Monitor program. Therefore it works well with Mitsubishi's KD30 debugger (the debugger must be put into 'free-running' mode) for ease of program development.

5.2.1 Capabilities

- 224KB of flash are available for data storage.
- Each dataset requires 24 bytes, so 9557 datasets can be stored.
- Programmable logging interval between 5 and 1000ms
- Total recording time between 159 minutes (1000ms logging interval) and 48 seconds (5ms logging interval). For wave recording (logging interval = 36ms), this allows recording for 344 seconds (5.7 minutes).

5.2.2 Software

The use of flash for data storage is complicated by the fact that the entire flash memory, although made up of several separate blocks, has a single flash mode control device. The significance of this is that, once a block of flash has started to be written or erased, it is not possible to read from any other block of flash. This means that the interrupt vector table and all interrupt service routines, and all code used to erase or write to flash, must be executed from RAM. That in turn requires that the code be relocatable, and reasonably compact in size. A relocation routine copies the code from ROM to RAM at start-up, and sets up the interrupt vector table in RAM to point to the RAM copies of the routines.

A new program cannot easily be loaded into part of flash memory without erasing the rest; therefore, both the data recording and data output functions must be part of the same program.

To allow for easier debugging, the entire program fits into flash between F8000h and FBFFFh. This causes some pressure on code size. A small increase in program size would have required the use of the F0000h-F7FFFh block of flash for program storage, and consequently reduced the data buffer size by 32K. This required some code optimisations:

- The FPUTC.C source code from the library was slightly customised. The standard version calls *fgetc()* (a large routine) to allow Ctrl-S/Ctrl-Q (XON/XOFF) handshaking for flow control.

- Similarly, the heap initialisation (which caused MALLOC to be linked in, although the heap isn't used) and initialisation of FAR memory spaces (unused -- no external memory) was removed from the startup module (NCRT0.A30) to reduce code size.

All Interrupt Service Routines (ISRs) and the flash erasing/writing routines were written in assembler. This was so that they could all be placed in the same 'section' and easily collected together by the linker. This also made it easy to ensure that none of this code contained absolute addresses. A side benefit of this is smaller code size and faster execution.

At reset, after the standard CPU setup, NCRT0.A30 copies the ISRs and flash writing routines to RAM. It then copies the interrupt vector table from flash to RAM. As it does this, it corrects all the vector table entries so that they point to the RAM copies, points the INTB registers at this table, and enables interrupts.

Next the data areas are initialised as usual, and *init()* is called. This sets up *stdout* to output via UART0, and sets the UART to 19200N81. RTS/CTS handshaking is disabled. The lack of handshaking does require that the computer receiving data from this port is fast enough to handle it as it comes in. That assumption is reasonable for a modern PC (eg 500MHz Pentium) saving data direct to disk via a terminal emulator program. The various peripheral devices (7-segment LEDs, timers, pushbuttons) are then initialised.

Finally, the *main()* program in LOGGER.C is executed. This displays the logging interval (in multiples of 10ms, and in hexadecimal) on the 7-segment displays. Several versions of the logger can be built using different logging intervals -- the display allows a double-check that the correct version is being used.

The main program waits for one of the INT0/INT1 pushbuttons to be pressed. A more sophisticated user interface could be built using UART0, but the logger is designed to record data on the logger entirely standalone – a PC or terminal is needed only when the data is being output by the logger, not whilst data is being recorded.

5.2.2.1 Data Logging

When INT0 is pressed, The CPU is put into a 'flash-writing' state -- wait states are inserted and the CPU clock slowed down as required for writing to flash. All flash from C0000h to F7FFFh is erased block by block.

The program then waits for a preset delay time, and then begins recording data until either flash memory is filled or the processor is stopped. The delay time is typically set to 5 minutes for buoy operations to allow the logger to be sealed in a watertight container and mounted on the buoy. In laboratory or road trials, the delay is set to 1 minute or less.

After the delay time has elapsed, the logger begins recording the sensor readings into flash memory. The data logging interval is preset at compile-time to a value between 10ms and over 1 second.

Each raw data point consists of three sets of numbers, one each for the X, Y, and Z axis readings. For each axis, three numbers are recorded: the pulse width and period of the accelerometer, stored as two 16-bit integers, and the pulse width of the magnetometer, stored as a 32-bit integer. Thus each data point requires 24 bytes to be stored.

Because flash must be written 256 bytes at a time, data is logged to RAM until at least 256 bytes are recorded. The dataset is 24 bytes in size which does not divide evenly into 256. Often, therefore, there will be a few bytes unwritten, and the buffer must be 256 + 24 bytes long. After a page is written to flash, any unwritten bytes are moved to the beginning of the buffer and logging continues immediately contiguous to the last unwritten byte. When over 256 bytes are again available for writing, the whole cycle begins again.

The standard C function *memcpy()* took 400ms to move the unwritten bytes to the beginning of the buffer. Clearly, this would preclude any fast logging rate. Therefore *memcpy()* isn't used, and instead an assignment statement is used to copy an entire dataset starting at *buff+256* down to *buff*. Writing a page to flash must be done in less than the logging interval... although this program does allow interrupts to happen whilst a flash write operation is in progress, it doesn't log data during that time.

This approach means that, in the output phase, data stored in flash can be viewed as contiguous datasets.

Data compression was considered but discarded because

- It is expected that the data will be continuously varying, therefore detecting patterns in the data to allow compression could get very complex, and
- Adding more code could reduce the amount of flash available for data

To minimise the program size, and therefore maximise data storage space, the data logger performs no analysis. A total program size (including copies of interrupt service routines and the interrupt vector table) of 24KB or less means that the program can be contained in blocks 0 & 1 of flash memory, leaving blocks 2-6 (a total of 224KB) available for data storage (see Figure 4-10).

There is a compromise here; analysing raw data would mean that the data could be stored more compactly, so a larger, more complex program might actually increase the data storage capability of the logger.

Given a total of 224KB available, a total of 9557 data points can be recorded. At the minimum required sampling interval of 36ms, this allows recording for 344 seconds (5.7 minutes).

5.2.2.2 Data Output

If INT1 is pressed after startup, the logger immediately starts outputting data from flash to the serial port (UART0) at 19,200bps. A communications program such as Windows' HyperTerminal is used to capture the text and store it to a file. The data is output as comma-delimited ASCII text so that it can be easily imported into programs such as MS Excel for analysis. This permits easy data visualisation, and algorithms can be rapidly tested and evaluated.

A typical text file size is 560KB, an average of 57 bytes per data point; this varies somewhat depending on the size of the numbers. At 19,200bps, it takes about 5 minutes to output the data from the logger. This time could be shortened by increasing the baud rate and/or transferring the data in binary rather than as text. However, at higher baud rates there is a greater risk of errors; if the PC receiving the data becomes busy it may miss a character or more. That in turn would require an error-detecting and –correcting protocol, increasing the complexity and size of the data logger program, and perhaps also needing a special program at the PC end. Similarly, transferring data in binary would potentially reduce the transfer time by about half, but would require a special "receiver" program on the PC.

5.2.3 Memory Map:

Address Range

```
00000 - 003FF     Special Function Registers
00400 - 008F5     Scratchpad RAM

02C00 - 03200     Stack

04800 - 04AFF     RAM_CODE (ISRs, Flash writing routines)
04B00 - 04BFF     RAM_vector (RAM version of Interrupt Vector Table)

04C00 - ???       Used by Monitor program

C0000 - F7FFF     Flash Data Storage

F8000 - FA6D3     Program -- Startup, Main Program, Library functions
FA900 - FAA58     ROM data
FBB00 - FBCA5     ROM_CODE (ISRs, Flash routines, to be copied to RAM)
FBD00 - FBDFF     ROM_vector (ROM copy of vector table, to be copied to RAM)

FBE00 - FBFFF     Unusable

FC000 - FFFFF     Monitor program
```

Note that the flash memory blocks get smaller above F0000 – this makes it slightly more convenient to store data starting at C0000. Secondly, the M16C startup code can't be located at C0000.

Because of the way that the vector table is moved, the RAM copy must start at an even page boundary (i.e. the origin of *RAM_vector* must be a multiple of 100h). Similarly, the *ROM_CODE* section shouldn't overlap a 64K boundary.

This source code is available in Appendix 1: Data & Programs.

5.3 Road Testing

The embedded system was used to record data whilst being driven in a car. This allowed the system to be tested without the environmental and other issues involved with deploying a buoy on the ocean. In addition, the motion sensed by the embedded system could be compared to known motion.

A suitable road for testing was chosen; this was Pukepapa Road, a rural road outside the town of Marton, New Zealand. Pukepapa Rd is a straight road which runs at 15° to

true north. The magnetic declination in the area is 21° East, so the road's direction is 354° Magnetic in one direction, and 174° Magnetic in the other. The road has several undulations which vary in height from a metre or so to about ten metres. By driving over these at various speeds, various frequencies of vertical motion can be generated.

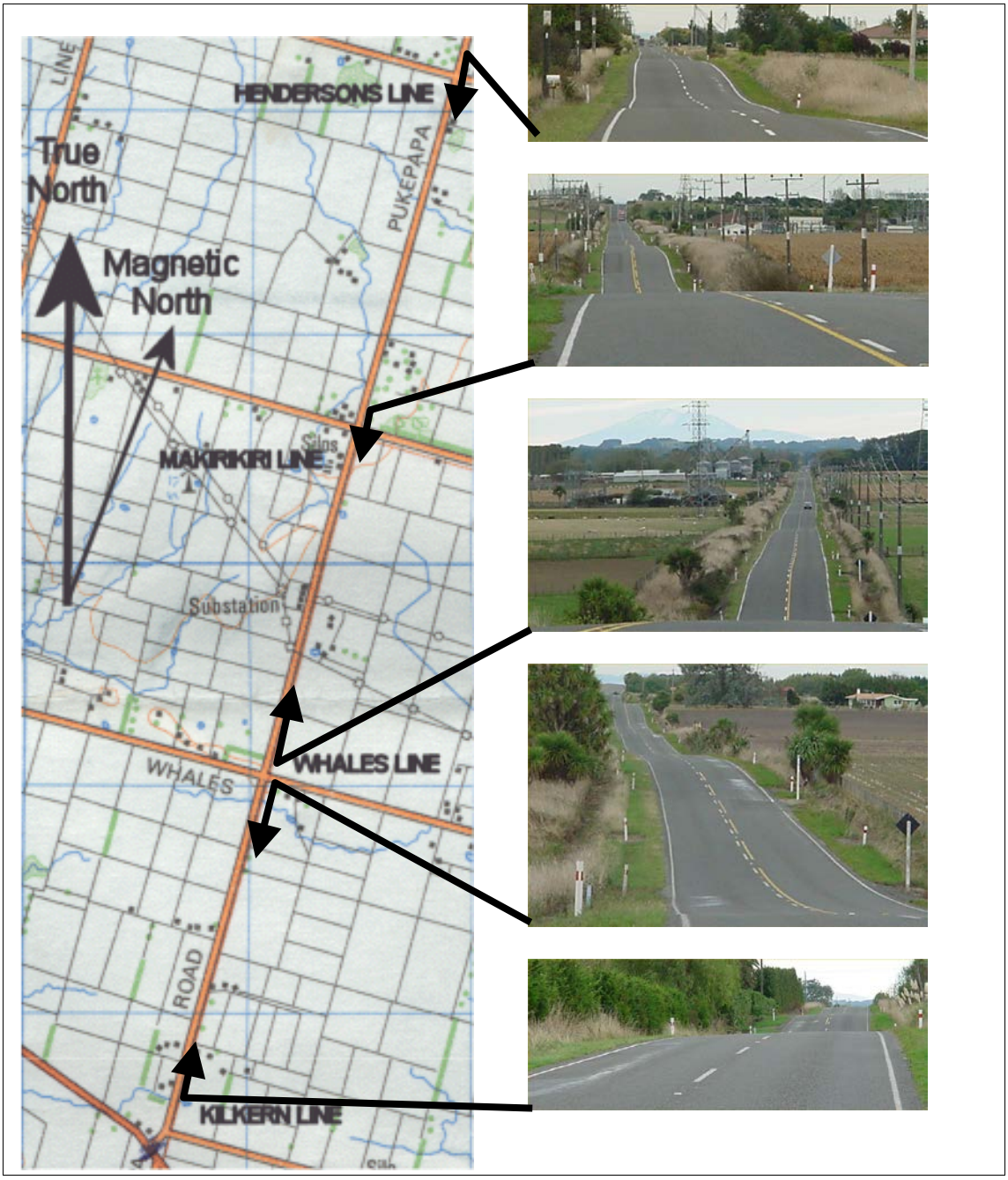

Figure 5-1: Topographic Map and photographs, Pukepapa Road area

The apparent highest point visible from Makirikiri Line and Henderson's Line is at the intersection with Whales Line.

The heights of various points along Pukepapa Rd were surveyed using GPS and an aircraft altimeter. Unfortunately, neither of these devices was sufficiently accurate to reliably measure accurate heights. Nevertheless, there was good general agreement between the two devices.

Four passes were then made over Pukepapa Rd from the intersection with Makirikiri Line to the intersection with Kilkern Line (see Figure 5-1):

- Pass 1: southbound, 100kph
- Pass 2: northbound, 70kph
- Pass 3: southbound, 100kph
- Pass 4: northbound, 100kph

During each of these passes the magnetometer and accelerometer outputs were logged and the data calculated, resulting in the profile shown in Figure 6-10.

5.3.1 Analysis

5.3.1.1 Accelerometers

- Calibration: Accelerometers were calibrated by rotating the sensor array fully in 3 dimensions so that each accelerometer was aligned with the gravity vector as described in section 4.2.4.
- Low-pass filter: To remove vibration, the accelerometer readings were passed through a Butterworth 2.5Hz (0.4 second period) low-pass filter.

5.3.1.2 Magnetometers

- Calibration: Magnetometers were calibrated as described in section 4.1.3.
- Linearisation: the magnetometer data were linearised as described in section 4.1.3 and "pre-filtered" to remove artefacts due to the M16C's interrupt handling
- Low-Pass Filter: The magnetometer readings were passed through a Butterworth 0.005Hz (200 second period) low-pass filter to give a long-term average reading for the orientation of the sensors in the magnetic field. This provides a reference of "horizontal" against which each reading may be compared. This is analogous to the 120-second period pendulum in the Waverider (see page 9). This low-pass filtered data was normalised to correct any calibration errors, and to avoid calculation errors in subsequent trigonometry.
- Band-pass filter: The magnetometer readings were also passed through a Butterworth 0.0625-0.625Hz (1.6-16 second period) band-pass filter to smooth any errors in the sensor readings, then normalised. The angles between the band-pass-filtered data and the low-pass-filtered data give the orientation of the sensors relative to the magnetic field.
- Rotation: The magnetic field readings were rotated to correct for the dip (24° from the vertical) of the Earth's magnetic field to give true direction. Because Pukepapa Road runs nearly North-South, the readings were simply rotated about the X axis by the dip angle to give an approximation of the true coordinate system.
- Azimuth, Pitch, Roll calculations: The azimuth (heading) was calculated from the X and Y low-pass-filtered readings. The arcsine of the rotated X and Y band-pass-filtered readings gave the pitch and roll respectively.
- With Pitch motion known, the accelerometer readings were rotated about the X axis to derive horizontal and vertical accelerations.
- The horizontal acceleration was integrated to calculate horizontal velocity, which was in turn integrated to calculate horizontal displacement. Similarly, vertical acceleration was doubly integrated to derive vertical displacement.
- The horizontal displacement was plotted against vertical displacements for each pass.

- These graphs were compared. Because accurate initial values for vertical and horizontal displacement and velocity were not known, values were selected so that obvious features on the graphs coincided. These graphs are shown in Figure 6-10.

This source code is available in Appendix 1: Data & Programs.

5.4 Buoy Testing

The data logger was then deployed on a buoy to provide raw data for later PC analysis.

To protect the electronics from the corrosive effect of seawater, they (including batteries) were mounted inside a waterproof plastic box. This in turn was sealed with waterproof tape. This system proved completely effective in protecting these sensitive components from seawater. As further insurance against seawater splashes (which proved unnecessary), the components and interface boards were placed inside plastic bags inside the plastic box.

Figure 5-2: Microcomputer & sensor package

The data logger was programmed with a preset delay on 60 seconds after start-up before data logging commenced. This was to allow time for sealing the plastic box, installing it on the buoy, and deploying the buoy into the sea. The buoy was tethered via a 20m long rope to allow easy retrieval after data collection was completed.

By re-deploying the buoy using multiple SK2 boards in sequence, several data sets could be logged on a single data collection trip. These SK2 boards were then returned to shore for download of the data and subsequent analysis.

5.4.1 Analysis

5.4.1.1 Accelerometers

- Calibration: Before leaving shore, the accelerometers were calibrated as described in section 4.2.4. The data was logged to an M16C data logger for later analysis.

5.4.1.2 Magnetometers

- Calibration: Magnetometers were to be calibrated as described in section 4.1.3.
- Linearisation: the magnetometer data were linearised as described in section 4.1.3 and “pre-filtered” to remove artefacts due to the M16C’s interrupt handling

- Low-Pass Filter: The magnetometer readings were passed through a Butterworth 0.005Hz (200 second period) low pass filter to give a long-term average reading for the orientation of the sensors in the magnetic field. This provided a reference of “horizontal”. This low-pass-filtered data was normalised to correct any calibration errors, and to avoid calculation errors in subsequent trigonometry.
- Azimuth calculations: The Y axis of the magnetometer reading was corrected for the dip (24° from the vertical) of the magnetic field. The azimuth (heading) is calculated from the X and Y low-pass-filtered readings. The arctangent of the X and corrected Y axis readings gives the azimuth.
- Band-pass filter: The pre-filtered magnetometer readings were also passed through a Butterworth 0.0625-0.2Hz (5-16 second period) band-pass filter to select a range of wave frequencies to extract. The angles between the band-pass-filtered data and the low-pass-filtered data give the pitch and roll of the sensors.

This source code is available in Appendix 1: Data & Programs.

6 Results

6.1 Road Testing

The graphs shown in Figure 6-1 and Figure 6-2 show the raw data readings measured during four passes up and down Pukepapa Road from the intersection with Makirikiri Line to the intersection with Kilkern Line:

Pass	Direction	Start Time	Finish Time	Speed
1	southward	00:00.0	01:45.3	100kph
2	northward	01:54.0	04:07.5	70kph
3	southward	04:17.0	06:09.7	100kph
4	northward	06:30.0	08:21.0	100kph

Note the readings between the end of each pass and the beginning of the next:

1. a deceleration in the Y (longitudinal) axis
2. a negative X (lateral) acceleration as the car is turned (all turns were clockwise)
3. simultaneously, an abrupt change in the X and Y magnetic field readings
4. finally a Y acceleration
5. little change in the Z (vertical) acceleration or magnetic field

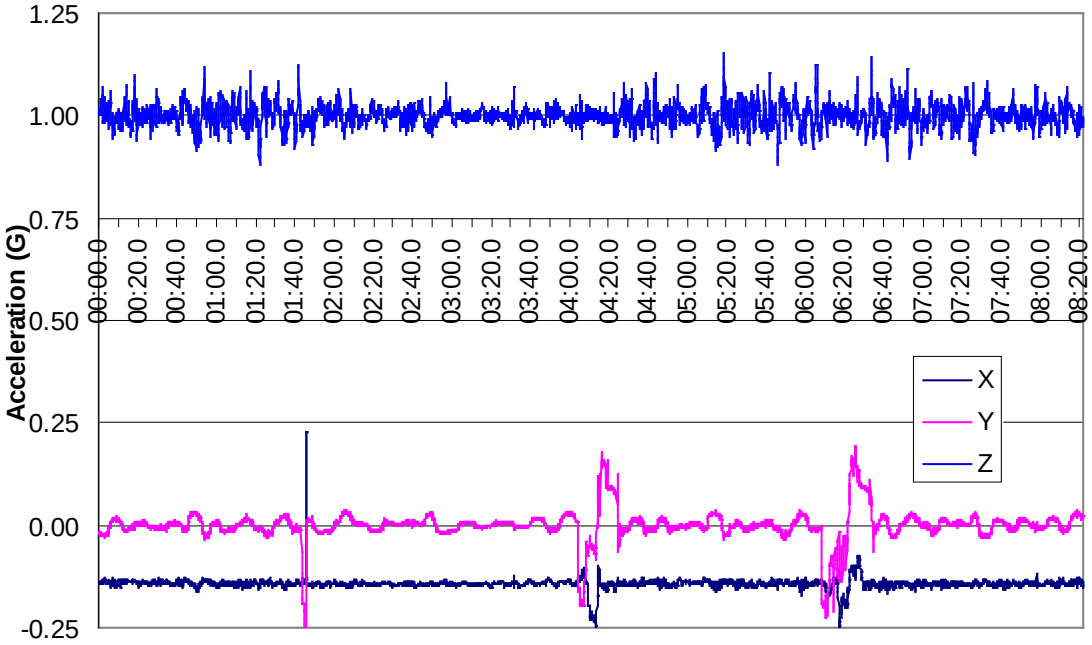

Figure 6-1: Pukepapa Rd Accelerations

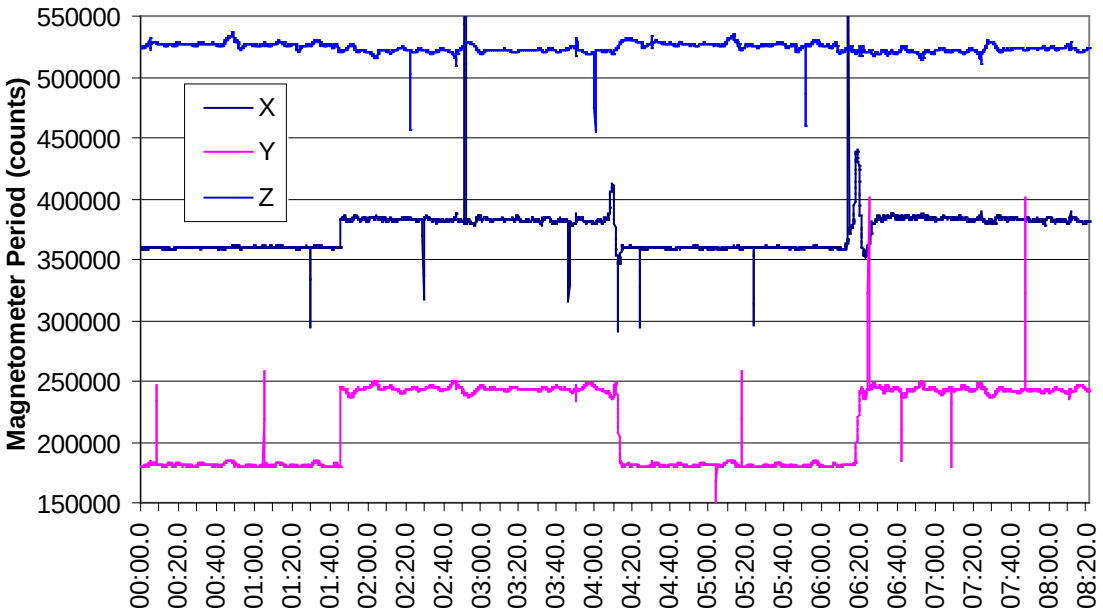

Figure 6-2: Pukepapa Rd Raw Magnetometer Counts

The large spikes in the magnetometer record above are artefacts of the M16C sampling procedure. When the counter overflows at 64K counts, an interrupt is generated. If processing of this interrupt is delayed due to a second interrupt occurring simultaneously, the overflow may be misread as being the end of a pulse, or vice versa.

These artefacts were removed manually. However, an automated procedure for detecting and removing them needs to be implemented (see section 7.8).

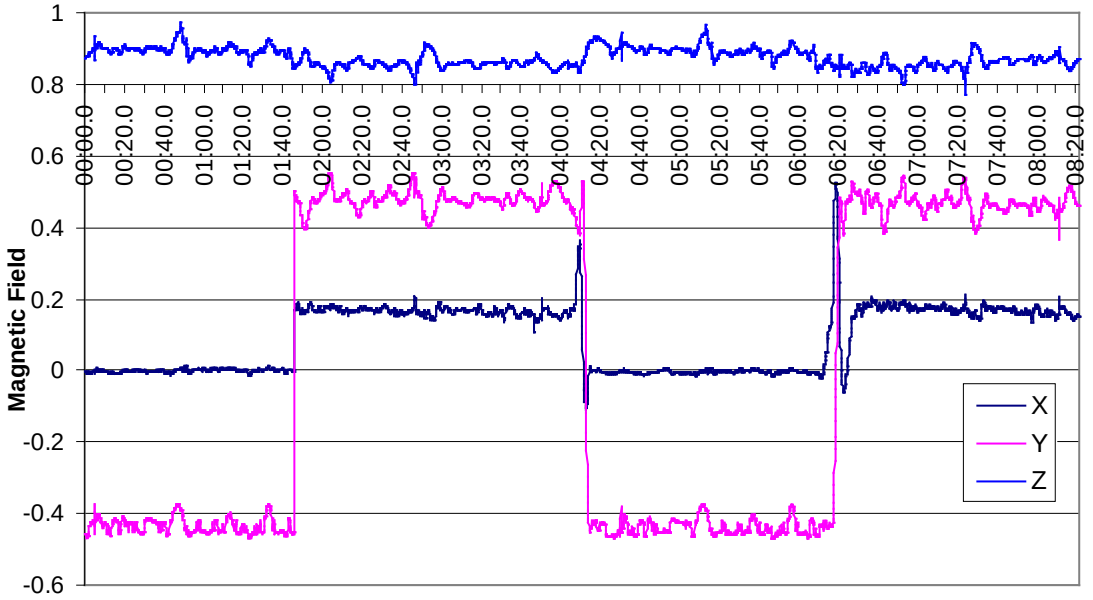

Figure 6-3: Pukepapa Rd Magnetic Field Components

These ‘pre-filtered’ magnetic field components were then passed through a Butterworth low-pass pass filter with a cut-off frequency of 0.005Hz.

At the beginning of each pass, the filter was re-initialised so that components read in the previous pass (in the opposite direction) would not distort the filtered data for the current pass. The resulting data is shown in Figure 6-4 below.

Similarly, the accelerometer data was passed through a Butterworth low-pass filter with a cut-off frequency of 0.4Hz to remove high frequency accelerations due to vibration.

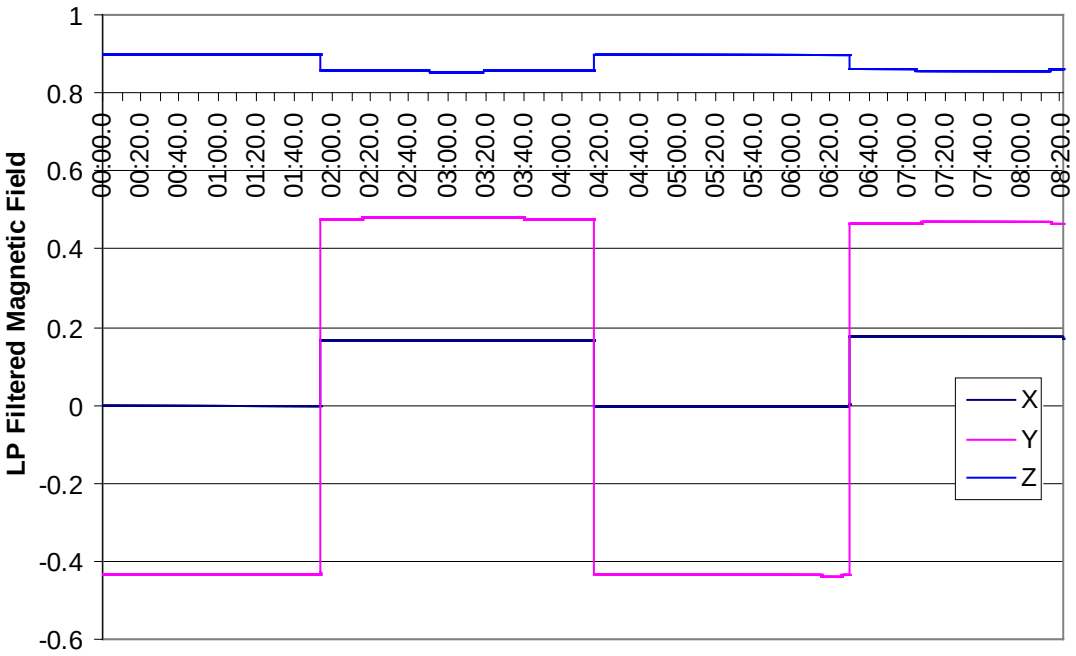

Figure 6-4: Pukepapa Rd Low-Pass Filtered Magnetic Field Components

The pre-filtered magnetic field components were also passed through a Butterworth filter with a pass-band of 0.0625-0.625 Hz, resulting in the data graphed below in Figure 6-5:

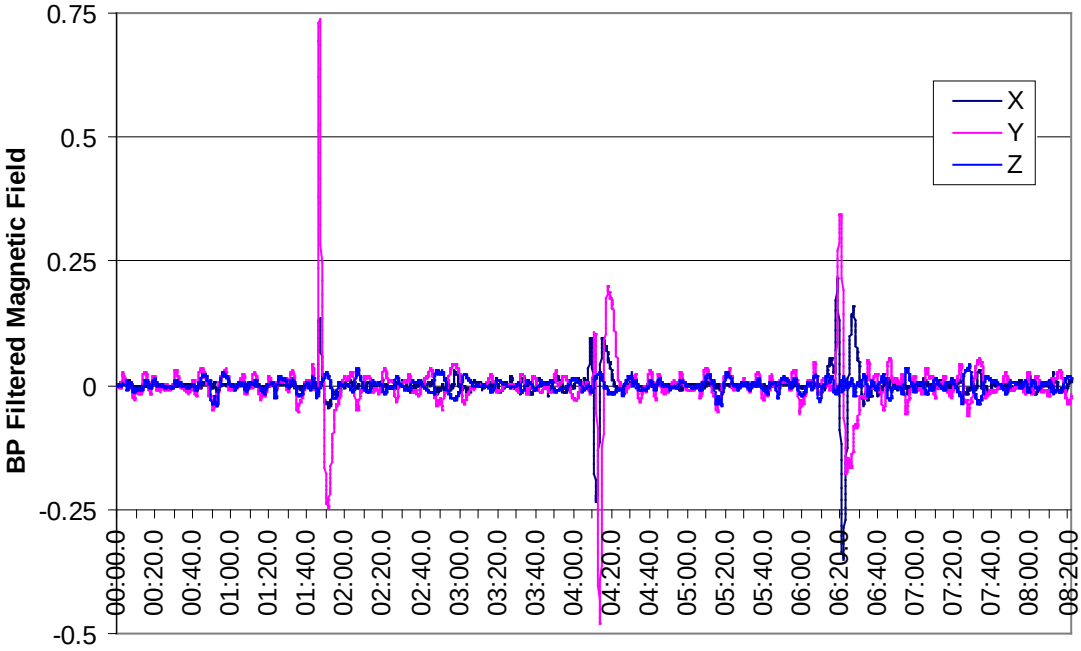

Figure 6-5: Pukepapa Rd Band-Pass Filtered Magnetic Field Components

From the X and Y low-pass filtered readings, azimuth (heading) was calculated. The Y and Z band-pass-filtered readings were rotated about the X axis to correct for the dip angle of the magnetic field (24º from vertical) to calculate pitch in world-coordinates.

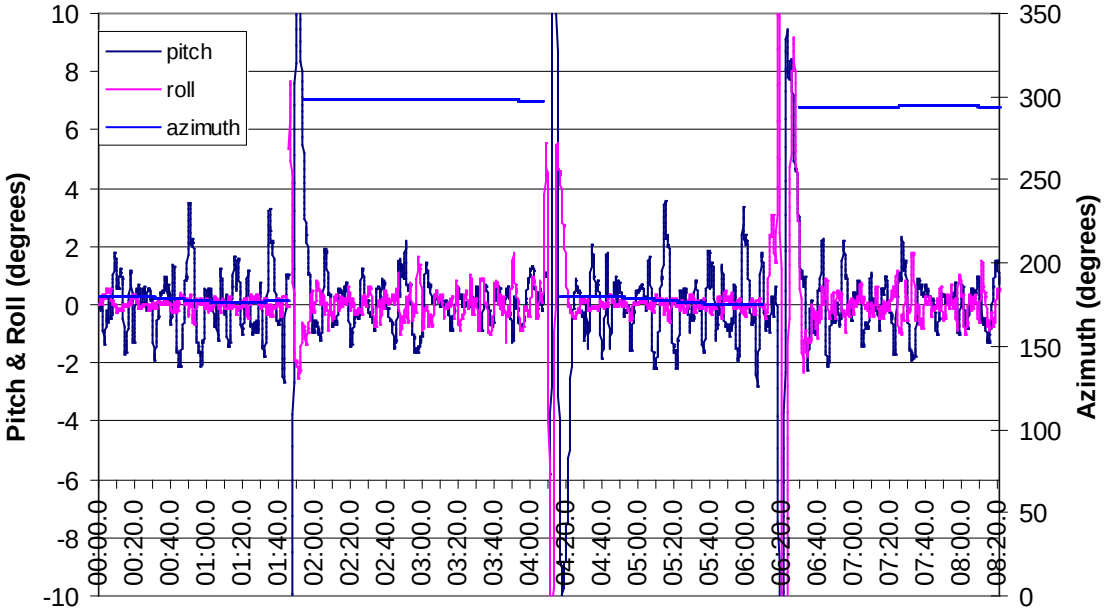

Figure 6-6: Pukepapa Rd Azimuth, Pitch, and Roll Components

With Pitch motion known, the accelerometer readings were rotated about the X axis to derive horizontal and vertical accelerations.

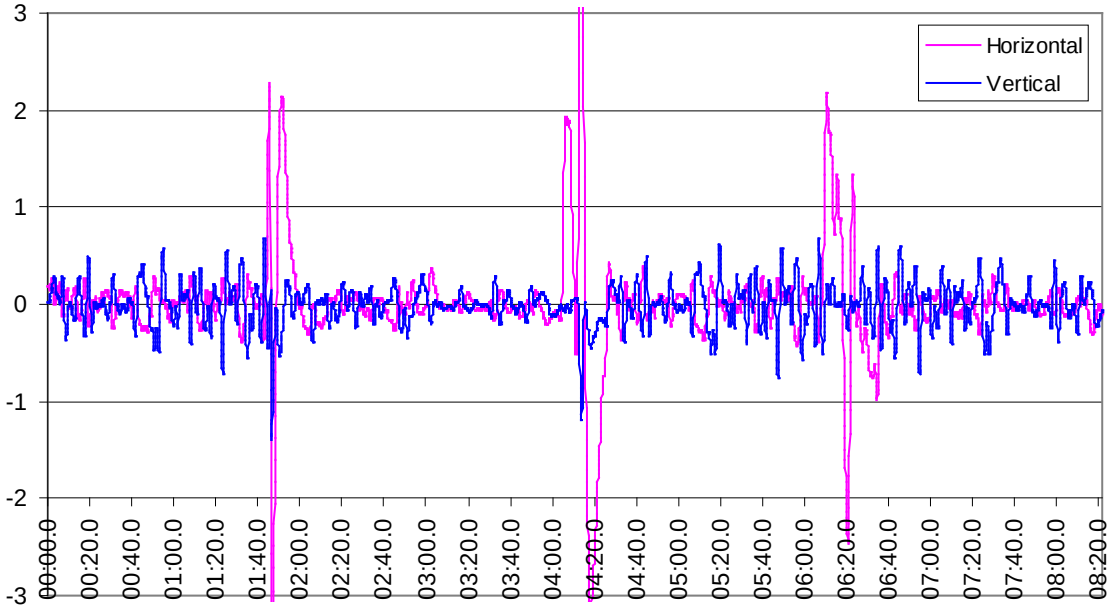

Figure 6-7: Pukepapa Rd Horizontal and Vertical Accelerations

The horizontal acceleration was integrated to calculate horizontal velocity, which was in turn integrated to calculate horizontal displacement. Similarly, vertical acceleration was doubly integrated to derive vertical displacement.

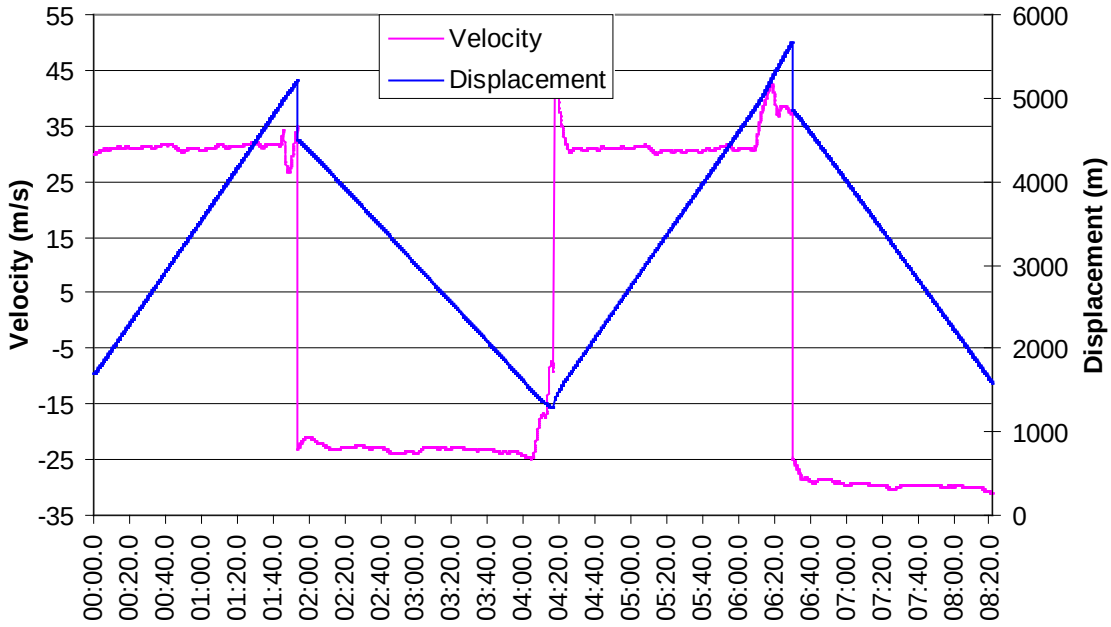

Figure 6-8: Pukepapa Rd Horizontal Velocity and Displacement

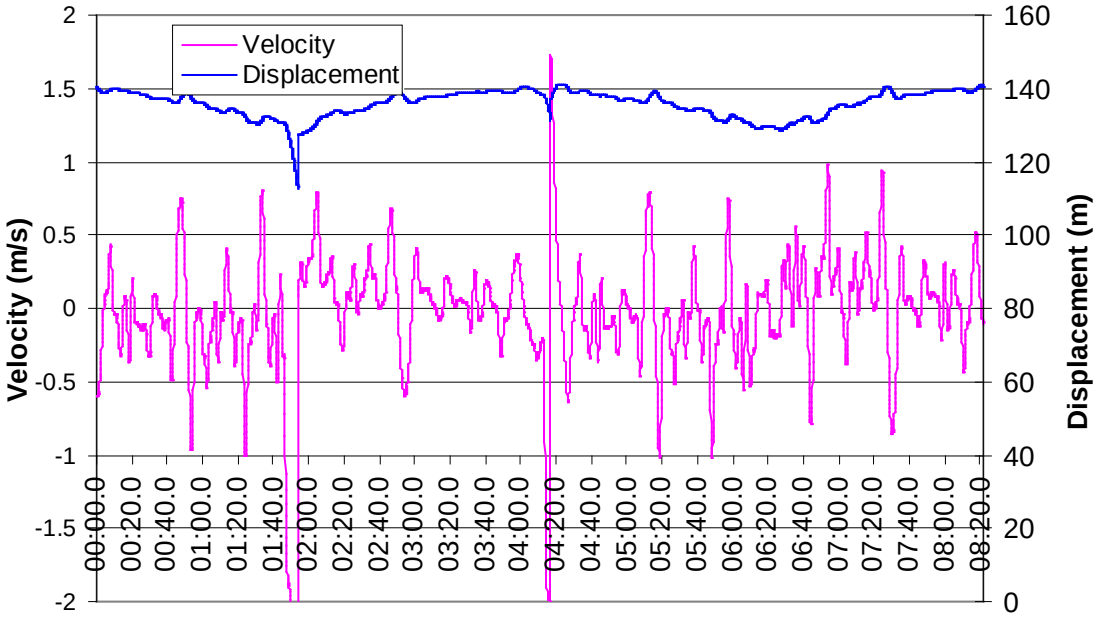

Figure 6-9: Pukepapa Rd Vertical Velocity and Displacement

The horizontal displacement was plotted against vertical displacements for each pass.

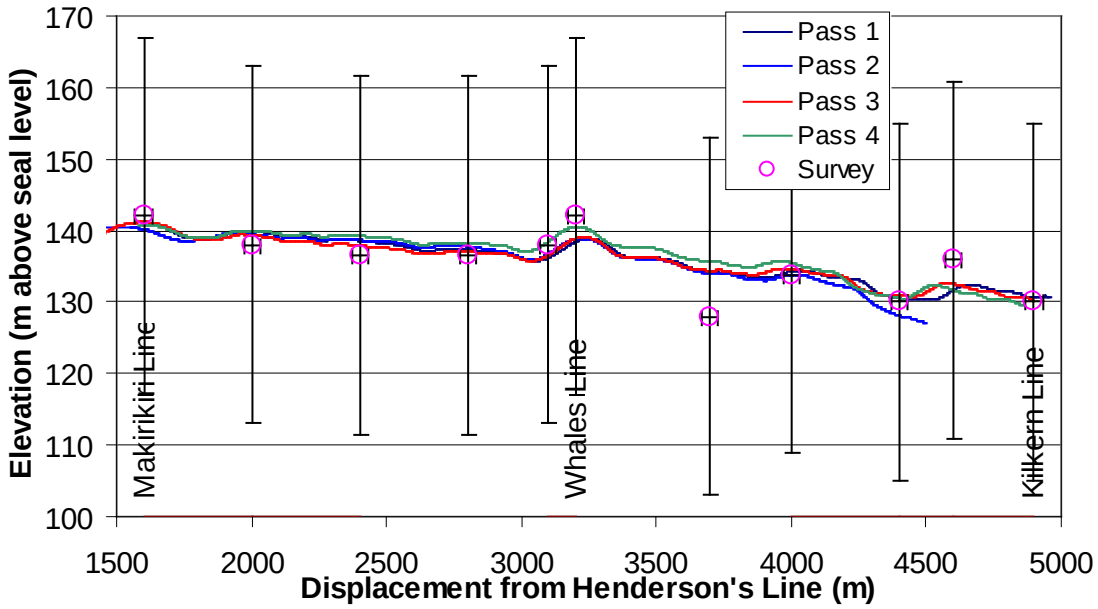

Figure 6-10: Pukepapa Rd Profile: Vertical vs Horizontal Displacement

The "Survey" points on this graph were measured using GPS. The horizontal and vertical error bars indicate the positional error in GPS readings.

Figure 6-11 shows a comparison, using Pass 1 data, of integration techniques described in section 3.2.3. It can be seen that the various integration techniques result in very similar outputs. The right-hand graph shows detail of a small segment from the right-hand of the main graph. This part of the graph shows the worst-case for accumulated errors, with a variation of less than 0.5m between the four methods. Note the apparent high-frequency error introduced by the Simpson's Rule technique.

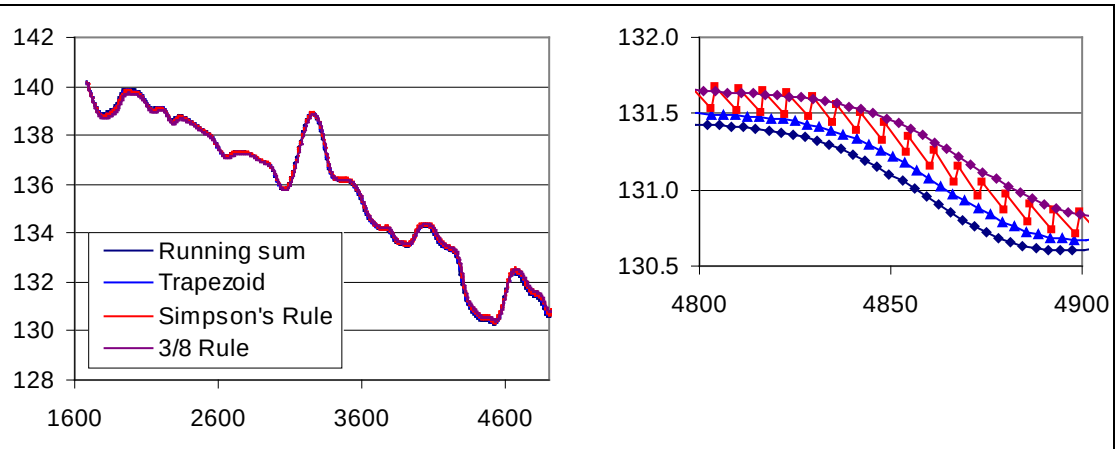

Figure 6-11: Comparison of integration techniques

Both the raw data and the analysed data is available in Appendix 1: Data & Programs as Microsoft Excel spreadsheets.

6.2 Buoy Testing

Two separate data collection trips were made:

- 20 December 2002: via sea kayak, from Kai-iwi beach, north-west of Wanganui. For this trip, since the water was expected to be relatively shallow, it was intended to analyse short wavelength (relatively high frequency) waves. Therefore the loggers were programmed to log at high sampling rates of 100Hz.

  Unfortunately, no useful data was collected on this trip. Whilst sitting in a kayak in motion, even though the sea was moderate, it took considerably longer than the one minute allowed to seal the plastic box. A second attempt at deploying using a surf rescue Inshore Rescue Boat resulted in (undetected) intermittent damage to the accelerometer connections due to the pounding whilst going out through the surf.

- 15 May 2003: via the "Gwenelda", offshore from Wanganui. The buoy was deployed into the water at 39º57'53.9"S, 174º57'59.5"E, approximately 5km offshore in 18m of water several times between 8:30am and 11:30am (See Figure 6-12). During this period, the boat itself drifted at 1.2km/hr on a course of 215º. The weather was fine with a southwesterly swell of approximately 1 metre. A light easterly breeze decreased to calm over this period of time. In addition, a record was taken of motion on board the boat at the same location, using the same sensors.

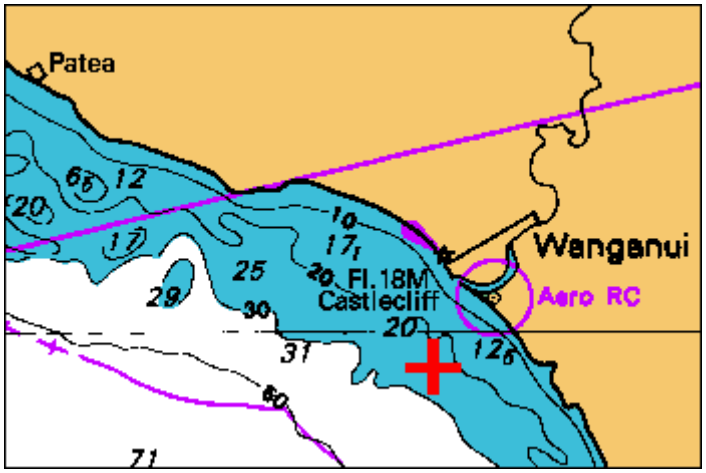

Figure 6-12: Buoy Location

After returning to shore, it was found that one of the accelerometer devices was giving faulty readings. This meant that only one channel (the horizontal Y axis) was useable. However, without the corresponding X and Z channels, no useful information could be extracted from this data.

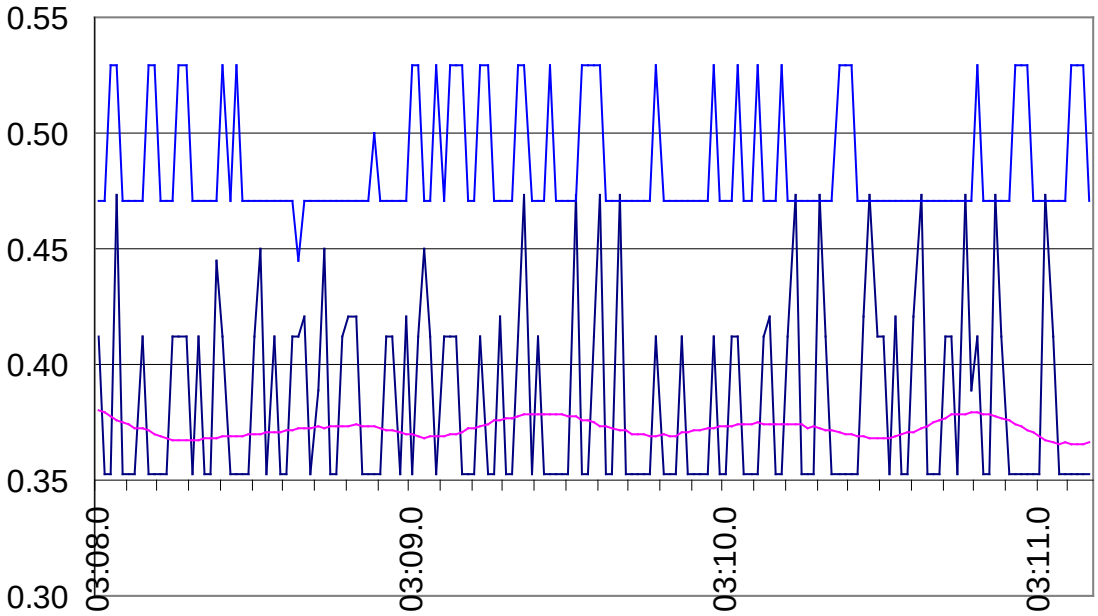

Figure 6-13: Buoy: Raw acceleration data

Before leaving shore, the accelerometers were calibrated by rotating the sensor array fully in 3 dimensions so that each accelerometer was aligned with the gravity vector. However, the data logged was not inspected until later.

The graph above shows a detailed view of the last few seconds of the accelerometer data logged during data collection. Note that the X and Z axis data are “quantised” into only a few discrete levels, whereas the Y axis data shows a continuous waveform. This quantisation is due to the frequency of the signals output from the X and Z accelerometers being approximately 20 times too high due to an intermittent power supply fault. The X and Z axis data are produced by a single 2-axis accelerometer chip; the Y axis data come from a second chip which was unaffected by the fault.

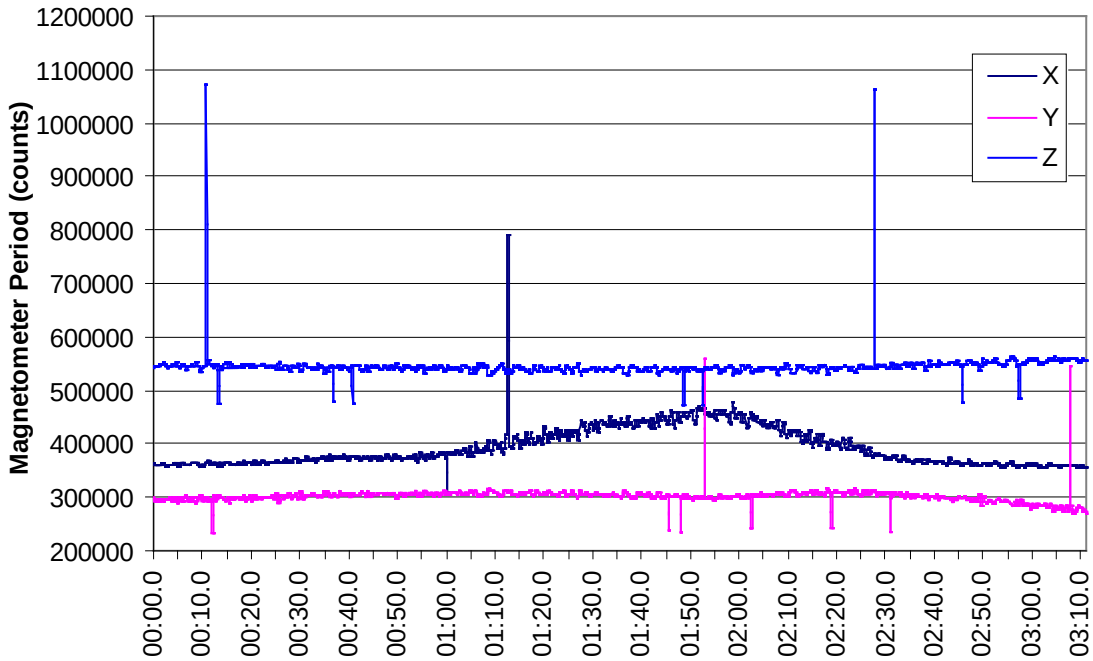

Figure 6-14: Buoy: Raw magnetometer data

The automatic calibration algorithm could not find a suitable set of points (see section 7.7). A special calibration program was used to scan through the entire data set to find a suitable set of calibration readings. These calibration settings were then used to calibrate the magnetometers for the data set.

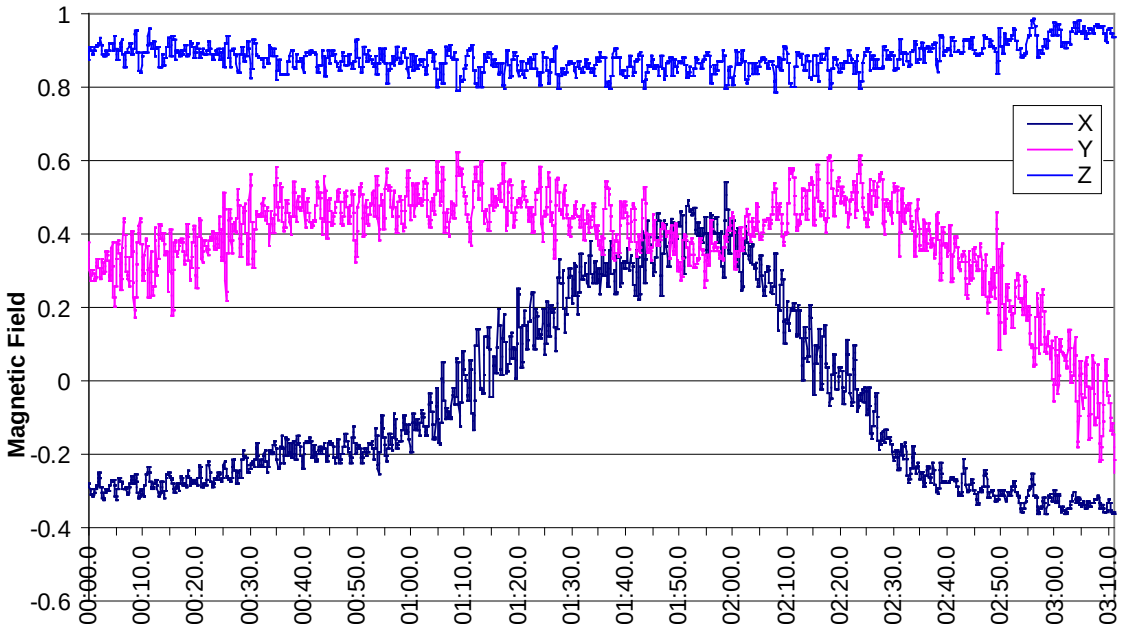

Figure 6-15: Buoy: Magnetic field components

These ‘pre-filtered’ magnetic field components were then passed through a Butterworth low-pass pass filter with a cut-off frequency of 0.005Hz. The resulting data is shown in Figure 6-16 below:

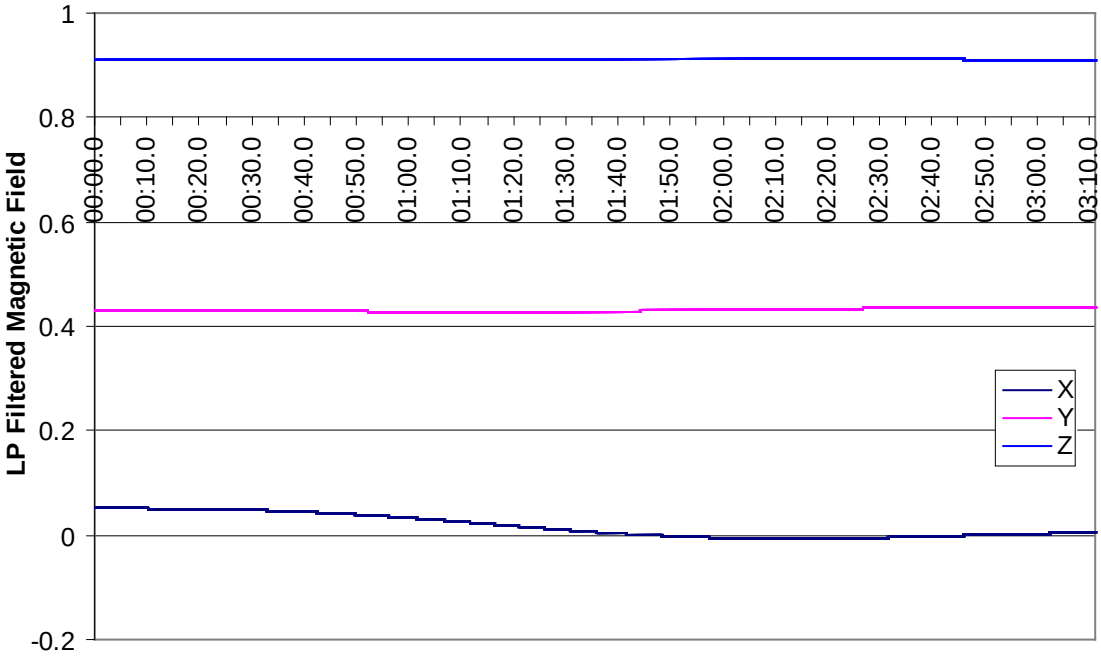

Figure 6-16: Buoy: Low-pass filtered magnetic field components

The pre-filtered magnetic field components were also passed through a Butterworth filter with a pass-band of 0.0625-0.625Hz, resulting in the data graphed below in Figure 6-17:

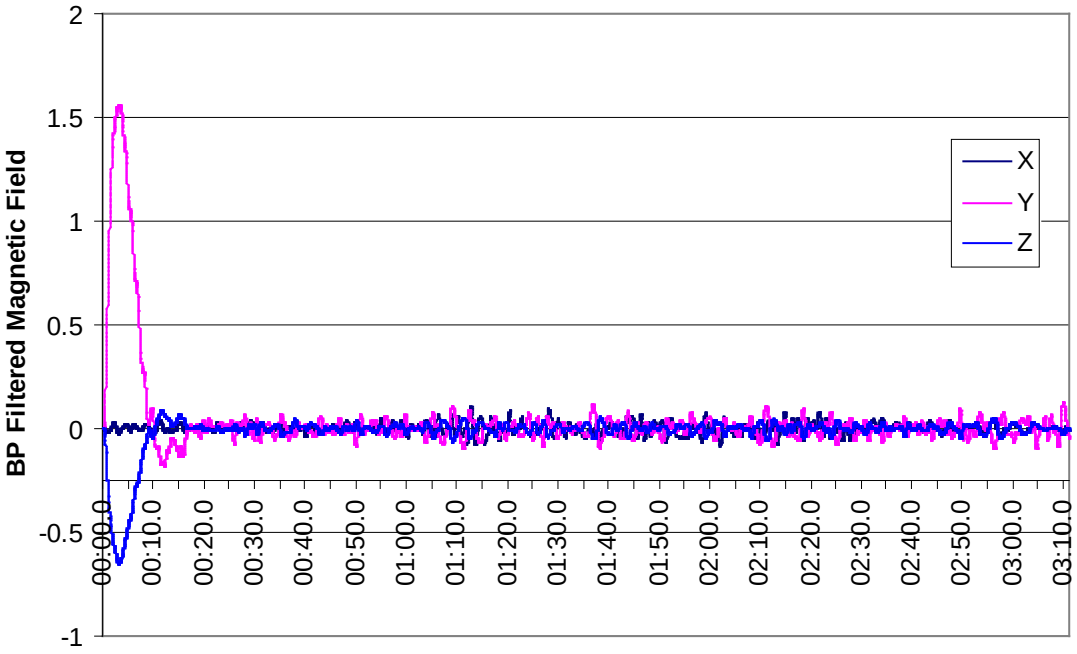

Figure 6-17: Buoy: Band-pass filtered magnetic field components

The initial, large-magnitude fluctuations in the apparent Y and Z axis magnetic field components occur whilst the filter is stabilising… the first 30 seconds of data in the data set cannot be used.

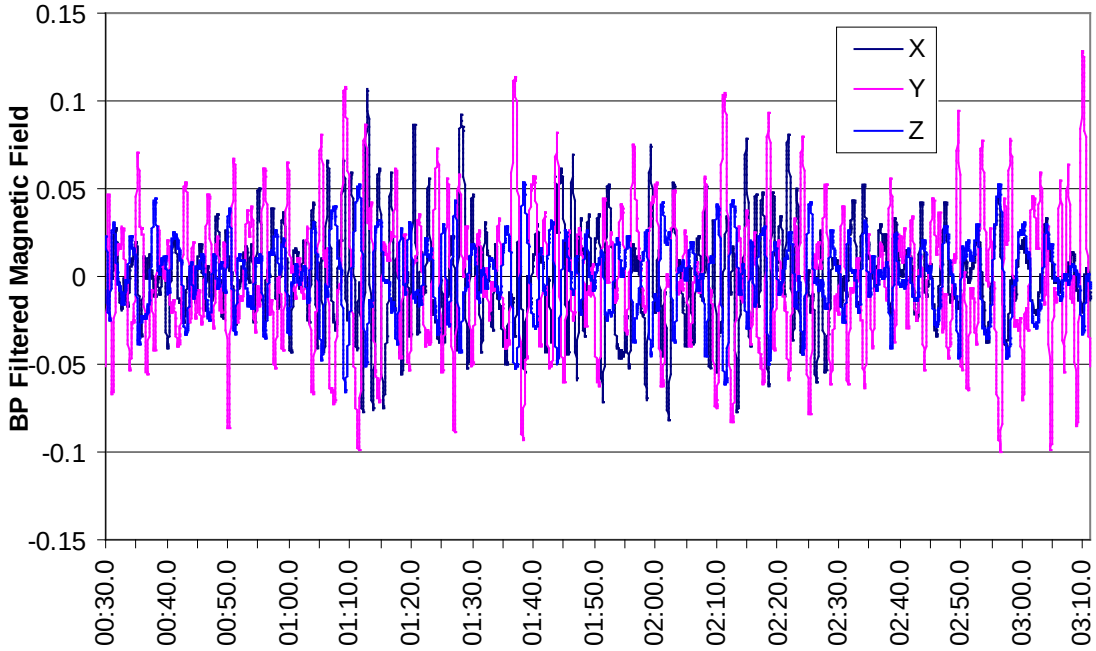

Figure 6-18: Buoy: Band-pass filtered magnetic field after 30 seconds

From the X and Y low-pass filtered readings, azimuth (heading) was calculated. The Y and Z band-pass-filtered readings were rotated about the X axis to correct for the dip angle of the magnetic field (24º from vertical) to calculate pitch in world-coordinates. In this particular case, this proved to be simple, since the azimuth is very close to due Magnetic North.

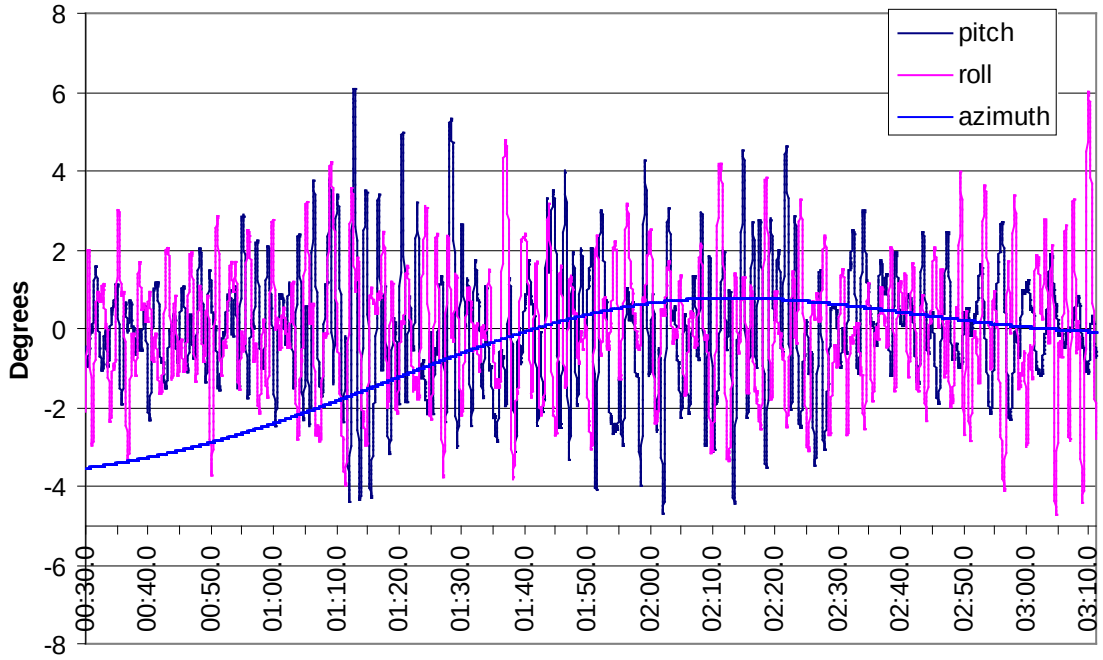

Figure 6-19: Buoy: Azimuth, pitch, and roll (.0625-.625Hz)

The data were also filtered using a pass-band of 0.0625-0.1Hz. The results of this are graphed below:

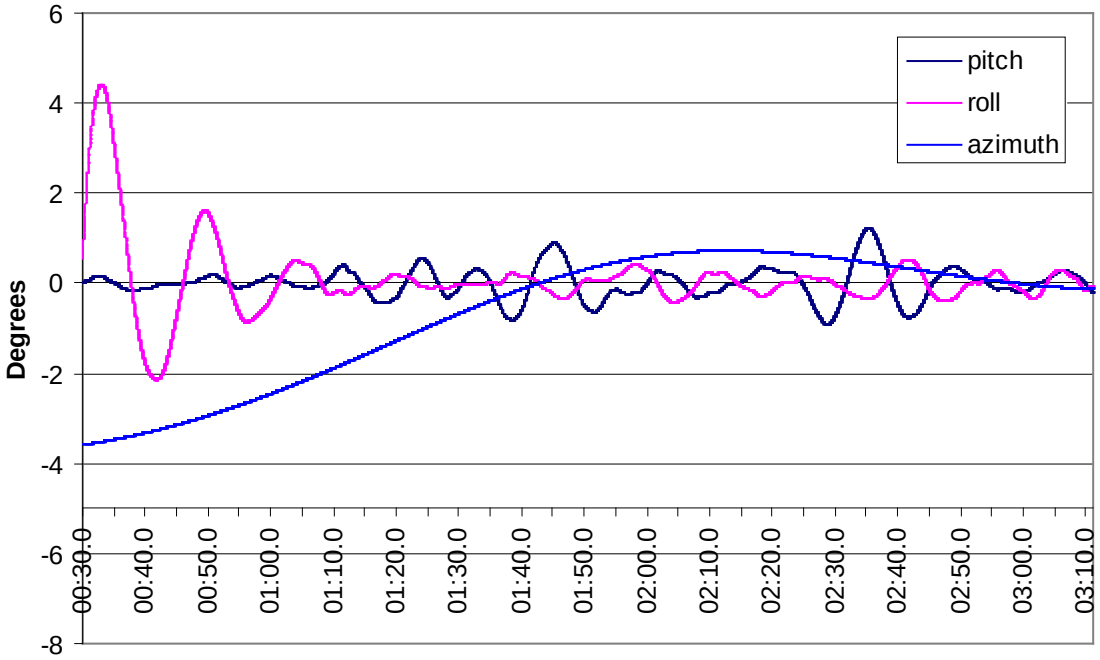

Figure 6-20: Buoy: Azimuth, pitch, and roll (.0625-0.1Hz)

Both the raw data and the analysed data is available in Appendix 1: Data & Programs as Microsoft Excel spreadsheets.

6.3 Boat Testing

On the 15 May 2003 data collection trip on the "Gwenelda", the sensor package was placed on the boat's deck. The resulting data set therefore gives a record of the motion of the boat itself.

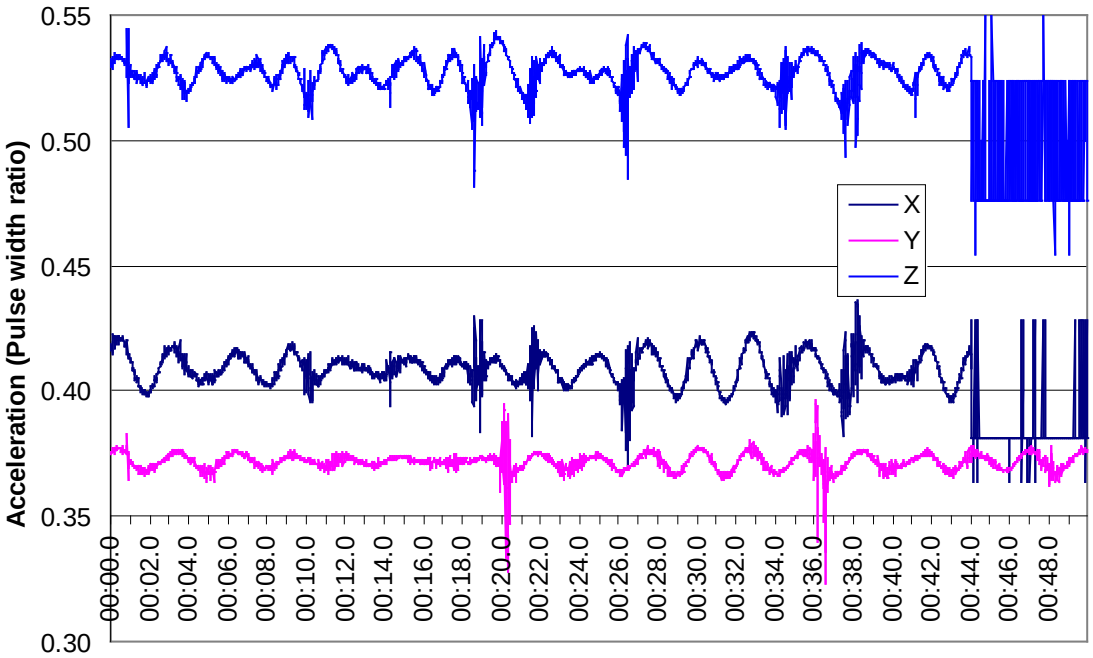

Figure 6-21: Boat: Raw acceleration data

The graph above shows the accelerometer data logged. Note that the X and Z axis data shows good data (a continuous waveform) for the first 44 seconds, then for the remainder of the data set exhibits the same fault as the buoy data in the previous section.

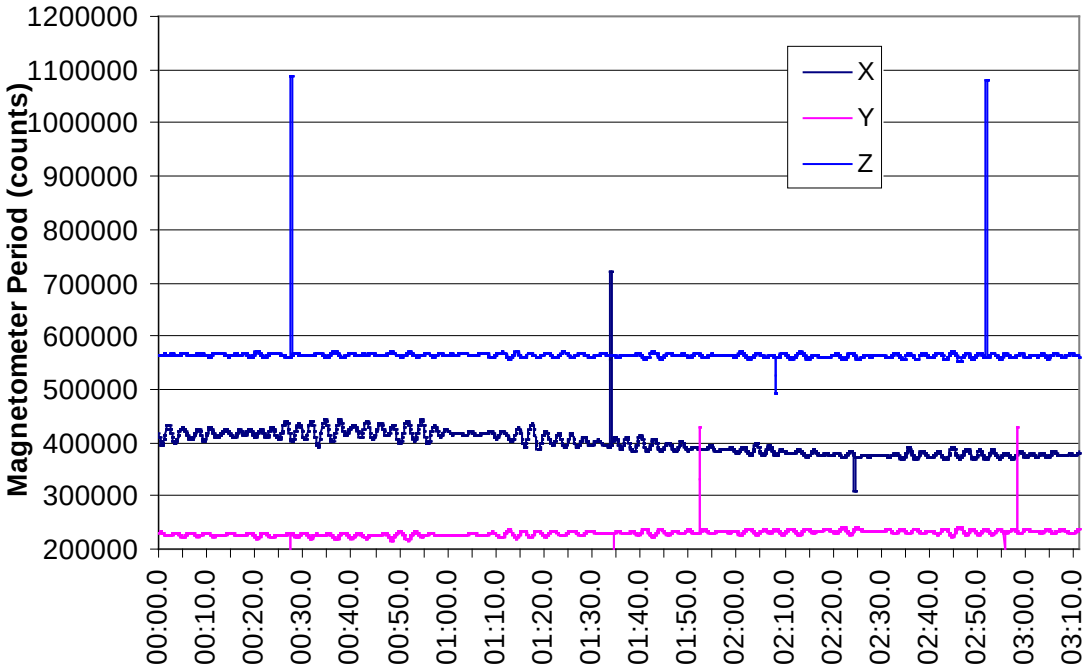

Figure 6-22: Boat: Raw magnetometer data

The same calibration settings were used to calibrate the magnetometers for this data set as for the buoy data.

The magnetic field data was processed in the same way as the buoy data, using a 0.0625-0.1Hz filter, resulting in the data graphed below in Figure 6-23:

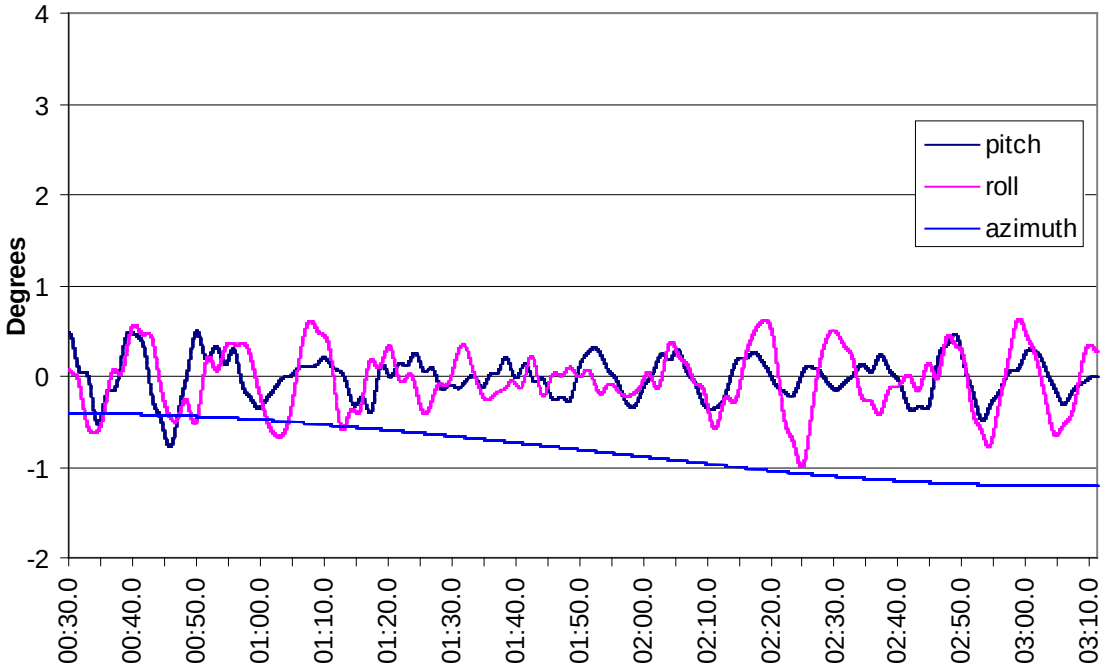

Figure 6-23: Boat: Azimuth, pitch, and roll

The initial, large-magnitude fluctuations in the apparent Y and Z axis magnetic field components occur whilst the filter is stabilising… the first 72 seconds of data in the data set cannot be used.

This is unfortunate, since the only valid accelerometer data is for the first 44 seconds of the data set.

Both the raw data and the analysed data is available in Appendix 1: Data & Programs as Microsoft Excel spreadsheets.

7 Future Directions

7.1 Radio link

The lack of feedback from the buoy and sensor package has meant that on many occasions no data was collected, or else erroneous data was collected unknowingly. Ideally, during experimentation real-time bidirectional data link would be maintained with a laptop computer.

This data link should

- Allow the experimenter to monitor data being output.
- Allow the laptop computer to log data, thus effectively removing limitations on logging rates and duration.
- Allow the experimenter to alter parameters (eg logging rate) interactively.
- Not compromise the environmental security of the sensor package
- Have low power consumption
- Have a range of up to 100m, so that the monitoring boat does not interfere with the buoy.
- Be easy to interface to the M16C microcontroller

The above suggest a radio data link via the M16C's serial port. Whilst IEEE 802.11b provides sufficient bandwidth and range, interfacing to the M16C would involve significant effort.

In the long term, it is envisaged that the final system will communicate its results back to a base station either via a cell phone link (for inshore applications) or via a satellite (for deployments in remote locations).

7.2 Buoy testing against known conditions

For this system to be useful, its accuracy needs to be proven. This may initially involve a mechanical system to emulate a wave of specified height and direction, but ultimately would require testing in the ocean and comparison of data with data from known good buoy.

7.3 Calculation Speed and Accuracy

Whilst it seems likely that the M16C's 256KB internal flash memory will be large enough to contain a program which does all the required calculations, it is still somewhat uncertain that a 16-bit CPU running at 16MHz will be sufficiently fast to perform the large amounts of floating point arithmetic required.

It may be possible to use suitable algorithms to replace many (or even all) of the most-used floating point calculations by integer arithmetic. This would result in a significant increase in processing speed.

There may be a trade-off possible between speed and accuracy… for example, reducing the order of digital filtering will reduce the amount of calculations required, but also reduce accuracy of the results. In this case, it is necessary to determine the sensitivity of the calculations' accuracy to the order of the filters to determine the minimum acceptable order.

It appears that magnetometer calibration, for example, is not critical to accuracy of wave measurement. It may be that fixed calibration settings may be adequate. Another trade-off is the location of the calculations: the more calculation that can be done on the buoy, the less data will need to be transmitted. This may consequently have a large impact on power consumption.

For example, a typical output from a wave recording system is a wave spectrum calculated via a Fast Fourier Transform (FFT). The input to the FFT is the series of surface displacement (height) readings. Thus, all height readings will need to be available at the location where the FFT is calculated. If the FFT is calculated at a base station rather than on the buoy, then all height readings will need to be transmitted to the base station, and consequently there will be a great deal of radio traffic, which may in turn use a great deal of power, and perhaps also be expensive monetarily.

If the transform is calculated on the buoy, then only the output of the FFT will need to be transmitted. It may be worth the cost, both in money and power terms, to use a more powerful processor, or perhaps a second M16C, on the buoy.

7.4 Power consumption

Whilst the M16C and the sensor datasheets suggest that considerable power savings might be possible, no investigation of this has been done.

Given the intended application, and consequently power being provided by solar cells, minimal power usage is a desirable property.

7.5 Hull designs

The prototype system has been tested on a buoy which includes fins in the water to ensure that the buoy's motion as closely as possible resembles the motion of the water it is floating in.

The intended environment for the device is on a boat-like autonomous vessel. Since this vessel is designed to move through the water, it will not follow the motion of the surface water particles accurately. Therefore it may be necessary to model the vessel's hydrodynamic behaviour to correct for inaccuracies induced in the sensors' motion by the boat not following the wave surface exactly.

Conversely, it may be possible to take advantage of the boat's controllability to provide better results (eg turn it into wind and command the propulsion system to maintain zero speed relative to the water).

7.6 Dedicated hardware design

The prototype, whilst it provides flexibility and easy modification, lacks robustness, and incudes many unused components (eg 7-segment LED displays).

A dedicated hardware design would include all the sensors and the microcontroller on a single PCB, providing a cheaper, stronger, more reliable device. The radio link mentioned earlier might also be included on the same PCB.

7.7 Sensor calibration

When deployed in the buoy, the automatic calibration system as described in section 4.1.3.3 failed to work. This was because the system required data points from 6 substantially different orientations. In the prevailing climate, the buoy's motion was close to a circular arc… that is, because waves were only coming from one direction, it was rotating in only one plane. The orientations were not different enough, over a short enough timeframe, to allow the algorithm to work.

A mechanical device to alter the orientation of the magnetic sensors may be needed to allow automatic calibration, especially in relatively small seas from a single direction. Alternatively, if deployed on an autonomous vessel, the vessel itself might turn to provide different orientations.

Alternatively, the low-pass filtered magnetic field data may be used to calibrate the sensors. The low-pass filter provides a virtual Z sensor that is always exactly vertical, along with two virtual X and Y sensors that are orthogonal to, and rotate about, the Z axis. It follows that the magnetic field apparent on the virtual vertical magnetometer should always be equal to the cosine of the angle of dip (the angle between the magnetic field vector and the vertical).

7.8 Pre-filtering

Several attempts were made to 'pre-filter' the data automatically to remove the spikes (see Figure 6-2). However, this proved to be extremely difficult... some of the spikes are quite small in amplitude, and difficult to distinguish from rapid changes in orientation of the sensors.

One approach might be to only remove the very large amplitude spikes, and leave the smaller amplitude spikes to be attenuated by the digital filtering which follows.

It may be that in buoy data, where rapid changes of orientation are unlikely, it may be much easier to distinguish spikes from data.

Another approach is to reduce the number of TimerB counts per magnetometer cycle; at present, the magnetometer signals are divided by 2048 (section 4.4.3), and the M16C uses the *f8* (500KHz) clock to measure the length of each cycle. This can be changed to use the *f32* clock (125KHz). By also reducing the hardware from 2048 to 512, the frequency of the magnetometer signals received by the microprocessor would be increased. The overall reduction in counts/cycle resolution by a factor of 16 would prevent overflow of the timer counters from occurring. Whilst this would add somewhat to the workload of the CPU, and would reduce the resolution of the resulting count, the problem should be solved.

8 Conclusions

This project demonstrates that detection and measurement of attitude and motion of a buoy by the use of low-cost magnetometers and accelerometers is achievable. Still to be determined is whether this can be done in real-time, and at reasonable cost in terms of power consumption. However, this does seem likely; if not immediately, then within the near future as processor speeds continue to increase, and power consumption continues to decrease.

It may be that this approach is applicable to other attitude measurement areas where, like buoys, the motion and attitude are constrained. For example, it may be possible to survey a section of road with some accuracy, simply by driving over it.

9 Bibliography

[Airy 1845] Airy G B, 1845, Tides and Waves, Encycl. Metrop., London.

[Allender 1989] Allender J, Andunson T, Barstow S F, Bjerken S, Krogstad H E, Steinbakke P, Vartdal L, Borgman L E, Graham C, 1989, The WADIC project: A comprehensive field evaluation of directional wave instrumentation, Ocean Eng., 16: 505-536.

[Alpers 1981] Alpers W R, Ross D B, Rufenach C L, 1981, The detectability of ocean surface waves by real and synthetic aperture radars; J. Geophys. Res., 86, 6481-6498

[Analog Web] http://products.analog.com/products/info.asp?product=ADXL202

[Anctil 1993] Anctil F, Donelan M A, Forristall G Z, Steele K E, Ouellet Y, 1993, Deep-water field evaluation of the NDBC-SWADE 3m discus directional buoy, J. Atmos. Oceanic Tech. 10, 97-112.

[Barber 1948] Barber N F, Ursell F, 1948, The generation and propagation of ocean waves and swell, Phil. Trans. Royal Soc. Lond., A, 240, 527-560

[Barber 1963] Barber N F, 1963, The directional resolving power of an array of wave recorders, In: Ocean Wave Spectra., Prentice-Hall, 137-150.

[Barber 1969] Barber N F, Ghey G, 1969, Water waves, ISBN: 0851090605

[Barrows 1996] Barrows A K, Gebre-Egziabher D, Hayward R, Xia R, Powell J D, 1996, GPS-Based Attitude and Guidance Displays for General Aviation, IEEE Emerging Technologies and Factory Automation '96, Kauai, HI

[Barton 1997] C.E. Barton, 1997, International Geomagnetic Reference Field: The Seventh Generation, J. Geomag. Geoelectr. 49, 123-148.

[Bascom 1980] Bascom W, 1980, Waves and Beaches, ISBN: 0385148445

[Beal 1986] Beal R C, Gerling T W, Irvine D E, Monaldo F M, Tilley D G, 1986, Spatial variations of ocean wave directional spectra from the seasat synthetic aperture radar, J. Geophys. Res., 91, 2433-2449.

[Black 1981] Black K P, Helay T R, 1981, Computer programs for wave analysis, wind wave generation, wave refraction diagrams, and fast Fourier analysis,

[Borgman 1977] Borgman L E, 1977, Directional Wave Spectra from Wave Sensors, In Ocean Wave Climate Symposium

[Borgman 1993] Borgman L E, Petrakos M, Li C, 1993, Evolutionary Fourier Analysis of Wave Data, In Ocean Wave Measurement and Analysis pp708-725

[Borgman 1998] Borgman L E, 1998, Directional Wave Polyspectra Beyond Stationarity, Proc. Offshore Technology Conf., OTC 8660

[Brisette 1994] Brisette F P, Tsanis I K, 1994, Estimation of wave directional spectra from pitch-roll buoy data, Jour. Waterway, Port, Coastal and Ocean Eng., 120: 93-115.

[Carvalho 2000] Carvalho J L B, Parente C E, 2000, Directional wave measurements using a slope array system., App Ocean Res (22) 95-101

[Chaffin 1993] Chaffin J N, Bell W, O'Neil K, Teng C-C, 1993, Design and Testing of the NDBC Wave Processing Module, In Ocean Wave Measurement and Analysis pp 277-286

[Datawell Web] http://www.datawell.nl/

[Davis 1977] Davis R, Davis L, Regier A, 1977, Methods for estimating directional wave spectra from multi-element arrays, Journal of Marine Research, pp 453-477.

[Draper 1986]	Draper L, 1986, Wave Measurements at North Atlantic weather stations India and Juliet in the 1970s, IOS Report No 222
[Earle 1979]	Earle M D, Malahoff A, 1979, Ocean Wave Climate, ISBN: 0-306-40079-0
[Earle 1993]	Earle M D, Orton R H, Selsor H D, Steele, K E, 1993, A Sonobuoy-Sized Expendable Air-Deployable Directional Wave Sensor, In Ocean Wave Measurement and Analysis pp302-315
[Ewing 1987]	Ewing J A, Laing A K, 1987, Directional spectra of seas near full development, J. Phys. Oceanogr. 17, 1696-1706.
[Gebre-Egziabher 2000]	Gebre-Egziabher D, Elkaim G H, Powell J D, Parkinson B W, 2000, A Gyro-Free Quaternion-Based Attitude Determination System Suitable for Implementation Using Low Cost Sensors, IEEE PLANS, San Diego, CA.
[Gnanadesikan 1993]	Gnanadesikan A, Terray E A, 1993, A comparison of three wave-measuring buoys, In Ocean Wave Measurement and Analysis pp 287-301
[Hanson 1997]	Hanson K L, Hara T, Bock E J, Karachintsev A B, 1997, Estimation of directional wave spectra from a towed research catamaran, J. Atmos. Oceanic Tech. 14, 1467-1482.
[Haug 1993]	Haug O, Krogstad H E, 1993, Estimation of directional spectra by ML/ME methods, In Ocean Wave Measurement and Analysis pp 394-405
[Hayward 1998]	Hayward R C, Powell J D, 1998, Real Time Calibration of Antenna Phase Errors for Ultra Short Baseline Attitude Systems, ION GPS '98 - Nashville, Tennessee
[Hidy 1971]	Hidy G M, 1971, The waves; the nature of sea motion, New York, Van Nostrand Reinhold Co
[Hofmann-Wellenhof 1994]	Hofmann-Wellenhof B, Lichtenegger H, Collins J, 1994, GPS Theory & Practice, ISBN: 3-211-82591-6
[Howell 1993]	Howell G L, 1993, Design of an in-situ directional wave gauge for one year deployments, In Ocean Wave Measurement and Analysis pp 264-276
[Huang 1998]	Huang M-C, Chen J-Y, 1998, Wave Direction Analysis from Data Buoys, Ocean Engng 25, No 8, pp621-637
[Hurn 1993]	Hurn J, 1993, Differential GPS Explained, Trimble Navigation Ltd
[Hwang 1993]	Hwang P A, Trizna D B, Wu J, 1993, Spatial measurements of short wind waves using a scanning slope sensor., Dyn. Atmos. Oceans, 20, 1-23
[Hwang 1997a]	Hwang P A, 1997, A study of the wavenumber spectra of short water waves in the ocean. Part II: Spectral model and mean square slope., J. Atmos. Oceanic Technol.14, 1174-1186.
[Jeffreys 1924]	Jeffreys H, 1924, On the formation of waves by wind, Proc. Roy. Soc., A, 107, 189-206.
[Jeffreys 1925]	Jeffreys H, 1925, On the formation of waves by wind II, Proc. Roy. Soc., A, 110, 341-347.
[Kaplan 1996]	Kaplan E D, 1996, Understanding GPS -- Principles & Applications, ISBN: 0-89006-793-7
[Keulegen 1940]	Keulegen G H, Patterson G W, 1940, Mathematical theory of irrotational translation waves, National Bureau of Standards, Rep. No. 1272, Washington DC, 47-101.
[Key 1999]	Key K W, Born G H, Leaman K D, Vertes P, 1999, A New GPS Data Processing Algorithm for the Positioning of Oceanographic Experiments, J Atmos & Oceanic Tech, Aug 1999, pp1127-1137
[Kinsman 1965]	Kinsman B, 1965, Wind waves, Prentice-Hall

[Kim 1993] Kim T, Lin L, Wang H, 1993, Comparison of directional wave analysis methods, In Ocean Wave Measurement and Analysis pp 554-568

[Kobune 1986] Kobune K, Hashimoto N, 1986, Estimation of directional spectra from the Maximum Entropy principle, Proc. 5th Intern. Conf. On Offshore mechanics and Arctic Engineering, Tokyo, 80-85.

[Korteweg 1895] Korteweg D J, de Vries G, 1895, On the change of long waves advancing in a rectangular canal and a new type of long stationary waves, *Phil. Mag.*, **5**, 422

[Krogstad 1988a] Krogstad H E, 1988, Maximum likelihood estimation of ocean wave spectra from general arrays of wave gauges, Modeling, Identification and Control, 9: 81-97. &#9

[Krogstad 1988b] Krogstad H E, Gordon R L, Miller M C, 1988, High-resolution directional wave spectra from horizontally mounted acoustic current meters, J. Atmos. Oc. Tech. 5, 340-352.

[Krylov 1966] Krylov V I, Shulgina E T, 1966, Manual on a numerical integration. Moscow, Nauka, 1-371 (in Russian).

[Leick 1995] Leick A, 1995, GPS Satellite Surveying (2nd Ed), ISBN: 0-471-30626-6

[Lefevre 1993] Lefevre H, 1993, The fibre-optic gyroscope, Artech House

[LeMehaute 1976] LeMehaute B, An Introduction to Hydrodynamics and Water Waves. Springer-Verlag, 1976., 1976, An Introduction to Hydrodynamics and Water Waves, ISBN: 0387072322

[Long 1979] Long R B, Hasselmann K, 1979, A variational technique for extracting directional spectra from multicomponent wave data, Jour. Phys. Ocean., 9: 373-381.

[Longuet-Higgins 1963] Longuet-Higgins M S, Cartwright D E, Smith N D, 1963, Observations of the directional spectrum of sea waves using the motions of a floating buoy, In: Ocean Wave Spectra, Prentice-Hall, 111-136.

[Luethi 2000] Luethi P, Moser T, 2000, Low Cost Inertial Navigation System, http://www.electronic-engineering.ch/study/ins/ins.html

[Markley 1988] Markley F L, 1988, Attitude Determination using Vector Observations and the Singular Value Decomposition, J Astronautical Sc, Vol 36, No 3, pp245-258

[Massel 1996] Massel S R, 1996, Ocean surface waves: their physics and prediction, ISBN: 9810216866

[McLeish 1980] McLeish W, Ross D, Shuchman R A, Teleki P G, Hsiao S V, Shemdin O H, and Brown W E Jr, 1980, Synthetic aperture radar imaging of ocean waves: comparison with wave measurements, J. Geophys. Res. 85, 5003-5011.

[Meindl 1992] Meindl E A, Hamilton G D, 1992, Programs of the national data buoy center, Bull. Am. Meteor. Soc. 73, 985-993.

[Melville 2002] Melville W K, Matusov P, 2002, Distribution of breaking waves at the ocean surface., Nature, 417, 58 - 63

[Mettlach 1993] Mettlach T, Gilhousen D, 1993, Instrumented Buoy Network Response to Ocean Swell, In Ocean Wave Measurement and Analysis pp 28-44

[Miche 1944] Miche M, 1944, Mouvements ondulatoires de la mer en profondeur constante ou decroissante, Annales des Ponts et Chaussees.

[Michell 1893] Michell J H, 1893, On the highest gravity waves on deep water, Philos. Mag, 56 (5), 430

[Mitsuyasu 1975] Mitsuyasu H, Tasai F, Suhara T, Mizuno S, Ohkusu M, Honda T, Rikiishi K, 1975, Observations of the directional spectrum of ocean waves using a cloverleaf buoy, J. Phys Oceanogr. 5, 750-760.

[National 1963] National Academy of Sciences Conference (Eds), 1963, Ocean Wave Spectra-Proceedings of a Conference ; NY, Prentice Hall, 1963, 357 pp, Compendium of wave spectra research by 40 well-known scientists & engineers.

[NDBC Web] NDBC, NDBC Web page, http://www.ndbc.noaa.gov

[National 1995] National Research Council, 1995, The Global Position System: A Shared National Asset, ISBN: 0-309-05283-1

[Noble 1996] Noble R, 1996, A new direction in orientation, Electronics World, pp40-44

[Noble 1997a] Noble R, Risk D, 1997, True orientation, Electronics World, pp197-200

[Noble 1997b] Noble R, 1997, Self-calibrating Compass, Electronics World, pp630-633

[Nwogu 1987] Nwogu O U, Mansard E P, Miles M D, Isaacson M, 1987, Estimation of directional wave spectra by the maximum entropy method, In: IAHR seminar : Wave analysis and generation in laboratory basins, 363-376.

[Qin 1992] Qin X, Gourevitch S, Ferguson K, Kuhl M, Ladd J, 1992, Dynamic short baseline calibration and attitude determination using Ashtech 3DF system, Proc 6th Int geodeitc symp on satellite positioning Mar 17-20 1992, Defense Mapping Agency

[OpenU 1994] Open University, 1994, Waves, Tides, and Shallow-water Processes, Pregamon, ISBN: 0-08-036371-7

[O'Reilly 1996] O'Reilly W C, Herbers T H C, Seymour R J, Guza R T, 1996, A comparison of directional buoy and fixed platform measurements of Pacific swell, J. Atmos. Oceanic Tech. 13, 231-238.

[Panicker 1970] Panicker N, Borgman L E, 1970, Enhancement of directional wave spectrum estimates (1974), Proceedings, 14th Coastal Engineering Conference, No. 3432, Woods Hole Oceanog. Inst. MA, Chapter 14, pp. 258-279

[Rabiner 1975] Rabiner, L R, Gold, B, Theory and application of digital signal processing, Prentice-Hall (1975), ISBN: 0139141014

[Rufenach 1991] Rufenach C, Olsen R B, Shuchman R A, Russel C A, 1991, Comparison of aircraft synthetic aperture radar and buoy spectra during the Norwegian Continental Shelf experiment of 1988, J. Geophys. Res. 96, 10423-10441.

[Sanford 1999] Sanford T B, Carlson J A, Dunlap J H, Prater M D, Lien R-C, 1999, An Electromagnetic Vorticity and Velocity Sensor for Observing Finescale Kinetic Fluctuations in the Ocean, Bull AMS Nov 1999, pp1647-1667

[Scarborough 1958] Scarborough J B, 1958, The gyroscope: Theory and Applications, NY Interscience

[Seymour 1993] Seymour R, Castel D, McGehee D, Thomas J, O'Reilly W, 1993, New Technology in Coastal Wave Monitoring, In Ocean Wave Measurement and Analysis pp 105-123

[Shay 1994] Shay L K, Walsh E J, Zhang P C, 1994, Orbital velocities induced by surface waves, J. Atmos. Oceanic Tech. 11, 1117-1125.

[Simpson 1969] Simpson J H, 1969, Observations of the directional characteristics of sea waves, Geoph. Jour. Roy. Astr. Soc., 17: 93-120.

[Speake Web] http://www.speakesensors.com/products.php

[Steele 1977] Steele K, Johnson A, 1977, Data Buoy Wave Measurements, In Ocean Wave Climate Symposium.

[Steele 1991] Steele K E, Earle M D, 1991, Directional ocean wave spectra using buoy azimuth, pitch, and roll derived from magnetic field components, IEEE J. Oceanic Engng. 16(4), 427-433.

[Steele 1992] Steele K E, Teng C C, Wang D W C, 1992, Wave direction measurements using pitch-roll buoys, Ocean Eng., 19(4): 349-375.

[Steele 1993] Steele K E, Mettlach T, 1993, NDBC Wave Data – Current and Planned, In Ocean Wave Measurement and Analysis pp 198-207

[Stiglitz 1986] Stiglitz M R, 1986, The global positioning system, Microwave J., 34-59.

[Stokes 1847] Stokes G G, 1847, On the theory of oscillatory waves, Trans. Cambridge Philos. Soc., 8, 441-473.

[Stokes 1880] Stokes G G, 1880, On the theory of oscillatory waves, Trans. Cambridge University Press, London.

[Tauxe Web] Tauxe L, http://sorcerer.ucsd.edu/es160/lecture8/web6/node6.html

[Teague 1979] Teague C C, 1979, Synthetic Aperture HF Radar Wave Measurement Experiments, In Ocean Wave Climate, pp203-220

[Trevorrow 1995] Trevorrow M V, 1995, Measurement of Ocean Wave Directional Spectra Using Doppler Side-Scan Sonar Arrays, J. Atmos. Oceanic Tech. 12, 603-616.

[Tricker 1964] Tricker R A R, 1964, Bores, Breakers, Waves & Wakes, Elsevier

[Trizna 1977] Trizna D B, Moore J C, Headrick J M, Bogle R W, 1977, Directional sea spectrum determined using HF Doppler radar techniques, IEEE Trans., AP25: 4-11.

[Trizna 1980] Trizna D B, Bogle R W, Moore J C, Howe C M, 1980, Observation by HF radar of the Phillips resonance mechanism for generation of wind waves, J Geophys Res (85) 4946.

[Tucker 1989] Tucker M J, 1989, Interpreting directional data from large pitch-roll-heave buoys, Ocean Eng., 16: 173-192.

[Tucker 1991] Tucker M J, 1991, Waves in ocean engineering: Measurement, analysis, interpretation, ISBN: 0-13-932955-2

[Tucker 1993] Tucker M J, 1993, Recommended standard for wave data sampling and near-real-time processing, Ocean Engng. 20, 459-474.

[Tyler 1974] Tyler G L, Teague C C, Stewart R H, Peterson A M, Munk W H, Joy J W, 1974, Wave directional spectra from synthetic aperture observations of radio scatter, Deep-Sea Res., 21: 989-1016.

[van der Hulst 2001] Van der Hulst F J, 2001, SRV Goodwill: A Vehicle for Research, Proc NACCQ Conf, Napier, New Zealand.

[Wang 1993] Wang D W, Teng C C, Ladner R, 1993, Buoy directional wave measurements using magnetic field components, In Ocean Wave Measurement and Analysis pp 316-329

[Wiegel 1960] Wiegel R L, 1960, A presentation of cnoidal wave theory for practical applications, DJ. Fluid. Mech., 7, 273-286.

[Young 1985] Young I R, Rosenthal W, Ziemer F, 1985, A Three Dimensional Analysis of Marine Radar Images for the Determination of Ocean Waves Directionality and Surface Currents. J. Geophys. Res. Vol. 90, pp. 1049-1059.

[Young 1994] Young Ian R, 1994, On the measurement of directional wave spectra, Applied Ocean Res., 16: 283-294.

[Young 1999] Young I R, 1999, Wind generated ocean waves, ISBN: 0080433170

10 Further Reading

Arribas M.A., Egozcue J J, 1994, Normalized maximum-likelihood estimators of the directional wave spectrum, J. Atmos. Oceanic Technol. 12, 668-673.

Atanassov V, Rosenthal W, Ziemer F, 1985, Removal of Ambiguity of Two-Dimensional Power spectra obtained by processing ship radar images of ocean waves, J. Geophys. Res. 90, 1061-1067.

Audunson T, Barstow S F, Krogstad H E, 1982, Analysis of wave directionality from a heave, pitch and roll buoy operated offshore Norway, Sci. Engng., 7, 291-319.

Banner M L, 1990, Equilibrium spectra of wind waves, J Phys Oceanog; 20:966-84

Barber N F, 1954, Finding the direction of travel of sea waves, Nature, 174, 1043-1050.

Barber N F, 1958, Optimum arrays for direction finding, N.Z.J. Sci., 1, 35-51.

Barber N F, 1958, Some relations to be expected between the directional spectra of swell observed at different times and places on the ocean, N.Z.J. Sci. 1, 330-341.

Barber N F, 1959, A proposed method of surveying the wave state of the open ocean, N.Z.J.Sci. 2, 99-108.

Barrick D E, Lipa B J, 1979, Ocean Surface Features Observed by HF Coastal Ground-Wave Radars: a Progress Review, In Ocean Wave Climate, pp129-152

Barrick D E, Lipa B J, 1979, A Compact Transportable HF Radars for Directional Coastal Wave Field Measurements, In Ocean Wave Climate, pp153-201

Barstow S F, Krogstad H E, 1984, General analysis of directional ocean wave data from heave/pitch/roll buoys, Modeling, Ident. Control, 5:47-70.

Barstow S F, Guddal J, 1987, A global survey on the need for and application of directional wave information., Marine Meteorology & related Oceanog. Activities. Report No. 19 WMO/TD No. 209

Barstow S F, Ueland G, Krogstad H E, Fossum B A, 1991, The WaveScan second generation directional wave buoy, IEEE J. Oceanic Engng., 17, 254-266.

Barstow S F, Haug O, v.d. Vlugt T, 1994, A field validation of a directional Waverider in a SEAWATCH buoy, Proc. Oceans 94 OSTAS conf., Brest, 32-37.

Beal R C, 1991, Directional ocean wave spectra, Johns Hopkins University Press. 30-33.

Beardsley R C, Enriquez A G, Friehe C A, Alessi C A, 1997, Intercomparison of aircraft and buoy measurements of wind and wind stress during SMILE, J. Atmos. Oceanic Technol. 14, 969-977.

Benoit M, 1992, Practical comparative performance survey of methods used for estimating directional wave spectra from heave-pitch-roll data, Proc 23rd intl conf coastal engng, Venice

Benoit M, Teisson C, 1994, Laboratory comparison of directional wave measurements systems and analysis techniques, Proc 24th intl conf coastal engng (ICCE), Kobe, 42-56.

Berger F B, 1957, The design of airborne Doppler velocity measuring systems, IRE Trans. Aeronaut. Nav. Elect. 157-175.

Berger F B, 1957, The nature of Doppler Velocity Measurement, IRE Trans. Aeronaut. Nav. Elect. 103-112.

Birch K N, Harrison E J, Beal S, 1976, A computer based system for data acquisition and control of scientific experiments on remote platforms, Oceans '76, 25B-1 - 25B-8.

Blair P M, 1974, Buoy for recording ocean wave height and period, Proc. Int. Symp. Ocean Waves Meas. Analy., 1, 254-263.

Bowden K F, White R A, 1966, Measurements of the orbital velocities of sea waves and their use in determining the directional spectrum, Geophys. J. R. astr. Soc. 12, 33-54.

Brigham E O, 1988, The Fast Fourier Transform and its Applications, Prentice Hall, 448 pp.

Briscoe M G, Goudriaan E, 1972, Research use of the Waverider buoy in deep water, Underwater J. 142-148.

Brisette F P, Tsanis I K, 1992, Maximum likelihood method techniques for directional analysis of heave-pitch-roll data, Proc. 3rd Int. Workshop on Wave Hindcasting and Forecasting., Montreal.

Bullock G N, Short I, 1985, Water particle velocities in regular waves, J. Waterway Port Coastal Ocean Engng. 111, 189-199.

Burdette E L, 1976, A study of the feasibility of using a triaxial magnetometer as an attitude sensor in a buoy mounted system for the measurement of ocean wave directional spectra, NDBC Technical Report.

Capon J, 1969, High-resolution frequency-wavenumber spectrum analysis, Proc. IEEE. 57, 1408-1418.

Cartwright D E, 1961, The use of directional spectra in studying the output of a wave recorder on a moving ship, In Ocean wave spectra, Prentice-Hall, 203-218.

Cartwright D E, Smith N D, 1964, Buoy techniques for obtaining directional waves from arrays at Adu Quir and Ras El-Bar, Egypt, Oceanology, Chapt 10, Marine Technology Society.

Chaffin J N, Bell W, Teng C C, 1992, Development of NDBC's Wave Processing Module, Proc. Mar. Tech. Soc., MTS '92, 2, 966-970.

Challenor P G, Srokosz M A, 1984, Extraction of wave period from altimeter data, Proc. Wkshp. ERS-1 Radar Altimeter Data Prod., 121-124.

Chaplin J R, 1977, Surface particle orbits in uniform waves, J. Waterway, Port, Coastal, Ocean Engng. 103, 205-213.

Chapman R D, Monaldo F M, 1991, The APL wave gauge system, JHU-APL report S1R-91U-041, Johns Hopkins University.

Chapman R D, Shay L K, Graber H C, Edson J B, Karachintsev A, Trump C L, and Ross D B, 1997, On the accuracy of HF radar surface current measurements: Intercomparisons with ship-based sensors, J. Geophys. Res., 102:C8, 18,737-18,748.

Chavez F, Herlien R, Thurmond G, Wright D, 1993, A novel ocean acquisition system for interdisciplinary science, MTS '93 Technol Req. Nineties Conf. Proc., 78-84.

Cooper C K, Forristall G Z, Hamilton R C, Ebbesmeyer C, , Utilization of offshore platforms for meteorological and oceanographic measurements, MTS J. 27, 10-23.

Cox C S, 1958, Measurements of slopes of high-frequency wind waves, J. Mar. Res., 16, 199-245.

Cox C, Deaton T, Webb S, 1984, A deep-sea differential pressure gauge, J. Atmos. Oceanic Technol. 1, 237-246.

Crisp G N, 1987, An experimental comparison of a shipborne wave recorder and a waverider buoy, Institute of Oceanographic Sciences Report No. 235. 181pp.

DeLeonibus P S, Simpson L S, 1972, Case study of duration-limited wave spectra observed at an open ocean tower, J. Geophys. Res. 77, 4555-4569.

DiMarco S F, Kelly F J, Zhang J, Guinasso N L Jr, 1995, Directional wave spectra on the Louisiana-Texas Shelf during Hurricane Andrew, J. Coastal Res. 21, 217-233.

Dobson E B, Monaldo F M, 1996, Radar altimeter wave height measurements, Remote sensing techniques for oceanographers., M Ikeda & F Dobson (eds), CRC Press.

Donelan M A, 1976, A method for the automatic measurement of wave frequency, J. Fisheries Res. Board Cda. 33, 2318-2322.

Donelan M A, Hamilton J, Hui W H, 1985, Directional spectra of wind-generated waves, Philos. Trans. Roy. Soc., A315: 509-562.

Donelan M A, Drennan W M, Magnusson A K, 1996, Non-stationary analysis of the directional properties of propagating waves, J. Phys. Oceanogr. 26, 1901-1914.

Donelan M A, Drennan W M, Terray E A, 1999, Wavenumber spectra of wind waves in the range of 1-50m, The wind-driven air-sea interface: electro-magnetic and acoustic sensing, wave dynamics and turbulent fluxes. Ed: M.L. Banner. Pub: Sch

Drennan W M, Donelan M A, Madsen N, Katsaros K B, Terray E A, Flagg C N, 1994, Directional wave spectra from a Swath ship at sea, J. Atmos. Oceanic Tech. 11, 1109-1116.

Drennan W M, Graber H C, Donelan M A, Terray E A, 1998, Directional wave measurements from the ASIS (Air-sea interaction spar) buoy, Proc. Oceans98, 414-418.

Driscoll F R, Lueck R G, Nahon M, 1998, The motion of a deep-sea remotely operated vehicle system. Part 1: Motion observations., Ocean Eng. (Submitted)

Driscoll F R, Lueck R G, Nahon M, 1998, The motion of a deep-sea remotely operated vehicle system. Part 2: Analytical model., Ocean Eng. (Submitted)

Dugan J P, Panichas S L, DiMarco R L, 1990, Decontamination of wind measurements from buoys subject to motions in a seaway, J. Atmos. Oceanic Tech. 8, 85-95.

Durden S L, Vesecky J F, 1985, A physical radar cross-section model for a wind-driven sea with swell, IEEE J. Oceanic Engng. OE-10, 445-451

Earle M D, Longman R W, 1983, An analysis of short pendulum heave sensors, Proc. Symp. on Buoy Technology, MTS and NOAA Data Buoy Centre, New Orleans.

Earle M D, Longman R W, 1986, An alternate hull pitch/roll system for use with NDBC DACT/DWA systems, MEC Systems Corp. (now Neptune Sciences, Inc.) report for National Data Buoy Center.

Earle M D, 1990, Evaluation and application of time series data from the NDBC prototype SWADE buoy, NDBC Technical Report.

Earle M D, Herchenroder B E, 1991, Investigation of filtering techniques for magnetometer-only determination of buoy heading, NDBC Internal Report.

Earle M D, Mettlach T R, 1996, Application of Wave Particle-Following Data Analysis to NDBC Directional Wave Data, National Data Buoy Center.

Elfouhaily T, Chapron B, Katsaros K, Vandemark D, 1997, A unified directional spectrum for long and short wind-driven waves, J. Geophys. Res. 102, 15781-15796.

Engen G, Krogstad H E, Barstow S F, 1994, Directional wave spectra by inversion of ERS-1 synthetic aperture radar ocean imagery, IEEE Trans. Geosci. Remote Sens., 32, 340-352.

Ewans K C, Kibblewhite A C, 1986, Spectral characteristics of ocean waves undergoing generation in New Zealand waters, 9th Australian Fluid mech. Conf. 1-4.

Ewing J A, 1986, Presentation and interpretation of directional wave data, Underwater technology, 12(3).

Ezraty R, , Using buoys and ships to calibrate ERS-1 altimeter and scatterometer, Proc. Wkshp, ERS-1 Wind Wave Calibration, 91-97.

Fenton J D, McKee W D, 1990, On calculating the lengths of water waves, Coastal Engineering., 14: 499-513.

Folsom R G, 1949, Measurements of ocean waves, Trans. Amer. Geophys. Union. 30, 691-699.

Ford J R, Timme R C, Trampus A, 1968, A new method for obtaining the directional spectrum of ocean surface gravity waves, IEEE Trans on Geoscience Electronics GE-6(4)

Foreman J W Jr, George E W, Jetton F L, Lewis R D, Thornton J R, Watson H J, 1966, 8C2-fluid flow measurements with a laser doppler velocimeter, IEEE J. Quantum Elec. QE2, 260-266.

Forget P, 1985, The wave field dynamics inferred from HF radar sea-echo, Ocean Surface, 257-262.

Forristall G Z, Ward E G, Cardone V J, Borgman L E, 1978, The directional spectra kinematics of surface gravity waves in Tropical Storm Delia., Jour. Phys. Oceanogr., 8: 888-909.,

Forristall G Z, Ewans K C, 1998, Worldwide measurements of directional wave spreading, J. Atmos. Oceanic Tech. 15, 440-469.

Gerling T W, 1992, Partitioning sequences and arrays of directional ocean wave spectra into component wave systems, J. atmos. Oceanic technol. 9, 444-458.

Gerstner J F, 1809, The Theory of Waves, Abh. koenigi. Bohm. Ges. Wissensch. 3, 1, 1408

Gilchrist A W R, 1966, The directional spectrum of ocean waves: an experimental investigation of certain predictions of the Miles-Phillips theory of wave generation, J. Fluid Mech., 25, 795-816.

Gilhousen D B, 1986, An accuracy statement for meteorological measurements obtained from NDBC moored buoys, Proc. MDS '86 Marine data systems Int. Symp. 198-204.

Gilhousen David B, Wang, 1998, Estimating Swell information for NDBC's Home Page, NDBC Technical Bulletin, 24 No 1, 11-12.

Gjessing D T, Hjelmstad J, 1986, Ocean waves and turbulence as observed with and adaptive coherent multifrequency radar, J. Geophys. Res. 91, 2461-2475.

Glad I K, Krogstad H E, 1992, A note on statistical properties of wave parameters from heave, pitch and roll buoys, J. Atmos. Oc. Tech. 9, 169-173.

Graber H C, Terray E A, Donelan M A, van Leer J, Drennan W M, 1995, A lightweight multi-spar buoy -- design and sea trials, RSMAS report 95-009.

Graber H C, Terray E A, Donelan M A, Drennan W M, Van Leer J, Peters D B, 2000, ASIS -- A new air-sea interaction spar buoy: design and performance at sea, J. Atmos. Oceanic Tech. 17, 708-720.

Grace R A, 1978, Surface wave heights from pressure records, Coastal Engng. 2, 55-67.

Guedes Soares C, Cavaco P, 1997, Analysis of directional spectra from the Portuguese coast, Proc. 27th IAHR Congress, San Francisco. Ed: E. Mansard.

Guillaume A., 1990, Statistical tests for the comparison of surface gravity wave spectra with application to model validation, J. Atmos. Oceanic technol. 7, 551-567.

Hale M R, Norrie D H, 1969, The analysis and calibration of the five-hole spherical pitot, Am. Soc. Mech. Engrs., 67-WA/FE-24.

Hamilton R C, Ward W G, 1974, Ocean Data Gathering Program – Quality and reduction of data, 6th Offshore Technology Conf., Houston, OTC 2108-A.

Hamilton G D, 1986, National data buoy center programs, Bull. Am. Metoer. Soc., 67, 411-415.

Hamilton G D, 1990, Guide to moored buoys and other ocean data acquisition systems, Report on Marine Science Affairs No 16, World Meteorological Org., Geneva.

Hammond D L, McClain C R, 1980, Spectral distortion inherent in airborne profilometer measurements of ocean wave heights, Ocean Engng. 7, 99-108.

Hashimoto N, Kobune K, Kameyama Y, 1987, Estimation of directional spectrum using the Bayesian approach and its application to field data analysis, The Port and Harbour Res. Inst., Rep. 26: 57-100.

Hashimoto N, 1997, Analysis of the Directional Wave Spectrum from Field Data, Adv. Coast. and Ocean Engin., 3, 103-143.

Hasselmann D E, Dunkel M, Ewing J A, 1980, Directional wave spectra observed during JONSWAP 1973, J.Phys. Oceanogr., 10, 1264-1280.

Hara T, Bock E J, Lyzenga D, 1999, In situ measurements of capillary-gravity wave spectra using a scanning laser slope gauge and microwave radars, J. Geophys. Res., 99, 1259-312602.

Hauser D, Caudal G, Rijckenberg G J, Vidal-Madjar D, Laurent G, Lancelin P, 1992, RESSAC: A new airborne FM/CW radar ocean wave spectrometer, IEEE Trans. Geosci. Remote Sensing, 30, 981-995.

Herbers T H C, Guza R T, 1990, Estimation of directional wave spectra from multicomponent observations, J. Phys. Oceanogr. 20, 1703-1724.

Herbers T H C, Lowe R L, Guza R T, 1991, Field verification of acoustic Doppler surface gravity wave measurements, J. Geophys. Res. 96, 17023-17035.

Holthuijsen L H, Smith D R, 1988, An evaluation of model estimates of ocean wave directions, Ocean engng. 15, 127-137.

Honda T, Mitsuyasu H, 1976, The statistical distributions for the elevation, velocity and acceleration of the surface of wind waves, Reports Res. Inst. Applied Mech. 31-48.

Hosom D S, Weller R A, Payne R E, Prada K E, 1995, The IMET (Improved Meteorology) Ship and buoy systems, J Atmos. Ocean Technol. 12, 527-540.

Hsu Y H L, 1986, Development of algorithms for use of a magnetometer measuring buoy pitch and roll motions, NDBC Technical Report DB-3505-3.

Hsu Y H L, 1986, A technique for the detection of inaccurate data being produced by the No-Hippy DWA system, NDBC Technical Report DB-3510.

Huang N E, Long S R, Tung C-C, Donelan M A, Yuan Y, Lai R J, 1992, The local Properties of Ocean Surface Waves by the Phase-Time Method, Geophysical Research Letters 19, 685-688.

Huang M-C, Chen J-Y, 1998, Wave Direction Analysis from Data Buoys, Ocean Engng 25, No 8, pp621-637

Huang N E, Shen Z, Long S R, 1999, A New View of Nonlinear Water Waves: The Hilbert Spectrum, Annu. Rev. Fluid Mech., 31, 417-457.

Hughes B A, Grant H L, Chappell R W, 1977, A fast response surface-wave slope meter and measured wind-wave moments, Deep-sea Res., 24, 1211-1223.

Hwang P A, Atakturk S, Sletten M, Trizna D B, 1996, A study of the wavenumber spectra of short water waves in the ocean, J. Phys. Oceanogr. 26, 1267-1285.

Hwang P A, Walsh E J, Krabill W B, Swift R N, 1997, Measuring Winds and Waves Using Altimeters, Proc. Waves 97.

Hwang P A, Teague W J, Jacobs G A, Wang D W, 1998, A statistical comparison of wind speed, wave height, and wave period derived from satellite altimeters and ocean buoys in the Gulf of Mexico region, J Geophys. Res. 103, 10451-10468.

Hwang P A, Wang D W, Walsh E J, Krabill W B, Swift R N, 2000, Airborne measurements of the wavenumber spectra of ocean surface waves. Part II: Directional distribution, J Phys. Oceanogr 30, 2768-2787

Ikeda, Motoyoshi / Dobson, Frederic W, 1995, Oceanographic Applications of Remote Sensing., ISBN: 0849345251

Isobe M, Kondo K, Horikawa K, 1984, Extension of MLM for estimating directional wave spectrum, Symp. Description and Modelling of Directional Seas, DHI and MMI, Copenhagen, 1-15.

Jackson F C, Walton W T, Peng C Y, 1985, A comparison of in Situ and airborne radar observations of ocean wave directionality, J. Geophys. Res. 90, 1005-1018.

Jackson F C, Walton W T, Baker P L, 1985, Aircraft and satellite measurement of ocean wave directional spectra using scanning-beam microwave radars, J. Geophys. Res. 90, 987-1004.

Jackson F C, Lyzenga D R, 1990, Microwave techniques for measuring directional wave spectra, II, 221-264.

Jefferys E R, Wareham G T, Ramsden N A, Platts M J, 1981, Measuring directional spectra with MLM, In Directional wave spectra applications., Weigel R L (ed) 203-219.

Kats A V, Spevak I S, 1980, Reconstruction of the sea-wave spectra from measurements of moving sensors, Izv. Acad. Sci. USSR, Atmos. Oceanic Phys. 16, 194-200.

Kenny J E, Uliana E A, Walsh E J, 1979, The surface contour radar, a unique remote sensing instrument, IEEE Trans. Microwave Theory, MTT-27, 1080-1092.

Kent E C, Taylor P K, Truscott B S, Hopkins J S, 1993, The accuracy of voluntary observing ships' meteorological observations- Results of the VSOP-NA, J. Atmos. Oceanic Technol., 10, 591-608.

Kjeldsen S P, 1989, The practical value of directional ocean wave spectra, JHU Tech. Dig. 11, 13-19.

Krogstad H E, 1989, Reliability and resolution of directional wave spectra from heave, pitch, and roll data buoys, In Directional Ocean Wave Spectra, Johns Hopkins University Press, pp66-71.

Krogstad H E, 1992, Calibration of the WAVESCAN Directional Wave Buoy, SINTEF Report STF-10-F92005. Available from Seatex A/S.

Krogstad H E, Barstow S F, Aasen S E, Rodriguez I, 1999, Some recent developments in wave buoy measurement technology, Coastal Engineering 37, 309-329

Kuik A J, van Vledder G Ph, Holthuijsen L H, 1988, A method for the routine analysis of pitch-and-roll buoy wave data, J. Phys. Oceanogr. 18, 1020-1034.

Laing A K, 1985, An assessment of wave observations from ships in southern oceans, J. Climate Applied Meteor. 24, 481-494.

Lawson L M, Long R B, 1983, Multimodal properties of the surface-wave field observed with pitch-roll buoys during GATE, J. Phys. Oceanogr. 13, 474-486.

Lipa B, 1990, Comparison of Hippy 40 and magnetometer-only systems on a 12-meter discus buoy, NDBC Technical Report.

Liu H T, Katsaros K B, Weissman M A, 1982, Dynamic response of thin-wire wave gauges, J. Geophys. Res., 87, 5686-5698.

Long R B, 1980, The statistical evaluation of directional spectrum estimates derived from pitch/roll buoy data, J. Phys. Oceanogr. 10, 944-952.

Long S R, Huang N E, Mollo-Christensen E, Jackson F C, Geernaert G L, 1993, Directional wind wave development, Manuscript.

Longuet-Higgins M S, 1962, The directional spectrum of ocean waves, and processes of wave generation, Proc. Roy. Soc., 265, 286-315.

Longuet-Higgins M, 1979, Spin and angular momentum in gravity waves, J. Fluid Mech., 97, 1-25.

Longuet-Higgins M S, 1985, Accelerations in steep gravity waves, Jour. Phys. Oceanogr., 15: 1570-1579.

Longuet-Higgins M S, 1986, Eulerian and Lagrangian aspects of surface waves, Jour. Fluid. Mech., 173, 683-707.

Lygre A, Krogstad H E, 1986, Maximum entropy estimation of the directional distribution in ocean wave spectra, Jour. Phys. Oceanogr., 16: 2052-2060.

Magoon O T, Hemsley J M, 1993, Ocean Wave Measurement and Analysis, ISBN: 0-87262-922-8

MacWhorter M A, Weller R A, 1991, Error in Measurements of Incoming Shortwave Radiation Made from Ships and Buoys, J. Atmos. Ocean. Tech., 8, 108

Maresca J W Jr, Georges T M, 1980, Measuring rms wave height and the scalar ocean wave spectrum with hf skywave radar, J. Geophys. Res. 85, 2759-2771.

Marom M, Shemer L, Thorton E B, 1991, Energy density directional spectra of a nearshore wave field measured by interferometric synthetic aperture radar, J. Geophys. Res. 96, 22125-22134.

Massel S R, Brinkman R M, 1998, On the determination of directional wave spectra for practical applications, App Ocean Res (20): 357-74

Mastenbroek C, de Valk C F, 2000, A semiparametric algorithm to retrieve ocean wave spectra from SAR, J Geophys Res (105)C2 3497-3516

Mathisen J, Bitner-Gregersen E, 1990, Joint distributions for significant wave height and wave zero-up-crossing period, Applied Ocean Res. 12, 93-103.

Mattie M G, Hsiao S V, Evans D D, 1981, Wave direction measured by four different systems, IEEE J. Oceanic Engng. OE-6, 87-93.

McClain C R, Chen D T, Hart W D, 1982, On the use of laser profilometry for ocean wave studies, J. Geophys. Res. 87, 9509-9515.

McClain C R, Huang N E, LaViolette P E, 1982, Measurements of sea-state variations across oceanic fronts using laser profilometry, J. Phys. Oceanogr., 12, 1228-1244.

McLaughlin D J, McIntosh R E, Pazmany A, Hevizi L, Boltniew E, 1991, A C-Band scatterometer for remote sensing the air-sea interface, IEEE Trans. Geosci. and Rem. Sensing, 29, 260-267.

McLeish W, Ross D B, 1983, Imaging radar observations of directional properties of ocean waves, J. Geophys. Res., 88, 4407-4419.

Michelena E, Elder F C, Soo H K, 1968, A triaxial flowmeter for wave motion measurements, Proc. 11th Conf. Great Lakes Res., 424-436.

Miller J H, Lynch J F, Chiu C-S, 1989, Estimation of sea surface spectra using acoustic tomography, J. Acoust. Soc. Am. 86, 326-345.

Mitsuyasu H, Honda T, 1974, The high frequency spectrum of wind-generated waves, J. Oceaongraphical Soc. Japan. 30, 185-198.

Mitsuyasu H, 1977, Measurement of the high-frequency spectrum of ocean surface waves, J. Phys. Oceanogr., 7, 882-891.

Mitsuyasu H, Tasai F, Suhara T, Mizuno S, Ohkusu M, Honda T, Rikiishi K, 1980, Observations of the power spectrum of waves using a cloverleaf buoy, Jour. Phys. Oceanogr., 10: 286-296.

Mitsuyasu H, Kusaba T, 1983, Directional wave spectra measured with a cloverleaf buoy during ARSLOE, IEEE J. Oceanic Engng. OE-8, 214- 220.

Mizuno S, 1976, Pressure measurements above mechanically generated water waves (I), Reports Res. Inst., XXIII, 113-129.,

Mollo-Christensen E, Jackson F C, Walsh E J, Hoge F, 1986, Oceanographic measurement capabilities of the NASA P-3 aircraft, Proc. Wkshp. ERS-1 Wind and Wave Calibration. 111-121.

Monaldo F, Lyzenga D R, 1986, On the estimation of wave slope- and height variance spectra from SAR imagery, IEEE Trans. Geosci. Remote Sens. GE-24, 543-551.

Monaldo F, 1988, Expected Differences Between Buoy and Radar Altimeter Estimates of Wind Speed and Significant Wave Height and their Implications on Buoy-Altimeter Comparisons, J. Geophys. Res., 93:C3, 2285-2302.

Moore M J, 1985, Radar sensing of the ocean, IEEE J. Oceanic Engng. OE-10, 84-113.

Muir L R, El-shaarawi A H, 1986, On the calculation of extreme wave heights: a review, Ocean Engng. 13, 93-118.

Munk W H, Wunsch C, 1979, Ocean acoustic tomography: a scheme for large scale monitoring, Deep-sea res. 26A 123-161.

Nagata Y, 1964, The statistical properties of orbital wave motions and their application for the measurement of directional wave spectra, J. Oceanogr. Soc. Jap. 19, 1-13.

Nagata Y, 1964, Observations of the directional wave properties, Coastal Engng. Japan, 7, 11-30.

Nagata Y, 1964, An electromagnetic current meter, J. Oceanogr. Soc. Japan. 20, 21-30.

NDBC, 1986, A study of hull-mooring data bases for wave measurement systems, Report No F-344-7. US Dept of Commerce, NDBC, NSTL, MS.

NDBO, 1978, Summary of NDBO wave measurement development activities, Report F-344-1. US Dept of Commerce, NDBC, NSTL, MS. 61-79.

Nichols C R, 1993, Operational characteristics of the Tampa Bay physical oceanographic real-time system, Proc. 1st Int. Conf. Hydro-Sci. Engng. Center Comput. Hydrosci. Engng. 1491-1498.

Nielson P, 1982, Explicit formulae for practical wave calculations, Coastal engng. 6, 389-398.

NOAA Data Buoy Office, 1973, Practical experience with buoys developed by the NOAA Data Buoy Office, US Dept of Commerce.

Nwogu O, 1989, Maximum entropy estimation of directional wave spectra from an array of wave probes, Applied Ocean Research, 11: 176-182.

Ocampo-Torres F J, Robinson I S, 1990, Wind wave directionality effects on the radar imaging of ocean swell, J. Geophys. Res. 95, 20347-20362.

Ochoa J, Dalgado-González O E, 1990, Pitfalls in the estimation of wind wave directional spectra by variational principles, Appl. Ocean Res. 12, 180-187.

Oltman-Shay J, Guza R T, 1984, A data-adaptive ocean wave directional spectrum estimator for pitch and roll type measurements, J. Phys. Oceanogr. 14, 1800-1810.

O'Reilly W C, Seymour R J, Guza R T, Castel D, 1985, Wave monitoring in the southern California Bight, Wave Monitoring. 448-457.

Park Y H, 1981, Study on the directional properties of ocean waves using the surface displacements and two components of horizontal velocity, Bull. Korean Ocean Res. Dev. Inst. 3, 1-6.

Pawka S S, Hsiao S V, Shemdin O, Inman D L, 1980, Comparisons between wave directional spectra from SAR and pressure sensor arrays, J Geophys Res (85):4987-95

Peep M, 1972, A wave follower for field study of air-sea interactions, IEEE Trans. Geosci. Electronics. GE-10, 24-32.

Phillips O M, 1988, Radar returns from the sea surface-Bragg scattering and breaking waves, J. Phys. Oceanogr., 18, 1065-1074.

Pierson W J Jr, Gerhard N, James R W, 1958, Practical Methods for Observing and Forecasting Ocean Waves by Means of Wave Spectra and Statistics, U.S. Naval Oceanographic Office, Washington, H. O. Pub. No. 603. 284 pp.

Pierson W J (ed), 1960, The directional spectrum of a wind-generated sea as determined from data obtained by the Stereo Wave Observation Project, New York Univ. Coll. Eng., Met. Pap. 2, 6.

Pierson W J Jr, 1990, Examples of, reasons for, and consequences of the poor quality of wind data from ships for the marine boundary layer: implications for remote sensing, J. Geophys. Res. 95, 13313-13340

Pitt E G, 1993, A new correction procedure for shipborne wave recorder data, In Ocean Wave Measurement and Analysis pp 726-739

Plant W J, Schuler D L, 1980, Remote sensing of the sea surface using one- and two-frequency microwave techniques, Radio Sci., 15, 605-615.

Plant W J, 1987, The microwave measurement of ocean-wave directional spectra, APL Tech. Digest, 8, 1, Johns Hopkins Univ., 55-59

Plant W J, Keller W C, Reeves A B, Uliana E A, Johnson J W, 1987, Airborne microwave Doppler measurements of ocean wave directional spectra, Int. J. Remote Sens. 8, 315-330.

Poulter E M, Smith M J, McGregor J A, 1990, Microwave radar measurements on ocean wave propagation – initial results, Geophys. Res. Let. 98, 7001-7010.

Poulter E M, Smith M J, McGregor J A, 1995, S-band FMCW radar measurements of ocean surface dynamics, J Atmos Oceanic Tech: 12: 1271-1286

Powers R L, Lewandowski L M, Dinger R J, 1996, High Frequency Surface Wave Radar - HFSWR, Sea Tech., November, 25-32.

Queffeulou P, 1983, SEASAT wave height measurement: A comparison with sea-truth data and a wave forecasting model - Application to the geographic distribution of strong sea states in storms, J. Geophys. Res. 88, 1779-1788.

Rao B V, Seetharamiah K, 1969, Swept back edge impact probe for measurement of three-dimensional flow field, Indian Inst. Sci., HY-7.

Regier L A, Davis R E, 1977, Observations of the power and directional spectrum of ocean surface waves, J. Mar. Res., 35, 433-451.

Rice S O, 1954, Mathematical Analysis of Random Noise, Sel. Papers on Noise and Stochastic Processes, Dover Pub, pp133-294

Rikiishi K, Mitsuyasu H, Honda T, 1976, Notes on the effects of data length and sampling interval upon the spectral estimates for wind waves, Reports Res. Ins. Applied Mech. XXIII, 131-147.

Rikiishi K, 1978, A new method for measuring the directional wave spectrum, Part I. Description. J. Phys. Oceanogr. 8, 508-517.

Rikiishi K, 1978, A new method for measuring the directional wave spectrum, Part II. Measurement of the directional spectrum and phase velocity of laboratory wind waves. J. Phys. Oceanogr. 8, 518-529.

Roerbaek K, Anderson H, 2000, Evaluation of Wave Measurements with an Acoustic Doppler Current Profiler, Oceans 2000 MST/IEEE Conference, Providence, Rhode Island, September 11 - 14, 2000

Santala M J, Terray E A, 1992, A technique for making unbiased estimates of current shear from a wave-follower, Deep-Sea Res. 39, 607-622.

Schuchardt J M, Newton J M, Morton T P, Gagliano J A, 1981, The coming of mm-wave forward looking imaging radiometers, Microwave J., 24, 45-62.

Schuler D L, 1978, Remote sensing of directional gravity wave spectra and surface currents using a microwave dual-frequency radar, Radio Sci., 13, 321-331.

Seddon A E, Anwar H O, 1963, Measuring fluid velocities optically, Engng. 196, 318-319.

Selsor H, 1993, An overview of the US Navy's AN/WSQ-6 (Series) Drifting Buoy Program, Proc. Int. Maritime Defense Conf.

Servain J, Busalacchi A J, McPhaden M J, Moura A D, Reverdin G, Vianna M, Zebiak S E, 1998, A Pilot research moored array in the tropical Atlantic, Bull. Am. Meteorol. Soc., 79, 2019-2031.

Sharma J, Dean R G, 1979, Second-order directional seas and associated wave forces, In: Proc. 11th Offshore technology conference, Houston (OTC 3645), 2505-2514.

Shearman E D R, 1986, A review of methods of remote sensing of sea-surface conditions by HF radar and design considerations for narrow-beam systems, IEEE J. Oceanic Engng. OE-11, 150-157.

Shemdin O, Brown W E Jr, Staudhammer F G, Shuchman R, Rawson R, Zelenka J, Ross D B, McLeish W, Berles R A, 1978, Comparison of In Situ and remotely sensed ocean waves off Marineland, Florida, Bound-Layer Meteor. 13, 193-202.

Sheres D, 1981, Remote and synoptic water-wave measurements by aerial photography: a model, experimental results, and an application, IEEE, OE-6., 63-69.

Sheres D, 1982, Remote synoptic surface current measurements by gravity waves; a method and its test in a small body of water, J. Phys. Oceanogr. 12, 200-207.

Sheres D, Kenyon K E, Bernstein R L, Beardsley R C, 1985, Large horizontal surface velocity shears in the ocean obtained from images of refracting swell and In Situ moored current data, J. Geophys. Res. 90, 4943-4950.

Sheres D, Chen D T, Valenzuela G R, 1987, Remote sensing of wave patterns with oceanographic implications, Int. J. Remote Sens. 8, 1629-1640.

Shkarbul S N, 1963, Static pressure tube for a three-dimensional flow, Measurement Tech., 9, 787-789.

Shonting D H, 1966, Measurements of particle motions in ocean waves, J. Mar. Res., 25, 162-181.

Shonting D H, 1967, Measurements of particle motion in ocean waves, J. Mar. Res., 25, 162-181.

Skafel M G, Donelan M A, 1983, Performance of the CCIW wave direction buoy at ARSLOE, IEEE J. Oceanic Engng. OE-8, 221-225.

Smith J A, Bullard G T, 1995, Directional surface wave estimates from doppler sonar data, J. Atmos. Oceanic Technol., 12, 617-632.

Smith M J, Poulter E M, McGregor J A, 1996, Doppler radar measurements of wave groups and breaking waves, J Geophys Res 101(C6): 14, 269-14, 282.

Smith M J, Poulter E M, McGregor J A, 1998, Doppler radar backscatter from ring waves, Int J Remote Sensing 19(2): 295-305

Snyder R L, 1974, A field study of wave-induced pressure fluctuations above surface gravity waves, J. Mar. Res. 32, 497-531.

Snyder R L, Long R B, Irish J, Hunley D J, Pflaum N C, 1974, An instrument to measure atmospheric pressure fluctuations above surface gravity waves, J. Marine Res. 32, 485-496.

Srokosz M A, 1986, On the joint distribution of surface elevation and slopes for a nonlinear random sea, with an application to radar altimetry, J. Geophys. Res. 91, 995-1006.

Srokosz M A, Longuet-Higgins M S, 1986, On the skewness of sea-surface elevation, J. Fluid. Mech., 164, 487-497.

Stanton B R, 1998, Ocean surface winds off the west coast of New Zealand: A comparison of ocean buoy, ECMWF model and land-based data, J. Atmos. Oceanic Technol. 15, 1164-1170.

Steele K E, Wolfgram P A, Trampus A, Graham B S, 1976, An operational high resolution wave data analyzer system for buoys, Proc. IEEE Conf. Oceans '76.

Steele K E, Earle M D, 1979, The status of data produced by NDBO wave data analyzer (WDA) systems, Proc. IEEE Conf. Oceans '79.

Steele K E, Lau J C-K, Hsu Y-H L, 1985, Theory and application of calibration techniques for an NDBC directional wave measurements buoy, IEEE J. Ocean. Eng., OE-10(4), 382-396.

Steele K E, Lau J C-K, 1986, Buoy azimuth measurements-correction for residual and induced magnetism, Proc. Marine Data Systems Int. Symp..

Steele K E, 1990, Measurement of buoy azimuth, pitch, and roll angles using magnetic field components, NDBC Technical Report 1804-91.03, 16pp.

Steele K E, Wang D, Teng C C, Lang N, 1990, Directional wave measurements with NDBC 3-meter discus buoys, Report No. 1804-01.05, NDBC, Stennis Space Centre, MS, 35 pp.

Stewart R H, Joy J W, 1974, HF radio measurements of surface currents, Deep-sea Res. 21, 1039-1049.

Stewart R H, 1977, A discus-hulled wave measuring buoy, Ocean Eng. 4, 101-107.

Stilwell D Jr, 1969, Directional energy of the sea from photographs, J. Geophys. Res., 74, 1974-1989.

Su M-Y, 1982, Three-dimensional deep-water waves, Part 1. Experimental measurement of skew and symmetric wave patterns. J. Fluid Mech. 124, 73-108.

Szabados M W, , Intercomparison of the offshore wave measurements during ARSLOE, 876-881

Taira K, 1971, Wave particle velocities measured with a Doppler current meter, J. Oceanogr. Soc. Japan, 27, 218-232.

Teng C C, Dagnall R, Remond F, 1991, Field evaluation of the magnetometer-only directional wave system from buoys, Proc. MTS ’91, 1216-1224.

Teng C C, Timpe G L, Dagnall R J, 1992, Field test and evaluation of NDBC’s Coastal Buoy, Proc. MTS ’92, 943-948.

Terray E A, Gordon R L, Brumley B, 1997, Measuring wave height and direction using upward-looking ADCPs, Proc. Oceans97.

Tilley D G, 1988, Estimating aircraft SAR response characteristics and approximating ocean wave spectra in the Labrador Sea, Proc. IGARSS '88 Symp. 399-402.

Trizna D B, 1978, Implications of Different Models of the Ocean Wave Directional Spreading Function: A) On Scaling Directional Sea Spectrum Estimates Using Radar Data and Buoy Data as Inputs and B) On Radar Cross Section of the Sea Versus Look Angle, Technical Memorandum

Trizna D B, Hansen J P, Hwang P A, Wu J, 1993, Ultra-wideband radar studies of steep crested waves with scanning laser measurements of wave slope profiles, Dyn. Atmos. Oceans, 20, 33-53

Tsai B M, Gardner C S, 1982, Remote sensing of sea state using laser altimeters, Applied Optics, 21, 3932-3940.

Tsanis I K, Donelan M A, 1989, Wave directional spectra in mixed seas, Proc. 2nd International Workshop on Wave Hindcasting and Forecasting, Vancouver, Environment Canada, AES-Downsview, 387-396.

Tucker M J, 1956, A shipborne wave recorder, Trans. R. Inst. of Naval Architects., 98, 236-250.

Tucker M J, 1959, The accuracy of wave measurements made with vertical accelerometers, Deep-Sea Res., 5, 185-192.

Tullock K H, Lau J C, 1986, Directional wave data acquisition and preprocessing on remote buoy platforms, Proc. Mar. Data Sys. Intl. Symp., MDS ’86.

Valenzuela G R, Laing M B, 1970, Study of Doppler spectra of radar sea echo, J. Geophys. Res., 75, 551-563.

Van Heteren J, Keijser H, 1982, Directional spectra: comparison of three methods, Proc Conf. On Directional Wave Spectra Applications, ASCE, p116-28

Veron F, Melville W K, 1999, Pulse-to-Pulse Coherent Doppler Measurements of waves and Turbulence, Bull AMS Vol 16, p1580

Walsh E J, Hancock D W III, Hines D E, Swift R N, Scott J F, 1981, Surface contour radar remote sensing of waves, Proc. Conf. Directional Wave Spectra applications. 281-298.

Walsh E J, Hancock D W III, Hines D E, Swift R N, Scott J F, 1982, Comparison of SCR microwave measurement of directional wave spectra with ARSLOW in-situ sensor, Oceans, 893-900.

Walsh E J, Hancock D W III, Hines D E, Swift R N, Scott J F, 1985, Directional wave spectra measured with the surface contour radar, J. Phys. Oceanogr., 15, 566-592.

Walsh E J, Hancock D W III, Hines D E, Swift R N, Scott J F, 1985, Elimination of directional wave spectrum contamination from noise in elevation measurements, IEEE J. Oceanic Engng. OE-10, 376-381.

Wang D W, Carolan R, 1991, Estimation of swell direction by a small discus buoy in high seas, Proc 5th Conf. on Meteorology and Oceanography of the Coastal Zone, 53-59.

Wang H, Leonard J W, 1992, Time Domain Solutions for the Motion of directional wave buoys, Proc. 11th Intl. Conf. on Offshore Mechanics and Arctic Eng. Vol 1 pp127-134.

Wang D W, 1993, Field evaluation of the wave processing module magnetometer-only version (WPM/MO), NDBC Technical Report 1804-01-06.

Wang H T, Freise C B, 1997, Error analysis of the directional wave spectra obtained by the NDBC 3-m pitch-roll discus buoy, IEEE J. Ocean. Engng. 22, 639-648.

Webb D J, 1981, A comparison of SEASAT 1 altimeter measurements of wave height with measurements made by a pitch-roll buoy, J. Geophys. Res. 86, 6394-6398.

Welch P D, 1967, The Use of Fast Fourier Transform for the Estimation of Power Spectra: A Method Based on Time Averaging Over Short, Modified Periodograms, IEEE Trans. Audio and Electroacoust., AU-15, 70-73.

Weller R A, Donelan M A, Briscoe M G, Huang N E, 1991, Riding the crest: a tale of two wave experiments, Bull. AMS 72, 163-183.

Wiegel R L, 1982, Directional Wave Spectra Applications, ISBN: 0872623033

Wilheit T T, Chang A T C, 1980, An algorithm for retrieval of ocean surface and atmospheric parameters from the observation of the Scanning Multichannel Microwave Radiometer (SMMR), Radio Sci., 15, 525-544.

Wilson W B, 1993, Data buoy aerodynamics, Mar. Tech. 30, 51-60.

Withee G W, Johnson A, 1975, Data report: Buoy observations during Hurricane Eloise (Sept 19 to Oct 11, 1975), Environmental Science Div., Data Buoy Office, NOAA, US Dept of Commerce.

Wu J, 1977, Directional slope and curvature distributions of wind waves, J. Fluid Mech., 79, 463-480.

Wyatt L R, 1986, The measurement of the ocean wave directional spectrum for HF radar Doppler spectra, Radio Sci. 21, 473-485.

Wyatt L R, 1988, Significant wave height measurement with HF radar, Int. J. Remote Sens., 9, 1087-1095.

Wyatt L R, Holden G J, 1994, Limits in direction and frequency resolution for HF radar ocean wave directional spectra measurement, Glob. Atmos. Ocean Syst., 2, 265-290.

Yamaguchi M, Tsuchiya Y, 1981, Directional spectra of wind waves in growing stage, Coastal Engng. 24, 93-104.

Yaplee B S, Shapiro A, Hammond D L, Au B D, Uliana E A, 1971, Nanosecond radar observations of the ocean surface from a stable platform, IEEE Trans. Geosci. Electronics. GE-9, 170-174.

Yoshimoto H, 1990, At-sea experiment of a floating offshore structure characteristics of directional wave spectra at a test field, JSNA 166, 1-9.

Ziemer F, Gunther H, 1994, A system to monitor ocean wave fields, Proc. Oceans'94.

Zwarts C M G, 1974, Transmission line wave height transducer, Int. Symp. On Wave measurement and Analysis, 605-620.

11 Appendices

Appendices are located on the CD-ROM attached to this document.

11.1 Appendix 1: Data & Programs

This appendix contains data, raw and analysed, collected from the data logger, as well as source code (C and M16C assembler) to analyse the data.

In general, the source code is contained in a subdirectory called SOURCE.

Files with .CSV extensions are comma-delimited text files containing raw data output from the logger program. Files with .XLS extensions are Microsoft Excel spreadsheets which have been generated by analysing the .CSV file with the same name. The various graphs included in this document have been generated by these spreadsheets.

11.1.1 Lab

Lab version of the software.

- BC3 code subdirectory
  Contains Borland C source code for retrieving data from the lab version of the M16C software, logging it, and displaying it graphically.
- M16C code subdirectory
  Contains M16C assembler and C source code for the lab version of the M16C software; inputting data, and outputting it via the serial port.

11.1.2 Logger

Contains M16C assembler and C source code for the logger version of the M16C software; inputting data, storing it in flash memory, and outputting it via the serial port.

11.1.3 Pukepapa

Data and source code relating to data logged on Pukepapa Rd

- SOURCE code subdirectory
  Contains Microsoft C source code for analysing data retrieved from the logger on Pukepapa Rd.
- pukepapa.csv
- pukepapa.xls

11.1.4 Mole

Two sets of raw data collected at the North Mole, Wanganui River Mouth, on 8th November 2002.

- 8Nov06.csv
- 8Nov11.csv

11.1.5 Kaiiwi

Data and source code relating to data logged off Kai-iwi Beach

- SOURCE subdirectory
- kaiiwi11.csv

- kaiiwi11.xls
- kaiiwi3.csv
- kaiiwi9.csv
- kaiiwi9.xls

11.1.6 Boat

Data and source code relating to data logged on 15th May 2003, on the "Gwenelda" data collection trip

- SOURCE subdirectory
- 10ms.csv: 10ms sampling interval buoy raw data
- 20ms.csv: 20ms sampling interval buoy raw data
- 20ms.xls: 20ms sampling interval buoy analysed data
- boat.csv: 20ms sampling interval boat raw data
- boat.xls: 20ms sampling interval boat analysed data

11.1.7 Trochoidal.xls

Excel spreadsheet for drawing trochoidal waveforms

11.2 Appendix 2: Papers

This directory includes academic and other documents downloaded from the Internet. They are included here because the transitory nature of the Internet means that they may not be available in the future.

11.2.1 ADXL202E datasheet.pdf

Datasheet published by Analog Devices for the ADXL202E accelerometer IC.

11.2.2 Kinematic DGPS.htm

Paper entitled "Development of Topographic Maps for Precision Farming with Kinematic GPS" by R. L. Clark and R. Lee

11.2.3 Attitude Determination

This subdirectory contains papers relating to attitude determination.

- Attitude Determination.pdf
  "Attitude Determination using Vector Observations and the Singular Value Decomposition"
  [Markley 1988]
- Attitude Estimation.pdf
  "Attitude Estimation" notes by Thomas Bak
  http://www.control.auc.dk/~raf/Aerospace/best_tb3.pdf
- bei gyro.htm
  A Micromachined Quartz Angular Rate Sensor for Automotive and Advanced Inertial Applications
  http://www.sensorsmag.com/articles/0899/26/main.shtml
- Chapter 4 attitude determination.doc
  Part of a course in Spacecraft Dynamics and Control by Chris Hall
  www.aoe.vt.edu/~chall/courses/aoe4140/attde.pdf

- Extended QUEST.pdf
  "Extended QUEST attitude determination filtering" by Mark L. Psiaki
  http://www.mae.cornell.edu/Psiaki/extended_quest.pdf

11.2.4 Wave Measurement

This subdirectory contains papers relating to ocean wave measurement.

- dbcp nz.html
  Data Buoy Cooperation Panel Annual Report (New Zealand)
  http://ioc.unesco.org/goos/ms/rpts/nz_r02.htm
- ndbc wave measurement.html
  "How are spectral wave data derived from buoy motion measurements?"
  http://seaboard.ndbc.noaa.gov/wave.shtml
- wavemeas.pdf
  Nondirectional and Directional Wave Analysis Procedures
  NDBC Technical Document 96-01
  http://www.ndbc.noaa.gov/wavemeas.pdf

11.2.5 Speake & Co

This directory contains documents relating to the FGM-series magnetometers

- AUTOCAL.DOC
  Application Note: Autocalibration algorithms for FGM type sensors
  http://www.fatquarterssoftware.com/Download/autocal.htm
- fgmapp.doc
  FGM-series Magnetic Field Sensors General Application Techniques
  http://www.fatquarterssoftware.com/Download/fgmapp.htm
- FGM_DS.DOC
  FGM-series Magnetic Field Sensors Datasheet
  http://www.fatquarterssoftware.com/Download/fgm_ds.htm
- scl004.doc
  SCL004 Integrated Circuit - Self Calibrating Compass
  http://www.fatquarterssoftware.com/Download/scl004.htm

11.2.6 Reference Lists

This directory contains various lists of papers and other references.

- asiref.html
  Will Drennan's list of references on Air-sea Interaction, geophysical turbulence, surface waves and related fields
  http://anole.rsmas.miami.edu/people/wdrennan/asiref.html
- attitude biblio.txt
  References related to attitude determination.
- hansrefs.html
  Hans Graber's List of References
- markrefs.html
  Mark Donelan's list of references
- Web References.doc
  Links to web sites which refer to GPS attitude determination, wave measurement, etc.
- Peak Picking Biblio.txt
  References related to peak picking.

11.3 Appendix 3: Hardware

This directory contains documents and images relating to the hardware construction required for this project. The schematic and PCB files were created with a software package called Protel DXP.

- accelerometer pcb.gif
  Image of the Accelerometer board PCB layout.
- accelerometer sch.gif
  Image of the Accelerometer board schematic.
- M16 Breakboard subdirectory
  Schematics, etc for construction of the M16C breakout board
- M16 Magnetometer board subdirectory
  Schematics, etc for construction of the Magnetometer interface board

11.4 Appendix 4: Media

This directory contains images and movies relating to this project.

11.4.1 Images

All images included in this thesis (excluding the graphs of data generated using Excel) are included in this directory.

11.4.2 Movies

Movies in this subdirectory were made using a Mavica digital camera. They are all short, and of relatively poor quality.

- 0.5m buoy floating (2).mpg
  The 0.5m buoy in the water at North Mole, Wanganui
- 0.5m buoy floating.mpg
  The 0.5m buoy in the water at North Mole, Wanganui
- Waves.mpg
  Waves breaking on the South Mole, Wanganui
- MVC-788W.MPG
  The 0.5m buoy in the water off Kai-iwi Beach, Wanganui
- MVC-789W.MPG
  The 0.5m buoy in the water off Kai-iwi Beach, Wanganui
- MVC-791W.MPG
  The 0.5m buoy in the water off Kai-iwi Beach, Wanganui
- MVC-792W.MPG
  The 0.5m buoy in the water off Kai-iwi Beach, Wanganui

12 Index